

**PEOPLE'S DEMOCRATIC REPUBLIC OF ALGERIA  
MINISTRY OF HIGHER EDUCATION AND SCIENTIFIC  
RESEARCH**

**University of M'hamed Bougara Boumerdes**



**Faculty of Technology  
Department of Electrical Systems Engineering**

**Field : Telecommunications**

**Option : Telecommunications Systems**

**DOCTORAT THESIS**

**By : BENLAKEHAL Mohamed Elamine**

**THEME**

---

**Analysis and Design of Terahertz Microstrip Antenna  
based on Photonic Band Gap Substrate  
Analyse et Conception d'une Antenne Réseau Térahertz  
Basée sur un Structure a Bande Interdite  
Electromagnétique**

---

**Presented and publicly defended on : 06/03/2024**

**Jury Members :**

<b>HAMADOUCHE M'Hamed</b>	<b>Professor</b>	<b>Univ. of Boumerdes</b>	<b>Chairman</b>
<b>HOCINI Abdesselam</b>	<b>Professor</b>	<b>Univ. of M'sila</b>	<b>Supervisor</b>
<b>KHEDROUCHE Djamel</b>	<b>Professor</b>	<b>Univ. of M'sila</b>	<b>Co-supervisor</b>
<b>MERAIHI Yassine</b>	<b>Professor</b>	<b>Univ. of Boumerdes</b>	<b>Examiner</b>
<b>BELKACEM Samia</b>	<b>MCA</b>	<b>Univ. of Boumerdes</b>	<b>Examiner</b>
<b>MESSAOUDENE Idris</b>	<b>MCA</b>	<b>Univ. of Bordj Bou Arreridj</b>	<b>Examiner</b>

**2023/2024**

# Acknowledgements

All thanks to “ALLAH” for giving me the strength, courage, and commitment that enabled me to start and finish this research work. This thesis work was carried out in the Systems Engineering and Telecommunications Laboratory at the University of Boumerdes.

First, I would like to express my sincere gratitude and appreciation to my family for all of their overall encouragement and provided support.

I would like to express my sincere gratitude and appreciation to my supervisor Prof. Abdeslam HOCINI and co-supervisor Prof. Djamel KHEDROUCHE for all their continuous support, availability, encouragement, and guidance throughout the accomplishment of this research work.

I would especially like to thank Prof. Yassine MERAIHI and Prof. Dalila ACHELI, who accompanied me at every step of my research work, advising and guiding me. I also greatly appreciate the precious time they devoted to proofreading my research work and the many constructive suggestions they have made.

I particularly would like to thank Prof. M’Hamed HAMADOUCHE for his availability, his scientific rigor and his sense of listening and exchange.

Additionally, I would like to strongly thank Dr. Idris MESSAOUDENE for his many tips which were very useful to me.

I would like to deeply thank Dr. Samia BELKACEM for the honor she gave me by taking the time to read and evaluate this research work.

I would also like to thank Dr. Mohamed Nasr Eddine TEMMAR for his assistance, advice, and valuable information, which he provided to me with an unparalleled degree of patience and professionalism, despite his multiple accusations.

I would like to express my sincere gratitude and appreciation to Prof. Ibraheem SHAYEA for all his support, encouragement, and advice throughout the accomplishment of this research work during the fruitful internship accomplished at Istanbul Technical University (ITU) under his guidance.

Finally, I would like to express my sincere thanks to the entire administrative and teaching staff at the University of Boumerdes for their keen interest in our training, interest and energy, in a pleasant and respectful environment.

# Abstract

## المخلص

في نظام الاتصالات اللاسلكية، يكتسب هوائي الميكروستريب أهمية باعتباره أحد أقوى اتجاهات التكنولوجيا وهو قابل للتطبيق لتطوير هوائي منخفض الوزن، منخفض التكلفة، وصغير الشكل وعالي الأداء. ومع ذلك، فإن هوائيات الميكروستريب التقليدية المصممة على التيراهيرتز تواجه عدة عيوب بما في ذلك عرض النطاق الترددي الضيق، والكسب المنخفض بسبب ارتفاع المسار الجوي، وانخفاض الكفاءة، وإثارة الموجات السطحية. للتغلب على كل هذه العيوب، تعد مصفوفات هوائي الميكروستريب المستندة إلى البلورات الضوئية مفيدة من خلال توفير أداء إضافي. الهدف الرئيسي من هذه الأطروحة هو تطوير وتحليل هوائيات المصفوفة العاملة في نطاق التيراهيرتز ( 0.1-10 هرتز) استنادًا إلى الهياكل البلورية الضوئية التي تلبّي المتطلبات المهمة المتمثلة في الاتجاهية العالية، الكسب العالي والكفاءة الإشعاعية والتي ستكون مرشحة للاستخدام في الموجات العالية ذات سرعة الاتصال، التحليل الطيفي الجزئي، التصوير الأمني، الاستشعار والتشخيص الطبي. ولتحقيق هذا الهدف، سيتم استخدام البرامج التجارية مثل Ansys HFSS و CST Microwave Studio . علاوة على ذلك، تم تصميم وتحليل مجموعة متنوعة على التيراهيرتز من مصفوفات هوائي الميكروستريب المستندة إلى ركائز فجوة النطاق الضوئية المعدلة. تم مقارنة الخصائص الإشعاعية للهوائيات المقترحة بالأبحاث التي تم الإبلاغ عنها مسبقًا. أخيرًا، تم تطوير ودراسة نظام MIMO اتصالات داخلي جديد يستخدم مصفوفة هوائي الميكروستريب  $2 \times 1$  قائمة على الجرافين استنادًا إلى ركائز مختلفة، بما في ذلك الركيزة المتجانسة، والركائز البلورية الضوئية الدورية و المحسنة لتعزيز سعة قناة اتصالات تيراهيرتز. هذا وأظهرت النتائج تحسنا ملحوظا مقارنة بالدراسات المبلغ عنها سابقا.

**الكلمات المفتاحية:** تيراهيرتز، هوائي الميكروستريب، مصفوفات الهوائي، الخصائص الإشعاعية، البلورة الضوئية، MIMO ، HFSS ، CST .

## Abstract

In a wireless communication system, a microstrip patch antenna is gaining importance as a most powerful technology trend and it is applicable for the development of minimal weight, low profile, low cost and high-performance antenna. However, the



designed conventional patch antennas in terahertz encounter several drawbacks including narrow bandwidth, low gain due to high atmospheric path loss, low efficiency, and surface wave excitation. To overcome these drawbacks, microstrip patch antenna arrays based on photonic crystals are advantageous by providing extra performance. The main objective of this thesis is to develop and analyze array antennas operating in the terahertz band (0.1-10 THz) based on photonic crystal structures that satisfy the important requirements of high directivity, gain and radiation efficiency which will be candidates for use in high-speed communication, spectroscopy molecular, security imaging, sensing and medical diagnosis. To achieve this goal, commercial software such as Ansys HFSS and CST Microwave Studio will be used. Further, a variety of microstrip terahertz patch array antennas based on modified photonic band gap substrates are designed and analyzed. The radiation characteristics of the proposed antennas are compared to previously reported papers. Finally, a novel MIMO indoor communication system using a graphene-based 1 x 2 microstrip patch antenna array is developed and studied based on different substrates, including homogeneous, periodic photonic crystals and optimized photonic crystals substrates for terahertz communications channel capacity enhancement. The outcomes showed a remarkable enhancement compared with previously reported studies.

**Keywords:** Terahertz, Microstrip patch antenna, Array configuration, Radiation characteristic, Photonic crystal, MIMO, HFSS and CST.

---

## Résumé

Dans un système de communication sans fil, une antenne patch microruban gagne en importance en tant que tendance technologique la plus puissante et elle est applicable au développement d'antennes de poids minimal, de profil bas, à faible coût et de haute performance. Cependant, les antennes patch conventionnelles conçues en térahertz rencontrent plusieurs inconvénients, notamment une bande passante étroite, un faible gain dû au chemin atmosphérique élevé, une faible efficacité et une excitation des ondes de surface. Pour surmonter ces inconvénients, les réseaux d'antennes patch microruban basés sur des cristaux photoniques sont avantageux en offrant des performances supplémentaires. L'objectif principal de cette thèse est de développer et d'analyser des antennes réseau fonctionnant dans la bande térahertz (0,1-10 THz) basées sur des structures de cristaux photoniques qui satisfont aux exigences importantes de directivité, de gain et d'efficacité de rayonnement élevées et qui seront candidates à une utilisation en hautes températures communication rapide, spectroscopie moléculaire, imagerie de sécurité, détection et diagnostic médical. Pour atteindre cet objectif, des logiciels commerciaux tels que Ansys HFSS et CST Microwave Studio seront utilisés. En outre, diverses antennes réseau à patch

térahertz microruban basées sur des substrats à bande interdite photonique modifiées sont conçues et analysées. Les caractéristiques de rayonnement du projet proposé les antennes sont comparées aux articles rapportés précédemment. Enfin, un nouveau système de communication intérieure MIMO utilisant un réseau d'antennes patch microruban 1 x 2 à base de graphène est développé et étudié sur la base de différents substrats, notamment des cristaux photoniques périodiques homogènes et des substrats de cristaux photoniques optimisés pour l'amélioration de la capacité des canaux de communication térahertz. Les résultats ont montré une amélioration remarquable par rapport aux études précédemment rapportées.

**Mots Clée:** Térahertz, antenne patch microruban, configuration réseau, caractéristique de rayonnement, photonique cristal, MIMO, HFSS et CST.

---

# Contents

<b>Acknowledgements</b>	<b>i</b>
<b>Abstract</b>	<b>iii</b>
<b>Contents</b>	<b>vi</b>
<b>List of Figures</b>	<b>ix</b>
<b>List of Tables</b>	<b>xiii</b>
<b>List of Abbreviations</b>	<b>xiv</b>
<b>List of Symbols</b>	<b>xvi</b>
<b>General Introduction</b>	<b>1</b>
0.1 Motivation . . . . .	1
0.2 Thesis Contributions and Organization . . . . .	1
<b>1 Terahertz Antenna Array Based on Photonic Band Gap Structures: State of the Art</b>	<b>4</b>
1.1 Introduction . . . . .	4
1.2 Terahertz Technology . . . . .	4
1.3 Microstrip Patch Antenna Array . . . . .	13
1.4 Photonic Crystals . . . . .	16
1.5 Design of Terahertz Microstrip Antenna Arrays Based on Photonic Crystals . . . . .	17

---

1.5.1	Design of a Single Patch Based on Photonic Crystals . . . . .	18
1.5.2	Design of 1x2, 1x4 and 2x8 Rectangular Microstrip Patch Antenna Arrays Based on Photonic Crystals . . . . .	20
1.5.3	Simulated Results and Discussion . . . . .	21
1.6	Summary . . . . .	30
<b>2</b>	<b>Design and Analysis of Novel Microstrip Patch Antenna Arrays Based on Photonic Crystals in Terahertz</b>	<b>32</b>
2.1	Introduction . . . . .	32
2.2	Design and Analysis of a novel 1x2 Microstrip Patch Antenna Array based on Photonic Crystals . . . . .	35
2.3	Design and Analysis of a novel 2x2 Microstrip Patch Antenna Array Based on Periodic and Non-Periodic Photonic Crystals Substrate . . . . .	44
2.3.1	Design and Analysis of a 2x2 Microstrip Patch Antenna Array Based on Periodic Photonic Crystals Substrate . . . . .	44
2.3.2	Design and Analysis of a 2x2 Microstrip Patch Antenna Array Based on Non-periodic Photonic Crystals Substrate . . . . .	51
2.4	Summary . . . . .	57
<b>3</b>	<b>Design and Analysis of Terahertz Microstrip Antenna Arrays Based on Modified Photonic Crystals</b>	<b>58</b>
3.1	Introduction . . . . .	58
3.2	Design and Analysis of a 1x2 Rectangular Microstrip Patch Antenna Array Based on Modified Photonic Crystals Substrate . . . . .	61
3.2.1	Antenna Array Design Based on Periodic Photonic Crystals . . . . .	61
3.2.2	Antenna Array Design Based on Aperiodic Photonic Crystals . . . . .	67
3.3	Design and Analysis of a 1x2 Circular Microstrip Patch Antenna Array Based on Modified Photonic Crystals Substrate . . . . .	76
3.3.1	Antenna Array Design Based on Cylindrical and Cuboid Photonic Crystal Substrate . . . . .	77
3.3.2	Antenna Array Performance Investigation . . . . .	83
3.4	Summary . . . . .	91

---

<b>4 Design and Analysis of MIMO System for Terahertz Indoor Communications</b>	<b>92</b>
4.1 Introduction . . . . .	92
4.2 Graphene Properties . . . . .	95
4.3 Antenna Array Design Based on Periodic and Non-Periodic Photonic Crystals With a Graphene Load . . . . .	98
4.4 MIMO System Design . . . . .	105
4.4.1 MIMO Antenna Array Design and Analysis With a Graphene Load . . . . .	105
4.4.2 Losses and Terahertz Channel Capacity . . . . .	109
4.4.3 Results and Discussion . . . . .	113
4.5 Summary . . . . .	118
<b>General Conclusion</b>	<b>119</b>
<b>Suggestions</b>	<b>122</b>
<b>Publications</b>	<b>123</b>
<b>Bibliography</b>	<b>125</b>

# List of Figures

1.1	THz band location in the frequency spectrum [1]. . . . .	5
1.2	Atmospheric path loss in different atmospheric conditions over a wide frequency range [1]. . . . .	7
1.3	Power performances of different sources at THz frequencies [1]. . . . .	10
1.4	The structure of a microstrip patch antenna. . . . .	13
1.5	Feeding method: (a) Series feed (b) Corporate feed (c) Series-Corporate feed. . . . .	14
1.6	Classification of PCs structures. . . . .	17
1.7	The geometry of the single element RMPA based on PBG substrate. . . . .	19
1.8	The geometry of the 1x2 RMPA array. . . . .	21
1.9	The geometry of the 1x4 RMPA array. . . . .	21
1.10	The geometry of the 2x8 RMPA array. . . . .	22
1.11	The return loss of the designed antennas. . . . .	25
1.12	Gain performance of the designed single element RMPA, 1x2, 1x4, 2x8 RMPA arrays in the frequency range 0.25-0.45 THz. . . . .	27
1.13	Polar plot of $E$ - plane and $H$ - plane for the designed single element RMPA, 1x2, 1x4 and 2x8 RMPA arrays. . . . .	29
2.1	The geometry of the proposed microstrip patch antenna array. . . . .	36
2.2	The magnitudes of the $S_{11}$ parameter of the designed antenna array based on the homogeneous and the PBG substrates using CST Microwave Studio and Ansys HFSS. . . . .	38
2.3	VSWR performance of the designed antenna array based on the homogeneous and the PBG substrates using CST Microwave Studio and Ansys HFSS. . . . .	39

---

2.4	The input impedance characteristics of the proposed antenna array. . . . .	40
2.5	Gain performance of the designed antenna array based on the homogeneous and the PBG substrates. . . . .	40
2.6	Radiation efficiency performance of the designed antenna array based on the homogeneous and the PBG substrates. . . . .	41
2.7	Polar plots of the directivity for the proposed antenna array. . . . .	41
2.8	3D radiation pattern of the directivity of the proposed antenna array based on the PBG substrate with maximum directivity of 12.21 <i>dBi</i> . . . . .	42
2.9	Surface current distribution of the proposed antenna array. . . . .	42
2.10	The geometry of the proposed 2x2 microstrip patch antenna array. . . . .	45
2.11	Magnitudes of the scattering parameter $S_{11}$ of the designed antenna array based on homogeneous and periodic PBG substrates using CST Microwave Studio and Ansys HFSS. . . . .	47
2.12	VSWR performance of the designed antenna arrays 0 and 1 using CST Microwave Studio and Ansys HFSS. . . . .	48
2.13	Polar plots of the radiation patterns for antenna arrays 0 and 1 at their resonance frequencies using CST Microwave Studio and Ansys HFSS. . . . .	49
2.14	Surface current distribution. . . . .	50
2.15	The geometry of the proposed antenna array based on non-periodic PCs substrate. . . . .	52
2.16	The magnitudes of the scattering parameter $S_{11}$ of the designed antenna arrays based on periodic and non-periodic PCs using CST Microwave Studio. . . . .	53
2.17	Gain and radiation efficiency performance of all designed antenna arrays in the frequency range 0.5-0.7 THz using CST Microwave Studio. . . . .	53
2.18	Surface current distribution. . . . .	55
3.1	The geometry of the square unit cell. . . . .	62
3.2	The geometry of the simulated PBG structure. . . . .	62
3.3	The relative permittivity of the designed PBG. . . . .	63
3.4	The geometry of the designed 1x2 RMPA array. . . . .	65
3.5	Magnitudes of the scattering parameter $S_{11}$ for antenna array 1 and antenna array 0. . . . .	65

3.6	Polar plots of the radiation patterns for antenna array 0 and antenna array 1 at their resonance frequencies for the $\theta$ and $\phi$ planes, which define the solid angle of the maximum radiation. . . . .	67
3.7	Current distribution. . . . .	68
3.8	The geometry of the proposed antenna array based on an aperiodic PCs substrate. . . . .	70
3.9	Magnitudes of the scattering parameter $S_{11}$ the proposed antenna arrays based on an aperiodic PCs substrate. . . . .	72
3.10	Gain and radiation efficiency of all proposed antenna arrays in the frequency range from 0.55-0.75 THz. . . . .	73
3.11	Polar plot of the proposed antenna arrays radiation patterns. . . . .	74
3.12	Current distribution. . . . .	75
3.13	The geometry of the unit cell. . . . .	78
3.14	The geometry of the proposed antenna arrays based on the homogeneous and periodic PBG substrates. . . . .	79
3.15	Return loss versus the frequency of the proposed antenna arrays. . . . .	80
3.16	Gain and radiation efficiency of all proposed antenna arrays in the frequency range of 0.58-0.70 THz. . . . .	80
3.17	The radiation pattern of proposed antenna arrays based on the periodic PCs and the homogeneous substrate at their resonant frequencies for the $\theta$ plane, which defines the solid angle of the maximum radiation. . . . .	82
3.18	Current distribution. . . . .	83
3.19	Single patch element performance based on PCs. . . . .	84
3.20	Geometry of the proposed antenna arrays based on non-periodic PCs. . . . .	85
3.21	Return loss of the proposed antenna arrays based on PCs versus the frequency. . . . .	85
3.22	VSWR of the proposed antenna arrays. . . . .	86
3.23	The input impedance characteristics of the proposed antenna arrays. . . . .	86
3.24	Effect of diameters of the PCs on the gain. . . . .	88
3.25	The radiation pattern of the proposed antenna arrays based on periodic and non-periodic PCs at their resonant frequencies. . . . .	88
3.26	Current distribution. . . . .	89



4.1	Intra-band conductivity of graphene. . . . .	97
4.2	Properties of graphene. . . . .	98
4.3	The geometry of the proposed 1x2 RMPA array based on the homogeneous substrate, periodic and non-periodic PCs with a graphene load. . . . .	100
4.4	The effective permittivity of the designed PBG substrate. . . . .	101
4.5	The radiation characteristics of the proposed 1x2 RMPA array based on the homogeneous substrate, periodic and non-periodic PCs with a graphene load. . . . .	103
4.6	The geometry of the designed MIMO antenna array based on the homogeneous substrate. . . . .	106
4.7	The geometry of the designed MIMO antenna array based on the periodic PCs with a graphene load. . . . .	106
4.8	The geometry of the designed MIMO antenna array based on the optimized PCs with a graphene load. . . . .	107
4.9	<i>S</i> Parameters of the designed MIMO antenna arrays. . . . .	108
4.10	The gain performance of the designed MIMO antenna arrays. . . . .	109
4.11	The far field radiation patterns of the designed MIMO antenna arrays. . . . .	110
4.12	The 3D far-field radiation pattern of the designed MIMO antenna array 2. . . . .	111
4.13	The performance of the designed MIMO antenna array based on the optimized PCs with different chemical potentials. . . . .	111
4.14	A scenario based on the MIMO antenna array. . . . .	113
4.15	The total path loss with different incident angles for a 2x2 MIMO system configuration. . . . .	114
4.16	The capacity performance for a 2x2 MIMO system configuration based on MIMO antenna arrays 0, 1 and 2. . . . .	114
4.17	The capacity performance for different system configurations. . . . .	114
4.18	The total path loss of the proposed MIMO system (2x2 system configuration). . . . .	115
4.19	The capacity of the proposed MIMO system (2x2 system configuration). . . . .	115
4.20	The total path loss of the proposed MIMO system (2x2 system configuration) for different $L_{ij}$ values. . . . .	116
4.21	The capacity of the proposed MIMO system (2x2 system configuration) for different $L_{ij}$ values. . . . .	116

# List of Tables

1.1	The calculated geometrical parameters of the proposed 1x2, 1x4 and 2x8 RMPA arrays based on the homogeneous substrate. . . . .	23
1.2	The optimized geometrical parameters of the proposed 1x2, 1x4 and 2x8 RMPA arrays based on the PBG substrate. . . . .	23
1.3	Comparison of the proposed designed antenna arrays and previously reported designs. . . . .	28
2.1	Parameters of the proposed antenna array based on PCs. . . . .	37
2.2	Comparison of the proposed designed antenna array and previously reported designs. . . . .	44
2.3	Parameter values for antenna array 0 based on the homogeneous substrate and antenna array 1 based on periodic PBG substrate. . . . .	47
2.4	Comparison of the proposed designed antenna arrays and previously reported designs. . . . .	56
3.1	Parameter values for antenna array 0 based on a homogeneous substrate and antenna array 1 based on a periodic PBG substrate. . . . .	66
3.2	The optimized radii air cylinder holes of the proposed antenna arrays. . . . .	69
3.3	Comparison of the proposed designed antenna arrays and previously reported designs. . . . .	71
3.4	Parameter values for antenna array 7 based on a homogeneous substrate, antenna array 8, and antenna array 9 based on a periodic PBG substrate. . . . .	78
3.5	Comparison of the proposed designed antenna arrays and previously reported designs. . . . .	90
4.1	Comparison of the proposed designed antenna arrays and previously reported designs. . . . .	104

# List of Abbreviations

<b>1D</b>	1 Dimension
<b>2D</b>	2 Dimension
<b>3D</b>	3 Dimension
<b>BW</b>	Bandwidth
<b>BWO</b>	Backward Wave Oscillator
<b>CMPA</b>	Circular Microstrip Patch Antenna
<b>CST</b>	Computer Simulation Technology
<b>CVD</b>	Chemical Vapor Deposition
<b>EM</b>	Electromagnetic
<b>DGS</b>	Defected Ground Structures
<b>ENZ</b>	Epsilon-Near-Zero
<b>Eqs</b>	Equations
<b>FEM</b>	Finite Element Method
<b>FIT</b>	Finite Integration Technique
<b>FTIR</b>	Fourier Transform Infrared
<b>GHz</b>	Gigahertz
<b>HFSS</b>	High-Frequency Structure Simulator
<b>HIS</b>	High Impedance Surfaces
<b>IMPATT</b>	Impact Ionization Avalanche Transit-Time
<b>IR</b>	InfraRed

---

<b>ITU</b>	International Telecommunication Union
<b>LAN</b>	Local Area Network
<b>MEMS</b>	Micro Electro Mechanical System
<b>MIMO</b>	Multiple Inputs Multiple Outputs
<b>MISO</b>	Multiple Inputs Single Output
<b>NMR</b>	Nuclear Magnetic Resonance
<b>OFDM</b>	Orthogonal Frequency-Division Multiplexing
<b>PAN</b>	Personal Area Network
<b>PBG</b>	Photonic Band Gap
<b>PCs</b>	Photonic Crystals
<b>PCB</b>	Printed Circuit Board
<b>QCL</b>	Quantum Cascade Laser
<b>RF</b>	Radio Frequency
<b>RMPA</b>	Rectangular Microstrip Patch Antenna
<b>SIMO</b>	Single Input Multiple Outputs
<b>SISO</b>	Single Input Single Output
<b>SoC</b>	System on Chip
<b>SPP</b>	Surface Plasmon Polaritons
<b>SRR</b>	Split Ring Resonators
<b>TE</b>	Transverse Electric
<b>THz</b>	Terahertz
<b>TM</b>	Transverse Magnetic
<b>UV</b>	Ultra Violet
<b>VNA</b>	Vector Network Analyser
<b>VSWR</b>	Voltage Standing Wave Ratio

# List of Symbols

$\mu_c$	Chemical potential
$P_{out}$	Output power
$P_{in}$	Input power
$\lambda$	Wavelength
$G_t$	Gain of the transmitter
$G_r$	Gain of the receiver
$P_{rad}$	Radiated power
$D$	Directivity
$\lambda_0$	Wavelength at free space
$h$	Substrate thickness
$\epsilon_r$	Relative permittivity
$\epsilon_{eff}$	Effective permittivity
$Z_0$	Characteristics impedance
$a$	Lattice constant
$r$	Radius
$W_p$	Width of the patch
$L_p$	Length of the patch
$W_s$	Width of the substrate
$L_s$	Length of the substrate
$T_s$	Substrate thickness
$T_g$	Ground thickness
$W$	Width of the feed line
$L$	Length of the feed line
$S$	Scattering parameter
$f_r$	Resonance frequency
$f$	Operating frequency
$E$	Electric field
$H$	Magnetic field
$\epsilon_0$	Permittivity of the free space
$\mu_0$	Permeability of the free space
$\mu_r$	Relative permeability
$c$	Speed of light
$t$	Ground thickness

---

$Z_c$	Characteristics impedance
$\Delta l$	Patch length extension
$K_0$	Wave number
$\eta_0$	Intrinsic impedance in free space
$\sigma_g$	Complex surface conductivity of graphene
$\sigma_{intra}$	Intra-band conductivity
$\sigma_{inter}$	Inter-band conductivity
$K_B$	Boltzmann's constant
$\omega$	Angular frequency
$T$	Temperature
$\hbar$	Reduced Planck's constant
$h$	Normal Planck's constant
$e$	Electron charge
$\tau$	Relaxation time
$f_d$	Fermi–Dirac distribution
$n_s$	Graphene carrier density
$V_f$	Fermi velocity
$W_g$	Graphene width
$A_{spread}$	Spreading loss
$A_{abs}$	Molecular absorption
$A_{ref}$	Reflection loss
$d$	Traveled distance
$\rho$	Roughness factor
$g$	Surface variation intensity
$\theta_I$	Angle of incidence
$\theta_O$	Angle of reflection
$\Delta$	Standard deviation coefficient
$L_{ij}$	Horizontal distance between transmitters and receivers
$d_{ij}$	Length of the radiation path
$Sp_i$	Distance between the transmitter and the corresponding indoor wall
$Sp_{ij}$	Distance between the receiver $j$ and indoor wall $i$
$d_t$	Spacing between transmitters
$d_r$	Spacing between receivers
$x$	Transmit signal
$y$	Receive signal
$w$	White Gaussian noise
$H$	Gain matrix
$N_0$	Noise power spectral density
$h_{ij}$	Gain matrix element between $i_{th}$ transmitter and $j_{th}$ receiver
$P_i$	Transmitted power from the $i_{th}$ antenna
$\lambda_i$	Singular values of the gain matrix
$n_{min}$	Rank of the gain matrix

# General Introduction

## 0.1 Motivation

In recent years, the Terahertz (THz) band has experienced rapid growth and research interest in many fields including radars and next-generation communication networks [1, 2], astronomic and atmospheric spectroscopy [3], semiconductor and pharmaceutical industry quality control [4], medicine [5], imaging and sensing [6], material characterization [7], chemical and biological detection [8], defense and security screening [9], etc. As the fundamental component for achieving unidirectional radiation with a high gain, antennas play an important role in THz research and technology advancements. The rapid development of THz communication systems has increased the demand for high-performance THz antennas. For this aim, many researchers have been conducted to achieve different performance highlights such as wider bandwidth, higher gain and radiation efficiency, however, there are still challenges in designing THz antennas with high gain, low profile, low cost, wideband and pattern characteristics (including polarization). Therefore, further improvements are needed for effective and efficient THz antennas [10].

## 0.2 Thesis Contributions and Organization

The contributions and outlines of this thesis are arranged as follows:

In Chapter 1, an overview of the THz frequency band is presented by covering its major impact, features and main challenges. Next, the importance of the microstrip

antenna is addressed and emphasized in this frequency band followed by an overview of Photonic Crystals (PCs) structures. Finally, different THz antenna array configurations including 1x2, 1x4 and 2x8 Rectangular Microstrip Patch Antenna (RMPA) arrays are designed and analyzed using PCs for improved gain performance and high radiation characteristics compared to those designed based on the homogeneous substrate around 0.35 THz [11], where there is a low atmospheric attenuation window. The designed antenna arrays were simulated with the aid of Computer Simulation Technology (CST) Microwave Studio, which is based on Finite Integration Technique (FIT), and validated with Ansys High-Frequency Structure Simulator (HFSS), which is based on Finite Element Method (FEM).

In Chapter 2, high gain novel microstrip patch antenna arrays were proposed and analyzed based on the PCs around 0.65 THz where the atmospheric path loss is relatively small in the THz band. The simulation was performed with the aid of two different simulation techniques, CST Microwave Studio and Ansys HFSS which showed the convergence. First, a novel 1x2 microstrip patch antenna array is designed based on a thick silicon substrate having a high relative permittivity and embedded air cylinder holes, and then the radiation characteristics of this antenna array are compared to the one that is mounted on the homogeneous substrate. For high radiation characteristics, the proposed antenna array resonated around 0.65 THz and showed significant improvements. The outcomes of this published work [12] are compared to previously reported works in the literature. Next, a novel 2x2 microstrip patch antenna array is designed and analyzed around 0.65 THz based on different substrates including periodic, non-periodic PCs and homogeneous substrates. The proposed antenna array was first designed based on a periodic PCs substrate in order to enhance its performance by suppressing the undesirable surface waves that are found in the homogeneous substrate. Finally, three different enhancements to the PCs substrate by introducing non-periodic PCs were described to improve the characteristics of the proposed antenna array. The simulated results presented in [13] are compared with other research papers, which are favorable.

In Chapter 3, several THz microstrip patch antenna arrays based on optimized PC



substrate are designed and analyzed around 0.65 THz to improve the performance of the conventional antenna array that is designed based on the homogeneous substrate by suppressing undesirable surface waves. First, six THz 1x2 RMPA arrays based on different substrates, including homogeneous, periodic PCs and five new aperiodic PCs substrates are analyzed. After that, modification of the patch shape is depicted followed by modifications in the PCs structures resulting in the construction of a 1x2 Circular Microstrip Patch Antenna (CMPA) array based on periodic and non-periodic air cylinders holes and air cuboids holes. The improvements of these antennas published in [14, 15] are compared with previously reported papers. The simulation in this chapter has been performed using CST Microwave Studio.

Chapter 4 covers the design and analysis of a novel Multiple Inputs/Multiple Outputs (MIMO) indoor communication antenna system with a graphene-based 1x2 RMPA array for THz communications channel capacity enhancement. First, the interesting features of the graphene load are discussed by varying its chemical potential ( $\mu_c$ ) from 0 to 1.5 eV. The impact of the graphene load and the PCs on the performance of the proposed antenna array were studied for different kinds of substrates that contain different air holes in square and triangular lattices [16]. Next, MIMO antenna array is designed in a common indoor communication scenario and analyzed using three different approaches such as homogeneous, periodic PCs, and optimized PCs [17]. Finally, the total path loss and channel capacity were numerically calculated for different system configurations and then compared with other results in the literature.

The conclusion of this thesis and proposals for further work are presented at the end of Chapter 4, respectively.

# Chapter 1

## Terahertz Antenna Array Based on Photonic Band Gap Structures: State of the Art

### 1.1 Introduction

Beyond the traditional application, the THz band is a key solution to potential wireless networking. Due to the exponential rise in population, big data is growing rapidly, requiring devices capable of transmitting and receiving the highest data rates possible at low power consumption. In this chapter, an overview of THz technology is provided by covering its main features, applications and corresponding challenges and then the importance of microstrip antenna array in this technology is addressed. Finally, different antenna array configurations based on PCs are studied and discussed.

### 1.2 Terahertz Technology

In most cases, the device bandwidth is around 10 % of its operating frequency [1]. Therefore, the large available bandwidths make high frequencies very attractive for

high data rate communication and sensing applications. According to the International Telecommunication Union (ITU), the THz frequency band is located between microwave and far-infrared and generally covers frequencies between 0.1 and 10 THz as shown in Fig.1.1.

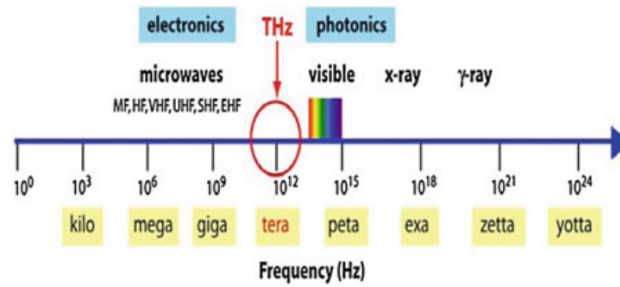


**Figure 1.1** – THz band location in the frequency spectrum [1].

The far-infrared region is essential due to its outstanding chemical and physical properties, but due to the lack of important devices such as interconnectors, detectors and powerful sources, this region has remained untouched for a long time by many researchers and has been named the “terahertz band gap”. Over the past decade, semiconductor technology has experienced rapid growth resulting in a significant impact on research into this band gap. With the continuous progress of research, the THz frequency band has many potential applications in biology/medicine, explosive and concealed weapon detection, earth and space science, imaging, time-domain spectroscopy, imaging of concealed items, semiconductor wafer inspection, agriculture and quality control. The wide application field of the THz band is because of its exceptional features, which are highlighted as follows [18]:

1. Penetration: With different levels of attenuation, a THz wave can pass through the different materials.
2. Resolution: Resolution in the THz range is much better than that in the microwave region, because image resolution increases as the wavelength decreases. The wavelength decreases at higher frequencies such as THz frequencies.
3. Spectroscopy: Many gaseous and solid materials show distinct spectral features in the 0.5-3.0 THz region, which can be utilized for detection.

4. Non-ionization: THz radiation shows a low ionization effect on the biological tissues, because of low-power levels in the microwatt range.
5. Scattering: The scattering is low in the THz band compared to the light wave, because it is inversely proportional to the wavelength.
6. Intensity: Wave collimation is easier in the THz band compared to the microwave region.

It should be taken into account that the characteristics of the device change at higher operating frequencies, so it is recommended to conduct an analysis of the various components of the THz wireless communication system. Due to the fact that this frequency band lies between two already well-explored regimes spectrum, it is feasible to use all electronics and photonic routes in the THz spectrum [19]. Although the THz frequency band offers some advantages, it also has some disadvantages compared to microwave and far-infrared. Therefore, the different advantages of this frequency band are highlighted as follows:

1. THz communications provide high bandwidth capacity compared to microwave.
2. THz communications provide high-capacity networks, secure communications, and protection against channel jamming attacks.
3. THz communications are inherently more directional than microwave or millimeter because of less free-space wave diffraction.
4. THz has a smaller signal attenuation compared to InfraRed (IR) under certain weather conditions such as fog.
5. At THz, the scintillation effect is smaller than that of IR. This effect is due to time-varying fluctuations in the real refractive index of the atmospheric path.
6. THz communication is a potential alternative to the last-mile and first-mile issues. These issues refer to the establishment of local, wide-area, multi-user wireless connections for high-speed networks, such as fiber optics.

7. Recent developments require new advanced modulation techniques like Orthogonal Frequency Division Multiplexing (OFDM) and coherent communications, but significant advances in data rate are slow in IR wireless communication systems compared to THz.

Despite all these facts, THz communication suffers from high atmospheric path loss. This loss is considered as a major obstacle resulting from different atmospheric conditions as shown in Fig.1.2.

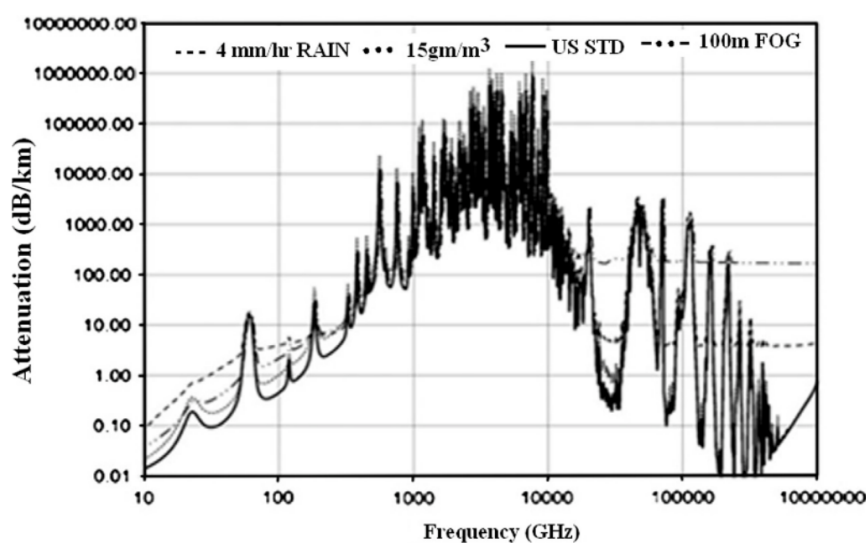


**Figure 1.2** – Atmospheric path loss in different atmospheric conditions over a wide frequency range [1].

From Fig.1.2, it is noted that as the frequency increases, the signal attenuation increases. The dashed line in the legend shows the signal attenuation in the 4 mm/h in rainy weather at sea level. The dotted line shows the water attenuation level in the soil at 15 gm/m<sup>3</sup>. The solid line shows the US standard weather conditions (59 % relative humidity), whereas, the dash-dot line shows the visibility at 100 meters in fog. As seen from Fig.1.2, the attenuation in a humid atmosphere is the main problem in THz communications, nonetheless, this attenuation is relatively smaller than the attenuation in the IR region. THz band encounters a higher degree of loss compared to the microwave region, however, the loss in the THz band is limited up to 1 THz. At 240 GHz ( for THz wave ), the average foggy attenuation is approximately

8  $dB/km$ . This value is less than the 200  $dB/km$  experienced by a 1.5  $\mu m$  wavelength infrared signal. Therefore, in extreme weather conditions, THz communication is a good selection against IR. However, THz propagation is related to the state of the atmosphere and the shift in attenuation frequency because of the change in temperature, altitude, etc. To overcome such situations, a robust network architecture is needed, otherwise, THz communication will still be restricted to either indoor wireless or inter-satellite connectivity only [20, 21]. Fortunately, there are several windows of low atmospheric attenuation in the THz range, within which wireless communications can be made. These windows showed low atmospheric loss below 100  $dB/km$  and could be located around 300, 350, 410, 650, and 850 GHz [22]. These windows can be used for short range wireless communications. Above 16  $km$ , which is referred to as inter-satellite communications, the attenuation is not significant since the effect of humidity is negligible.

The signal attenuation in the THz range is greater than in a conventional microwave link although there are a number of low attenuation windows below 1 THz. To combat this restriction, wireless communication channels must be optimized using different software and hardware parameters. Therefore, among the hardware equipment, further development and research are required in the domain of high-power sources, low-loss interconnects, sensitive detectors and high-gain antennas. This will support the creation of a low-profile, lightweight and cheap THz wireless communication network. THz has remained a band gap due to the lack of high energy sources, however, with the growth in science and engineering, different THz sources above 1 THz have been reported, among them the optical photo-mixing technique where two laser offset frequencies are merged to generate a THz wave, but this technique can not be applied to wireless communication, since a wireless communication needs to be established in lower attenuation windows of less than 1 THz [23, 24]. Nevertheless, the THz wave can be generated with the help of Backward Wave Oscillator (BWO) below than 1 THz, but due to the strong magnetic fields, the size of this device is overly massive [25]. Furthermore, there are numerous devices capable of generating a low-power THz signal as a THz system requires miniature and integrated devices

such as semiconductor devices. THz semiconductor devices are still being improved in the industry and will clearly eliminate the terahertz band gap. These devices are inherently low-power devices that have been used in microwaves and millimeters which encompass Impact Ionization Avalanche Transit-Time (IMPATT), Schottky diode, Tunnel diode, and Gunn diode [26, 27, 28, 29, 30, 31, 32, 33, 34, 35, 36, 37, 38]. However, due to manufacturing limitations, they cannot be used at the THz band frequency. Various types of sources below 1 THz were studied, and it was observed that as operating frequency increases, the output power decreases. The difference in the output of various semiconductor sources at THz band frequency is shown in Fig.1.3 [29]. In traditional sources such as IMPATT diode, Gunn Diode, Tunnel Diode, and Schottky Diode, the output power is approximately 0.01 mW at 1 THz. For a better generation of THz signal, the Quantum Cascade Laser (QCL) among the semiconductor sources can produce a power up to 90 mW, but it works above 1 THz, to make it works below 1 THz where the THz link is feasible, further design modifications are needed [33, 39, 40]. Moreover, microwave frequency multiplication to generate THz signal has been widely used. This technique uses solid-state devices to produce low-frequency outputs and the carrier frequency is shifted to a larger value by a frequency multiplier [35, 41, 42]. In addition, a solid-state wideband mixer is also designed for 835- 900 GHz [26, 38]. In fact, the use of solid-state instruments as a source for 580 GHz scanning radars has been studied [43]. In the frequency multiplication technique, it is feasible to convert the signal to the intermediate frequency level and then recover the baseband signal [35, 43]. Essentially, by applying the heterodyne principle, it becomes possible to receive a baseband signal using a THz link.

As mentioned before, the major constraint to THz communications is the atmospheric loss. Therefore, high-power transmitters and efficient detectors must be improved to overcome such constraint. However, only a certain amount of the source power can be raised where the outpower of most sources is limited to milliwatt scale. Because of the source's limitation, the function of the antenna in wireless communication is growing. Due to power limitations, the antenna gain in a THz network

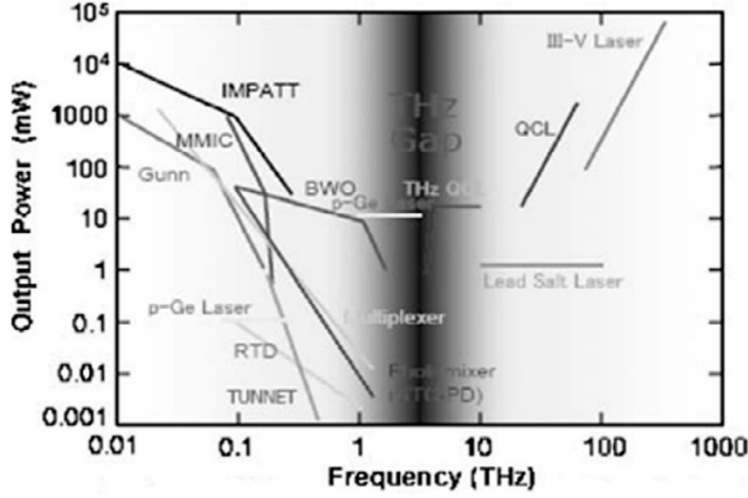


**Figure 1.3** – Power performances of different sources at THz frequencies [1].

must be increased in order to extend the signal over a longer range. Antennas are fundamental components in wireless communication systems, they also have applications in imaging and sensing. Their functionality can be comprehended with the aid of Friis equation and Brown analysis [44, 45]. The power supplied to the receiving antenna load is given by:

$$P_{out} = P_{in} \left( \frac{\lambda}{4\pi d} \right)^2 G_t G_r F_r(\theta_r, \phi_r) F_t(\theta_t, \phi_t) \tau \epsilon_p \quad (1.1)$$

where  $P_{out}$  is the output power.  $P_{in}$  is the input power of the transmitting antenna.  $G_t$  and  $G_r$  are the gain of the transmitting and receiving antenna, respectively.  $d$  is the space between the transmitting and receiving antenna.  $\lambda$  is the wavelength.  $\epsilon_p$  is the polarization coupling efficiency.  $\tau$  is the path power transmission factor.  $F$  is a function of the normalized intensity pattern.  $\theta$  and  $\phi$  are the angles at either the transmitter or receiver in a spherical coordinate system. Based on Eq.(1.1), it is observed that the output power to the load is directly proportional to the gain and inversely proportional to the distance between the receiving and transmitting antenna. Therefore, at THz communication, it is desirable to increase the antenna gain to cover the longer distance and the constraint of the source power  $P_{in}$ . The gain and directivity of the antenna are related as shown in Eq.(1.2) [46], where it is



noted that directivity is proportional to gain.

$$G_t = \eta D_t \quad (1.2)$$

where  $\eta$  is the antenna efficiency (or radiation efficiency), which can be written as the ratio of the radiated power to the input power of the antenna as:

$$\eta = \frac{P_{rad}}{P_{in}} \quad (1.3)$$

To penetrate the hostile environmental influence, the THz link must be directional. Therefore, highly directivity antennas are needed to overcome atmospheric attenuation and path losses in THz communications. To achieve this goal, different THz antennas have been studied and developed by many researchers including the corner cube reflector antenna [47, 48], the corner reflector array antenna [49], Bow-Tie in bi-conical shape antenna [50, 51], and a twin slot antenna [52]. In addition, lens antennas were also studied in [53, 54, 55], however, as the length increases, the antenna compactness is impacted and it becomes difficult to introduce all types of primary sources into the lens. These types of antennas are costly and sensitive to environmental conditions. Moreover, they incur relatively large dielectric losses due to the high relative material usage resulting in shock waves, which are created between the substrate and the permittivity of the air. To overcome the limitations of shock waves and increase directivity, materials with low permittivity can be used, but this will directly increase the size of the antenna [56].

Nevertheless, the aforementioned antennas are not equally suitable for the communication system for several reasons including complexity, cost, larger size, poor impedance matching, substrate mode generation, complex fabrication, inability to integrate into the System-on-Chip (SoC) design for the wireless communication in THz band. The waveguide horn and the planar antennas are the two most suitable candidates for establishing wireless communications at THz [1, 35]. The waveguide horn antennas offer low loss and excellent performance, but their key issue are not

compatible with the SoC design conception to operate at higher frequencies. On the other hand, planar antennas offer a greater potential and provide certain benefits such as low profile, low cost, design simplicity and ease of manufacture, furthermore, they have integration compatibility with other planar device [57]. However, the main drawbacks of this type of antenna are the low gain and directivity which cannot be sufficient to meet the requirements. Therefore, further developments and approaches are required to improve the directivity of this type of antenna. For this reason, several THz microstrip antennas have been studied and reported over recent years [58, 59, 60, 61, 62, 63]. Their performance can be improved by using an array of antennas instead of a single patch or by diminishing the conductor and substrate loss. However, in any type of antenna, the loss of the conductor still exists since the conductor loss is related to the metallic radiator. Also, the substrate loss or dielectric loss is linked to the relative dielectric permittivity of the substrate material, this loss can be minimized for better substrate material selection. A low permittivity substrate can be used in the THz antenna development, however, a low permittivity substrate increases the antenna size. Basically, substrate loss is a major challenge for millimeter and sub-millimeter wave patch antennas [64].

Instead of using the conventional substrate, the photonic band gap layer as a substrate of the microstrip patch antenna is used in order to decrease the effective permittivity of the material in which surface wave losses can be reduced, thereby improving the performance of the antenna. In the development of the microwave and the millimeter-wave antenna, this approach was employed. The primary radiation characteristics of this type of antenna at THz frequency are reported in [65, 66]. In addition, another approach to address this challenge is to use a multilayered substrate in contrast to the conventional substrate. This approach has been extensively studied at microwave and millimeter waves in order to increase both antenna directivity and bandwidth [67]. In THz antenna design, it has been reported within this approach, the antenna achieved a 34 % -10 dB impedance bandwidth improvement [67].

Besides the microstrip patch antenna, the planar patch array antenna (Yagi-Uda type structure) can also be used in THz communications [68, 69]. This type of antenna

provides a high gain and front-to-back ( $F/B$ ) ratio. However, this type of antenna has a limited frequency range and requires a large number of elements, which may increase the size of the antenna.

Therefore, THz communication strives to provide low-cost, low-profile, lightweight and high-performance antennas to overcome the narrow bandwidth of wireless communication networks and high path loss. Hence, further improvements and developments are needed for effective and efficient THz antennas.

### 1.3 Microstrip Patch Antenna Array

Antenna design has become one of the most active areas in communications research over the years. Antennas are essential components of a wireless communication system that provide a lower-cost alternative and a flexible way to communicate which are mainly used to transmit and receive nonionizing Electromagnetic (EM) fields [70]. One common type of antenna is microstrip patch antenna. Microstrip antennas are currently gaining importance as the strongest technology trend due to their advantages such as low profile, low cost, conformability, ease of design and manufacturing [71, 72]. Microstrip patch antenna is a single-layer design, its simplest form encompasses four major parts: ground plane, substrate, feeding line and radiating patch as illustrated in Fig.1.4.

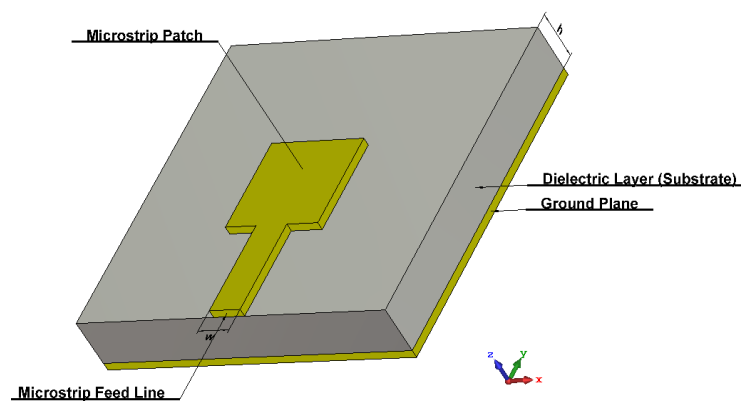


**Figure 1.4** – The structure of a microstrip patch antenna.

The radiating patch comes in various shapes like square, rectangular, circular, triangular, and other irregular shapes too that can be fed by various feeding techniques [73], however, the most commonly used configurations are circular and rectangular. The ground plane and the radiating patch are usually made from the same conducting material of high conductivity such as copper, nickel or gold. The substrate material and its corresponding thickness play a major role in determining the dimensions of the antenna as well as providing mechanical support between the ground plane and the patch. To achieve a good response, a variety of substrates can be employed while the dielectric constants are typically in the range of  $2.2 \leq \epsilon_r \leq 12$  [74]. To avoid surface waves excitation, the thickness of the dielectric substrate for the conventional microstrip antennas is usually in the range of  $0.003\lambda_0 \leq h \leq 0.05\lambda_0$  [75]. A substrate with a lower dielectric constant can provide greater bandwidth and better efficiency but at the cost of a larger element size. However, in some applications, smaller-sized antennas are needed. For a better selection, a thick substrate with a high dielectric constant is highly desirable, but in this case, larger losses appear such as surface waves which degrade the antenna performance resulting in low gain, narrow bandwidth and low efficiency [74, 75]. These drawbacks can be overcome by constructing multiple patches forming array configurations.

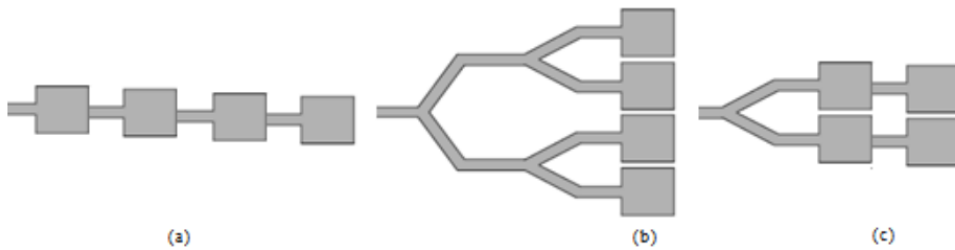


**Figure 1.5** – Feeding method: (a) Series feed (b) Corporate feed (c) Series-Corporate feed.

Here term array stands for geometrical and electrical arrangements of patch elements. As we increase the number of patch elements to form an array, improvement in performance is observed depending on the feeding network [76]. In the microstrip

array, radiating patches can be fed by a single line or multiple lines in a feed network arrangement. Therefore, feeding methods are categorized as follows: series feed network, corporate feed network and corporate-series feed network [77, 78] as shown in Fig.1.5. The corporate feed is widely used in parallel feed configuration, which has a single input port and multiple feed lines in parallel with the output port. Each of these feed lines terminates at an individual radiated patch. This technique has greater control over the feed of each element and is ideal for scanning phased arrays and multi-beam arrays. The phase of each element can be controlled using phase shifters while the amplitude can be adjusted using either amplifiers or attenuators [79, 80]. T-Junction power divider is a common technique used mainly in the configuration of the array antenna, this technique provides that the incident power is equally split of  $2k$  (where  $k = 2; 4; 8; 16. \dots$ ) and distributed to the individual antenna elements. This can be achieved by using either quarter-wavelength impedance transformers or tapered lines [78, 80, 81]. The series feed technique usually has a continuous transmission line, through which a small proportion of the power is gradually coupled to the individual element along the line, which may also constitute a traveling wave array if the feed line is terminated in a matching load [80, 82, 83, 84]. To feed the radiating patches and achieve an input impedance of  $50 \Omega$ , microstrip transmission line Eqs.(1.4) and (1.5) are used and represented in [85] by:

$$\frac{W}{h} = \frac{8e^A}{e^{2A} - 2} \quad (1.4)$$

for  $\frac{W}{h} < 2$  where

$$A = \frac{Z_0}{60} \sqrt{\frac{\epsilon_{reff} + 1}{2}} + \frac{\epsilon_{reff} - 1}{\epsilon_{reff} + 1} \left( 0.23 + \frac{0.11}{\epsilon_{reff}} \right)$$

$$\frac{W}{h} = \frac{2}{\Pi} \left[ B - 1 - \ln(2B - 1) + \frac{\epsilon_{reff} - 1}{2\epsilon_{reff}} \left\{ \ln(B - 1) + 0.39 - \frac{0.61}{\epsilon_{reff}} \right\} \right] \quad (1.5)$$

for  $\frac{W}{h} > 2$  where

$$B = \frac{377\Pi}{2Z_0\sqrt{\epsilon_{reff}}}$$

where  $\epsilon_{ref}$  is the effective dielectric constant and  $Z_0$  is the characteristics impedance of the microstrip transmission line of  $50 \Omega$ .  $W$  is the width of the feed line and  $h$  is the substrate thickness. The ratio  $\frac{W}{h}$  is determined according to the equations above.

Although the array configuration provides improved performance compared to a single patch antenna, however, surface wave excitation remains a major factor that affects microstrip antenna array performance. The excitation of surface waves leads to a mutual coupling effect between the adjacent elements of the array. This effect becomes progressively worse at higher operating frequencies, higher substrate permittivity and thicknesses resulting in blind spots and confinement of the angular scanning region in the array [84, 86, 87]. Mutual coupling can be reduced by widening the gap between the elements, but undesirable grating lobes appear [88]. A variety of approaches were described by many researchers to reduce mutual coupling in an array such as Defected Ground Structures (DGS) [89, 90], High Impedance Surfaces (HIS) [91], Split Ring Resonators (SRR) [92] and Photonic Crystals (PCs) [93]. Thus, incorporating Photonic Band Gap (PBG) structures in between the array patches is a hot research topic in the antenna community.

## 1.4 Photonic Crystals

PCs are one of the fastest materials growing sub-fields in optical physics. PCs are materials patterned with a periodicity in dielectric constant or metallic cells, which include various types such as 1D, 2D, and 3D structures depending on their periodic arrangements, and generally possessing ranges of forbidden frequencies called PBG in which light and electromagnetic waves cannot propagate through the structure [94]. Fig.1.6 represents the classification of the PCs based on the dielectric periodicity [95].

The first artificial PCs with a full PBG were first proposed by Yablonovitch in 1991 [96]. The "Yablonovite structure" was produced by drilling an array of holes in plexiglass between 13 and 15 GHz. This first demonstration fascinated researchers and sparked a race for the first PCs to operate at shorter wavelengths [97]. 2D and

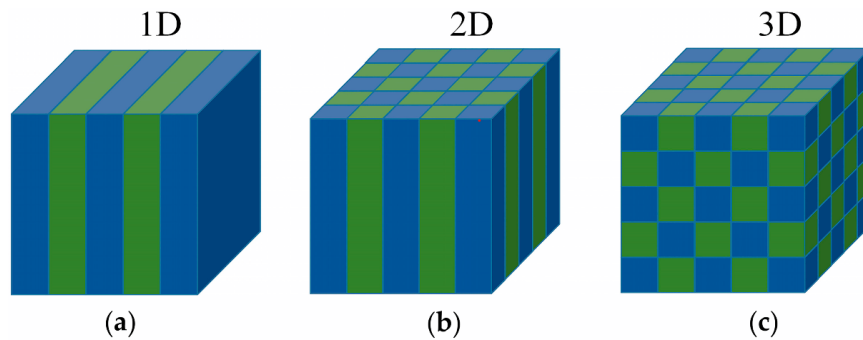


**Figure 1.6** – Classification of **PCs** structures.

**3D PCs** are an important extension of **1D PCs**, however, **2D PCs** have been more extensively examined compared to their **3D** counterparts because they are much easier to design and fabricate. Although their band gap is incomplete, **2D PCs** exhibit most of the properties of their **3D** counterparts [98].

**2D PCs** are formed from air holes having circular, hexagonal, triangular and elliptical shapes which are drilled in the dielectric substrate. The properties of **2D PCs** are essentially defined by the parameters  $a$ ,  $r$  and  $\epsilon$ , where  $a$  is the lattice constant and  $r$  is the radius, while  $\epsilon$  is the permittivity of the substrate. The type of lattice comes in different shapes, but the square lattice and the hexagonal lattice (sometimes called the triangular lattice) are the most popular lattices in **2D PCs** design because they result in large absolute **PBGs** which further suppress surface waves [99, 100]. Overall, the **PCs** structures have been proposed by many researchers at different frequencies for developing high-performance microstrip patch antennas.

## 1.5 Design of Terahertz Microstrip Antenna Arrays Based on Photonic Crystals

In this section, different antenna array configurations including 1x2, 1x4 and 2x8 Rectangular Microstrip Patch Antenna (**RMPA**) arrays are designed and analyzed using **PCs** for improved gain performance and high radiation characteristics compared to the ones that are designed based on the homogeneous substrate in the frequency

range of 0.25-0.55 THz. The design of the antenna arrays based on the homogeneous substrate and the PCs structures are made by using the designed single element RMPA as the basic building element and then they were fed by the parallel feeding structure. The designed antenna arrays were simulated using CST Microwave Studio software and validated with the aid of Ansys HFSS simulator. For high radiation characteristics, the proposed antenna arrays resonated around 0.35 THz which is a low loss frequency window in the THz band. The main results were obtained in terms of the gain, bandwidth, return loss and directivity.

### 1.5.1 Design of a Single Patch Based on Photonic Crystals

The proposed antenna array design was developed from a single element patch to a 16-element patch array antenna in order to increase the gain and perform various functions which would be difficult to do with a single element RMPA. Therefore, designing an antenna array with multiple patches is related to determining the dimension of a single patch. The single patch antenna is designed based on the PCs that are embedded in the substrate with a dielectric constant of 2.7 and loss tangent of 0.002 whose thickness is 84.97  $\mu m$ , however, the air holes have a lattice constant and radius of 124.45  $\mu m$  and 26.19  $\mu m$ , respectively. So, the dimensions of the square unit cell are 124.45x124.15  $\mu m^2$ , where the feed line, radiating patch and ground plane are made of copper of thickness 21.65  $\mu m$ , respectively. In THz and microwave frequency generally, the permittivity has a main role in determining microstrip antenna geometry aspects. The design of a single element RMPA is initiated by determining its patch dimension, where  $W_p$  and  $L_p$  were initially calculated using Eqs.(1.6) and (1.7) [101].

$$W_p = \frac{c}{2f_r} \sqrt{\frac{2}{\epsilon_{reff} + 1}} \quad (1.6)$$

$$L_p = \frac{c}{2f_r \sqrt{\epsilon_{reff}}} - 2\Delta l \quad (1.7)$$



where

$$\Delta l = 0.412h \frac{(\epsilon_{reff} + 0.3)\left(\frac{W_p}{h} + 0.264\right)}{(\epsilon_{reff} - 0.258)\left(\frac{W_p}{h} + 0.8\right)} \quad (1.8)$$

where  $c$  is the speed of light in free space,  $f_r$  and  $h$  are the resonant frequency and substrate thickness, respectively.  $\epsilon_{reff}$  is the effective dielectric constant provided that  $\epsilon_{reff} > 0.258$ . In the case of the homogeneous substrate, the effective permittivity  $\epsilon_{reff}$  is equal to the relative permittivity  $\epsilon_r$  of the substrate which is 2.7. Therefore, the calculated width and length of the rectangular radiating patch based on the homogeneous substrate are equal to  $369 \mu m$  and  $184 \mu m$ , respectively. After employing the PBG substrate, the dielectric permittivity of the substrate is reduced which is taken as the effective permittivity  $\epsilon_{reff}$ , and the value of  $\epsilon_{reff}$  is found via CST Microwave Studio as 2.11. Therefore, the calculated width and length of the rectangular radiating patch based on the PBG substrate are equal to  $344 \mu m$  and  $214 \mu m$ , respectively. Then, optimization of the calculated width and length of the single patch was performed using the CST Microwave Studio tool. The augmented dimension of the microstrip feed line is  $25.13 \mu m \times 105 \mu m$ . Finally, the configuration of the single patch antenna based on the PBG structure is shown in Fig.1.7.

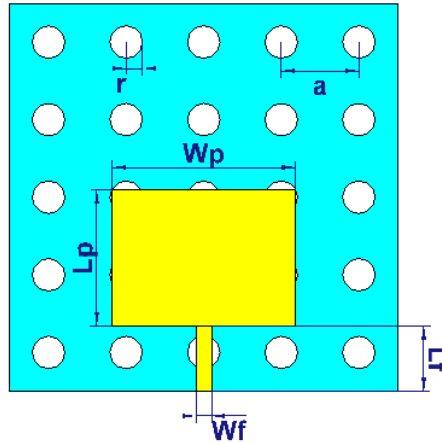


**Figure 1.7** – The geometry of the single element RMPA based on PBG substrate.

### 1.5.2 Design of 1x2, 1x4 and 2x8 Rectangular Microstrip Patch Antenna Arrays Based on Photonic Crystals

To obtain enhanced performance over a single patch antenna and to observe the significance of the PBG substrate structure on the antenna arrays, the designed antenna arrays are assumed to resonate at the same resonant frequency around 0.35 THz, mounted on the same PBG substrate structure with the same dielectric constant, same thickness substrate, same PBG hole radius and PBG cylindrical distance as single element RMPA. Starting with the 1x2 RMPA array which is designed with the parallel feed arrangement based on the PBG substrate structure which consists of two similar patches with the same dimension as a single element antenna. After designing the 1x2 RMPA array, the design of the 1x4 RMPA array is made, which consists of four similar elements patches that can be fed by the parallel or the corporate feed technique, which has a single input port and multiple feed lines in parallel with the output port. Each of these feed lines is terminated at an individual radiating element and operates at the same frequency around 0.35 THz. The design specifications of the 1x4 RMPA array are similar to the 1x2 RMPA array. At the end of this modeling investigation, the number of radiating patches is increased from 4 to 16 in order to understand the trends for a large array size, which should outperform the 1x4 RMPA array in terms of gain and directivity. The design of the 2x8 RMPA array based on the PBG substrate structure contains 4 similar 1x4 RMPA arrays, that are fed by the parallel feed method with the same parameters. To compute the width  $W$  of the feed for an impedance of  $50 \Omega$  in the case of the homogeneous substrate, Eq.(1.5) is used where the calculated values of  $B$  and  $W$  were  $7.20$  and  $229.42 \mu m$ , respectively. Again, to compute the width  $W_f$  of the feed for an impedance of  $100 \Omega$  in the case of the homogeneous substrate, Eq.(1.4) is used where the calculated values of  $A$  and  $W_f$  were  $2.39$  and  $63.73 \mu m$ , respectively. Similarly, in the case of the PBG substrate, the widths  $W$  and  $W_f$  were found using Eqs.(1.5) and (1.4), respectively, where the final values were optimized. The feeding lines lengths provide impedance transformation and phase matching on the radiated patches in equal parts, where their values were optimized using Genetic algorithm in CST Microwave Studio for

both designed substrates. Finally, the summary results of the design calculations and optimizations for various parameters of the designed antenna arrays based on the homogeneous substrate and the PBG substrate structure are presented in Table 1.1 and Table 1.2, respectively. While, Fig.1.8, Fig.1.9 and Fig.1.10 show the geometry of the designed 1x2, 1x4 and 2x8 RMPA arrays based on the PBG substrate structure and the homogeneous substrate, respectively.

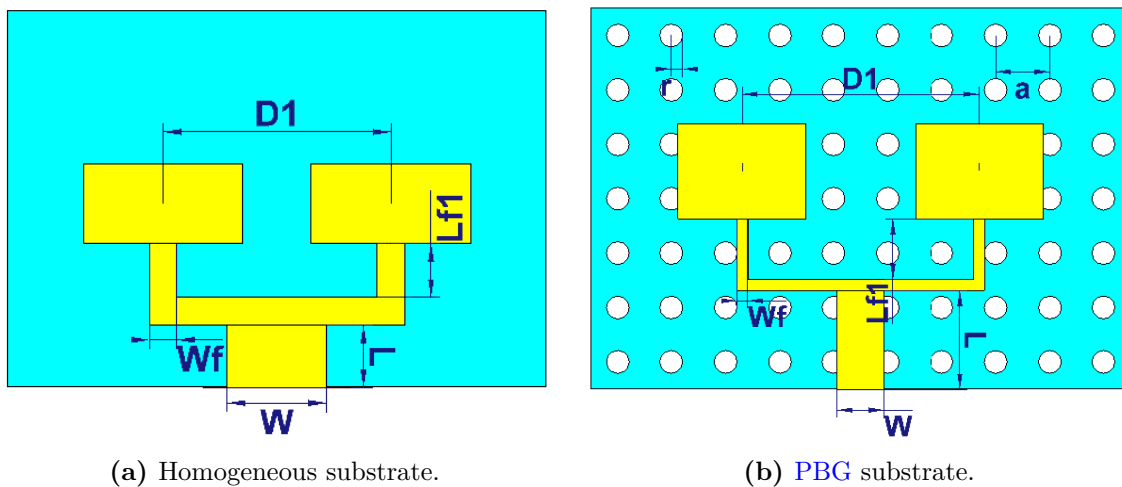


**Figure 1.8** – The geometry of the 1x2 RMPA array.

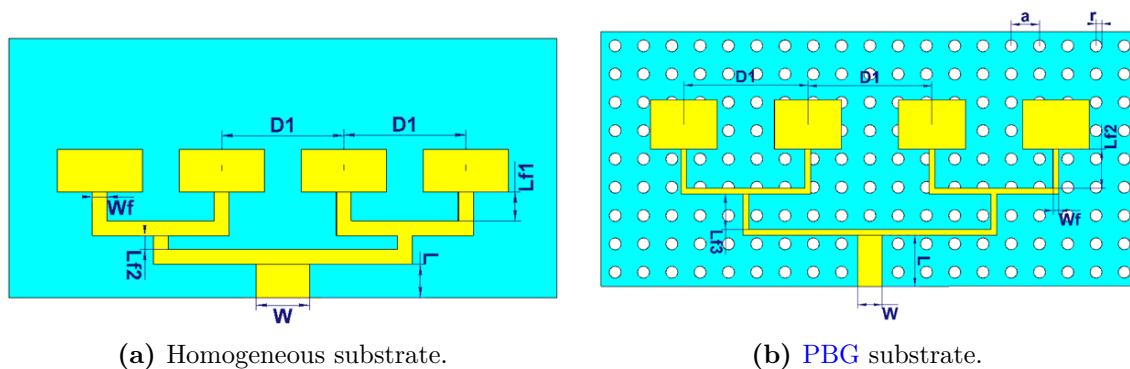
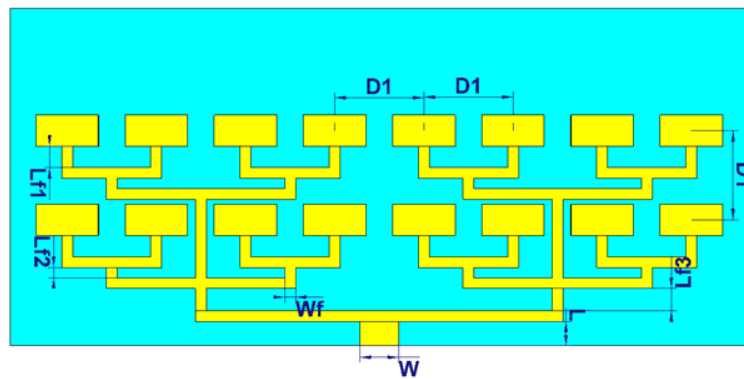


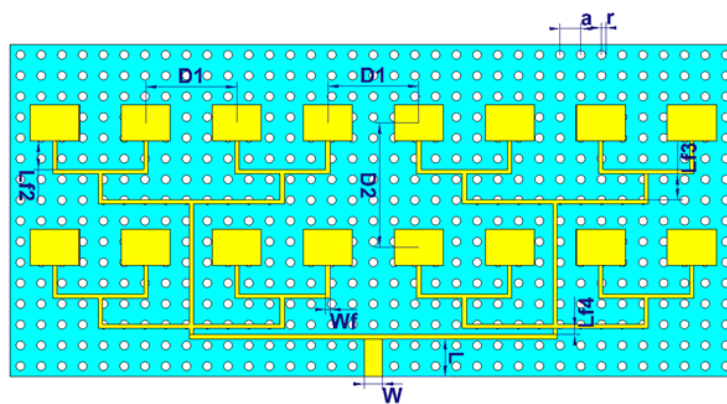
**Figure 1.9** – The geometry of the 1x4 RMPA array.

### 1.5.3 Simulated Results and Discussion

In order to observe the significance of the PBG substrate and the effect of adding many patches to form the antenna array, the designed single element RMPA, 1x2, 1x4 and



(a) Homogeneous substrate.



(b) PBG substrate.

**Figure 1.10** – The geometry of the 2x8 RMPA array.

2x8 RMPA arrays based on the homogeneous substrate and the PBG structure were simulated with the aid of the CST Microwave Studio simulator tool which is based on Finite Integration Technique (FIT) in the frequency range of 0.25-0.55 THz. Then, the comparison is done by analyzing different radiation characteristics like gain ( $dB$ ), bandwidth (GHz), return loss  $S_{11}$  ( $dB$ ) and directivity ( $dB_i$ ).

### Comparison of The Designed Single Element RMPA Based on The Homogeneous and The PBG Substrates

Here, single element RMPA based on the homogeneous and the PBG substrates is analyzed, the results are presented in Fig.1.11 and Fig.1.12, it is observed that the initial prototype antenna based on the homogeneous substrate provides at a resonant

**Table 1.1** – The calculated geometrical parameters of the proposed 1x2, 1x4 and 2x8 **RMPA** arrays based on the homogeneous substrate.

Parameters	Value( $\mu m$ )
Width of the patch ( $W_p$ )	369
Length of the patch ( $L_p$ )	184
Distance between the two patches ( $D_1$ )	526.27
Substrate thickness ( $h$ )	84.97
Ground thickness ( $T_g$ )	21.65
Width of 50 $\Omega$ microstrip ( $W$ )	229.42
Length of of 50 $\Omega$ microstrip ( $L$ )	144
Width of 100 $\Omega$ microstrip ( $W_f$ )	63.73
Length of of 100 $\Omega$ microstrip ( $L_{f1}$ )	125
Length of of 100 $\Omega$ microstrip ( $L_{f2}$ )	60
Length of of 100 $\Omega$ microstrip ( $L_{f3}$ )	130

**Table 1.2** – The optimized geometrical parameters of the proposed 1x2, 1x4 and 2x8 **RMPA** arrays based on the **PBG** substrate.

Parameters	Value( $\mu m$ )
Width of the patch ( $W_p$ )	293.94
Length of the patch ( $L_p$ )	217.73
Distance between the two patches ( $D_1$ )	545.64
Distance between the two patches ( $D_2$ )	747.07
Substrate thickness ( $h$ )	84.97
Ground thickness ( $T_g$ )	21.65
Lattice constant ( $a$ )	124.45
Cylinder radius ( $r$ )	26.19
Width of 50 $\Omega$ microstrip ( $W$ )	107.55
Length of of 50 $\Omega$ microstrip ( $L$ )	225.67
Width of 100 $\Omega$ microstrip ( $W_f$ )	25.13
Length of of 100 $\Omega$ microstrip ( $L_{f1}$ )	138.54
Length of of 100 $\Omega$ microstrip ( $L_{f2}$ )	171.46
Length of of 100 $\Omega$ microstrip ( $L_{f3}$ )	155.46
Length of of 100 $\Omega$ microstrip ( $L_{f4}$ )	37.62

frequency of 0.394 THz a return loss ( $S_{11} \leq -10$  dB) of -16.98 dB, absolute bandwidth of 78.4 GHz approximately and a gain of 6.17 dB. After implementing **PCs** in the substrate layer, it could be clearly observed that the single element **RMPA** based on the **PBG** substrate resonates at the frequency of 0.351 THz which is close to

the desired frequency of 0.35 THz and offers a minimal return loss ( $S_{11} \leq -10$  dB) of  $-35.95$  dB, a bandwidth of 44.03 GHz and a gain of 7.68 dB. Thus, there were remarkable enhancements after implementing the PBG structure in the gain and the return loss. However, the bandwidth did not show much improvement, this is mainly due to the resonant frequency. The antenna bandwidth is a certain percentage of its resonating frequency, therefore, an antenna with a high resonant frequency can offer high bandwidth. The resonant frequency is that frequency at which most of the power fed to the radiating patch occurs when the best impedance matching happens between the feed line and the radiating patch with very less power reflection. The reason why the resonance frequencies are different in the case of the homogeneous substrate versus the PBG substrate is due to the different dimensions of the radiating patches, feed lines as well as the employed substrate that needs more power consumption.

### Comparison of The Designed 1x2 RMPA Array Based on The Homogeneous and The PBG Substrates

Despite the fact that by using the PBG substrate, the single element RMPA had an improved performance over the one that is designed based on the homogeneous substrate, however, still with a low gain and narrow bandwidth which may limit its wide applications, hence the designed 1x2, 1x4 and 2x8 RMPA arrays based on the PBG substrate assumed to achieve higher radiation characteristics than the single element RMPA. The results of the designed 1x2 RMPA array based on the homogeneous and the PBG substrates are presented in Fig.1.11 and Fig.1.12. It is clearly noticed that the designed 1x2 RMPA based on the homogeneous substrate provides at a resonant frequency of 0.313 THz a return loss ( $S_{11} \leq -10$  dB) of  $-26.32$  dB, a bandwidth of 31.23 GHz and a gain of 8.78 dB. However, by using the PBG substrate, the designed 1x2 RMPA provides at a resonant frequency of 0.315 THz, a deeper return loss ( $S_{11} \leq -10$  dB) of  $-59.04$  dB, a wider bandwidth of 215.81 GHz and a higher gain of 9.72 dB. Thus, by using the array configuration with the PBG substrate, more enhancements in the gain, bandwidth and return loss are obtained while the resonant frequency remains near 0.35 THz.

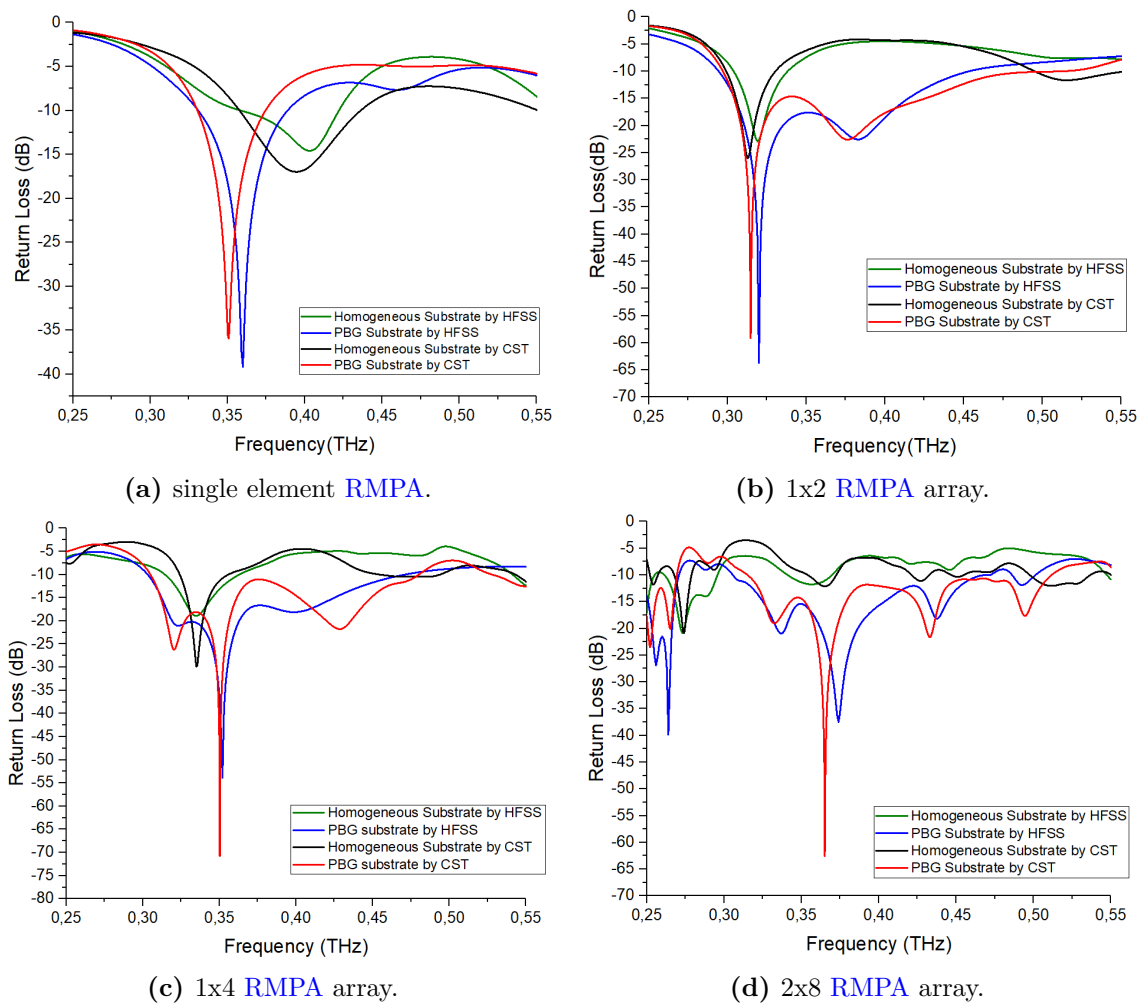


**Figure 1.11** – The return loss of the designed antennas.

### Comparison of The Designed 1x4 **RMPA** Array Based on The Homogeneous and The **PBG** Substrates

The results of the designed 1x4 **RMPA** array based on the homogeneous and the **PBG** substrates are presented in Fig.1.11 and Fig.1.12. It is observed that the increase in the number of patches leads to a higher gain, larger bandwidth and minimal return loss, while the resonate frequency remains around 0.35 THz, which means that the designed antenna arrays are functioning properly. So, the designed 1x4 **RMPA** array based on the homogeneous substrate resonates at the frequency of 0.335 THz and offers a return loss ( $S_{11} \leq -10$  dB) of -29.80 dB, a bandwidth of 31.58 GHz and

a gain of 12.03 *dB*. However, the designed 1x4 **RMPA** array based on the **PBG** substrate resonates exactly at the frequency of 0.35 THz, with a deeper return loss ( $S_{11} \leq -10$  dB) of -70.81 *dB*, a bandwidth of 175.10 GHz and a higher gain of 13.11 *dB*.

### Comparison of The Designed 2x8 **RMPA** Array Based on The Homogeneous and The **PBG** Substrates

The results of the designed 2x8 **RMPA** array based on the homogeneous and the **PBG** substrates are presented in Fig.1.11 and Fig.1.12. It is observed that both antenna arrays resonate at the same frequency of 0.365 THz, but the designed 2x8 **RMPA** array based on the **PBG** substrate exhibits higher performance with a minimal return loss ( $S_{11} \leq -10$  dB) of -62.56 *dB*, larger bandwidth of 196.57 GHz and higher gain of 16.75 *dB* compared to the one that is designed based on the homogeneous substrate which offers a return loss ( $S_{11} \leq -10$  dB) of -12.12 *dB*, narrow bandwidth of 18.52 GHz and gain of 14.13 *dB*.

The radiation characteristics such as the resonance frequency, return loss and bandwidth of the single element **RMPA**, 1x2, 1x4 and 2x8 **RMPA** arrays based on the homogeneous and **PBG** substrates are validated with the aid of Ansys **HFSS** simulator which is based on **FEM**. The obtained results were comparable and showed convergence. The small discrepancies between simulation results are due to the different simulation techniques.

In the case of the homogeneous substrate, it was found that as the number of the patches increases from 1 to 16, the gain increases proportionally, however, the designed 1x2, 1x4 and 2x8 **RMPA** arrays based on the homogeneous substrate showed very limited bandwidth and higher return loss, this is due to the fact that the size of the antenna became larger and, consequently, more losses such as dielectric and conductor losses appeared, moreover, surface waves excitation which leads to a mutual coupling effect between the adjacent elements of the array. This effect is very strong in **THz** band which contributes to the degradation of antenna array performance.



This effect is reduced after using of **PBG** substrate instead of the homogeneous substrate which improves the antenna array performance. Thus, taking into account the obtained results of the gain, bandwidth and return loss, it is clear that using the **PBG** substrate instead of the homogeneous substrate and increasing the number of patches forming an array at the same time leads to a better gain, larger bandwidth and high radiation characteristic which is really a powerful method for reducing surface waves and enhancing antenna performance in **THz**.

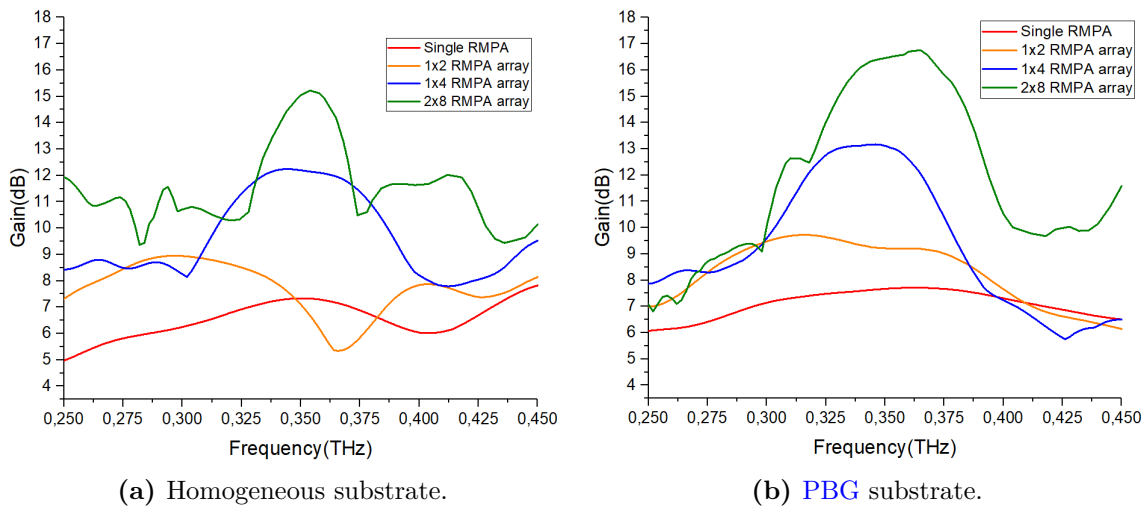


**Figure 1.12** – Gain performance of the designed single element **RMPA**, 1x2, 1x4, 2x8 **RMPA** arrays in the frequency range 0.25-0.45 THz.

Directivity is a fundamental of an antenna parameter. It is a measure of how directional an antenna radiation pattern is, so the main objective of an antenna design is to achieve the highest level of directivity and low side lobe level. Fig.1.13 shows the polar plot of both *E*-plane and *H*-plane from a single patch to the 16-element patches based on the homogeneous and **PBG** substrates. The directivity of the designed single **RMPA**, 1x2, 1x4 and 2x8 **RMPA** arrays based on the **PBG** substrate is 7.76 *dBi*, 9.87 *dBi*, 13.54 *dBi* and 17.40 *dBi*, respectively. Whereas, the directivity of the designed single **RMPA**, 1x2, 1x4 and 2x8 **RMPA** arrays based on the homogeneous substrate is 6.88 *dBi*, 9.16 *dBi*, 12.43 *dBi* and 14.62 *dBi*, respectively. It is clearly noticed that the directivity has improved a lot, this increase is due to the utilization of many patches and using the **PBG** substrate instead of the homogeneous

**Table 1.3** – Comparison of the proposed designed antenna arrays and previously reported designs.

	Antenna size ( $\mu m^2$ )	$f_r$ (THz)	$S_{11}$ (dB)	BW (GHz)	Gain (dB)	D (dBi)	Beamwidth $E$ -plane (degree)	Beamwidth $H$ -plane (degree)
1x2 array [102]	500 x 960	0.312	-51.24	22.68	5.6	-	57.1	86.5
4x4 array [103]	3000 x 2730	0.3	-	-	-	11.7	-	-
2x2 array [104]	2000 x 2000	0.6	-27.7	60	-	-	-	-
1x5 array [105]	780 x 2900	0.584	-21.29	6.35	9.95	11.7	-	-
Single RMPA (Homogeneous Substrate)	622.25 x 622.25	0.394	-16.98	78.04	6.17	6.88	77.5	92.2
Single RMPA (PBG Substrate)	622.25 x 622.25	0.351	-35.95	44.03	7.68	7.76	75	74.3
1x2 array (Homogeneous Substrate)	1244.50 x 871.15	0.313	-26.32	31.23	8.78	9.16	80.6	45.2
1x2 array (PBG Substrate)	1244.50 x 871.15	0.315	-59.04	215.81	9.72	9.87	72.6	49.9
1x4 array (Homogeneous Substrate)	2364.55 x 1120.05	0.335	-29.80	31.58	12.03	12.43	72.2	25.1
1x4 array (PBG Substrate)	2364.55 x 1120.05	0.35	-70.81	175.1	13.11	13.54	48.8	21.9
2x8 array (Homogeneous Substrate)	4355.75 x 1991.20	0.365	-12.12	18.52	14.13	14.62	29.5	11
2x8 array (PBG Substrate)	4355.75 x 1991.20	0.365	-62.56	196.57	16.75	17.40	23.3	11.8

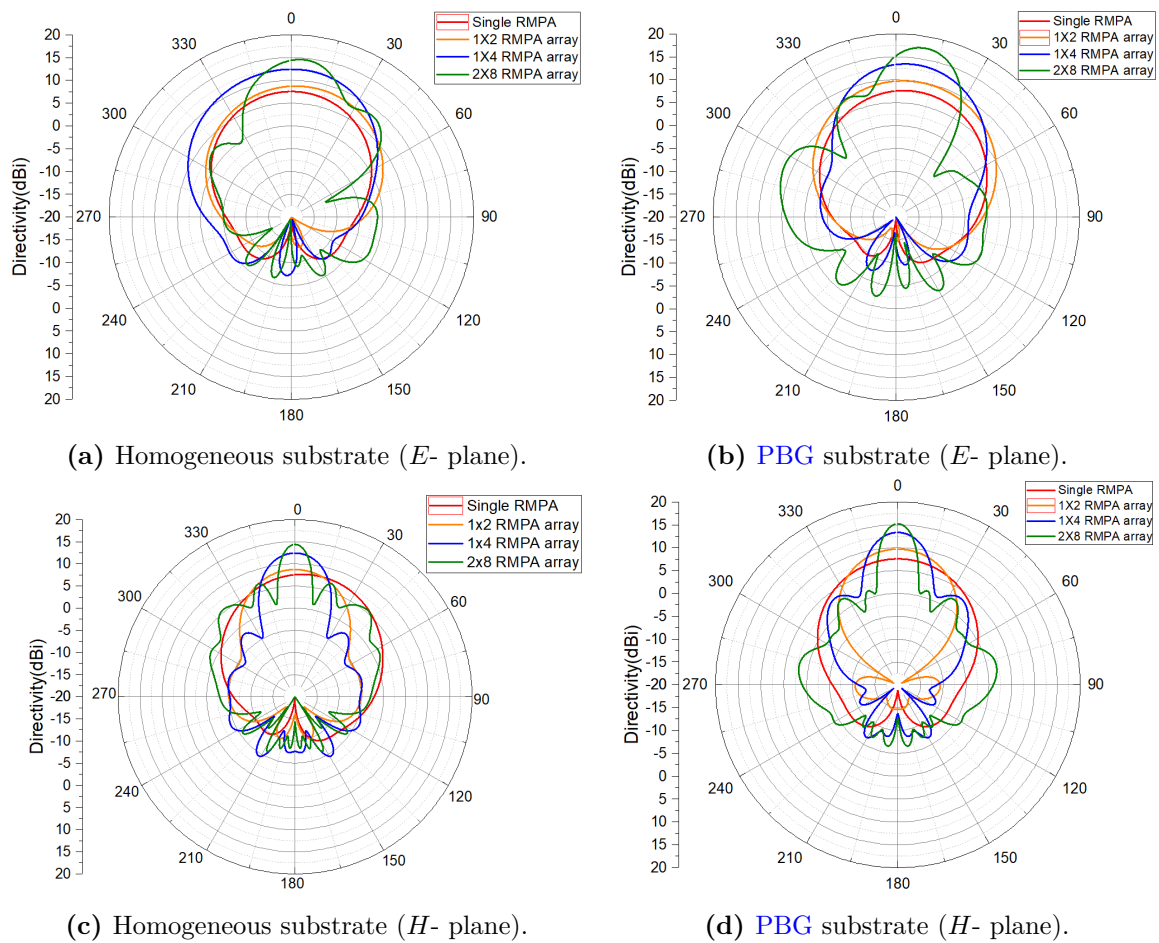


**Figure 1.13** – Polar plot of  $E$ - plane and  $H$ - plane for the designed single element RMPA, 1x2, 1x4 and 2x8 RMPA arrays.

substrate, the higher number of patches based on the PBG substrate leads to higher directivity.

The beamwidth of an antenna is the angular span of the main lobe of the antenna radiation pattern, which is the region of the pattern where most of the power is radiated. The beamwidth is usually measured in degrees relative to the  $E$  or  $H$  planes. There is an inverse relationship between antenna gain and beamwidth, a small beamwidth leads to a higher gain because the power transmission will increase in a certain direction with a smaller beamwidth. The beamwidth of the designed antennas is presented in the comparison Table 1.3.

The simulation results demonstrate that in order to increase antenna performance,

it is efficient to use the **PBG** substrate structure as a powerful technique and increase the number of patches at the same time, which yields to better performance compared to a homogeneous substrate in terms of the gain, bandwidth, return loss and directivity due to the suppression of the undesirable surface waves found in the homogeneous substrate. The radiation characteristics of the suggested single element **RMPA**, 1x2, 1x4 and 2x8 **RMPA** arrays are finally compared with the existing designs and illustrated in Table 1.3. It is evident that the radiation performance of the designed antenna arrays based on the **PBG** substrate is significantly enhanced as assumed compared to the ones that are designed based on the homogeneous substrate. These **THz** antenna arrays may have favorable applications in wireless communications, surveillance and medical diagnosis.

## 1.6 Summary

In this chapter, a literature review on the **THz** frequency band is demonstrated by involving its potential impact, key characteristics and corresponding challenges. Next, an introduction to **PCs** is demonstrated followed by simulation work using **CST** and **HFSS** where different **THz** antenna array configurations including 1x2, 1x4 and 2x8 **RMPA** arrays are designed and analyzed. The objective of this design was to enhance the radiation characteristics of these antenna arrays by suppressing undesirable surface waves that are found in the homogeneous substrate around 0.35 THz where there exists a low atmospheric attenuation window. This window has received great attention from many researchers in the fields of sensing and next-generation wireless communications. The main results showed that the designed antenna arrays based on the **PBG** substrate structure outperform the antenna arrays based on the homogeneous substrate in terms of gain, bandwidth, return loss and directivity. The designed 2x8 **RMPA** array based on the **PBG** substrate exhibited excellent performance improvement and achieved the highest directivity of 17.40 *dBi* compared to 14.62 *dBi*. Whereas, the designed 1x4, 1x2 **RMPA** arrays and single **RMPA** achieved directivity of 13.54 *dBi*, 9.87 *dBi* and 7.76 *dBi*, respectively, compared to the ones that are

---

designed based on the homogeneous substrate that achieved 12.43 *dBi*, 9.16 *dBi*, and 6.88 *dBi*, respectively. Thus, using the [PBG](#) substrate structure and increasing the number of patches improves the performance of the antenna at this band of frequency.

# Chapter 2

## Design and Analysis of Novel Microstrip Patch Antenna Arrays Based on Photonic Crystals in Terahertz

### 2.1 Introduction

Over the last decade, the THz band (0.1–10 THz) which is located between microwave and infrared frequencies has gained a lot of attention from many researchers. This is because of its inimitability characteristics such as high spectral resolution, less diffraction than the microwave, high bandwidth which leads to a high data rate that may reach several tens of Gbits per second and non-ionizing property [106, 107, 108, 109, 110]. In particular, this frequency band has various interesting applications in wireless communication [111], astronomy and space science [112], imaging applications [113], surveillance systems [114] and medical science [115]. Unfortunately, high path loss and signal attenuation are considered as the main issues in the THz band, due to the high atmospheric attenuation [116], which restricts the distance of THz communication. Because of these restrictions, THz communication

is generally limited to Personal Area Network (PAN) or Local Area Network (LAN) networks [117]. To overcome the impact of these losses, it is necessary now-a-day to increase the gain to use THz efficiently, which can be obtained by designing antennas.

In the THz band, antennas are critical components that are able to achieve high gain, a lot of researchers have discussed various types of antennas such as Yagi-Uda [118], Bow Tie [119], On-chip antenna [120], Wave Guide antennas [121], Leaky wave antenna [122] and Lens antenna [123], however, still the structure design and the size of the antenna the major concerns. To overtake those challenges, the planar antenna technology is suitable for a greater potential of integration. In THz, the demand of miniaturization for which the planar microstrip patch antennas are the best suited. Microstrip patch antennas are widely used for numerous applications such as satellite and mobile communications [124] due to their low cost, low profile, ease of design and fabrication and compatibility with Integrated Circuit (IC) technology such as THz System-on-Chip (SoC) technologies based on silicon. The use of such integrated on-chip antennas in silicon technology is promising in the THz band, which eliminates the need for sophisticated packaging such as external transmission line connections and therefore it may be more cost effective than the conventional packaging of an external antenna with transceivers in terms of packaging cost and compactness [125]. By using a silicon substrate, basically, two types of modes propagate: slow wave and quasi-TEM. However, increasing the substrate thickness of the conventional microstrip patch antenna introduces three main loss mechanisms resulting in deteriorated performance such as narrow bandwidth, low gain and radiation efficiency: conductor loss (ohmic loss), dielectric or substrate loss, and radiation loss. The conduction loss is mainly due to the low resistivity of the silicon substrate and the finite conductivity of the metallization. Dielectric losses occur mainly due to the substrate material with higher permittivity and larger loss tangent, these losses lead to serious surface wave loss in the form of sock waves at the substrate interface. Furthermore, the low resistivity and the high permittivity of the silicon form phenomena called dielectric relaxation frequency which has an effect on the cutoff frequency [126, 127, 128]. In addition to those losses, a factor that

contributes to the degradation of the microstrip patch antenna performance at such high frequencies and affects the conductivity of the utilized metals in the design is called surface roughness [129, 130, 131]. To overcome these difficulties and improve the performance of the microstrip patch antenna, many researchers have been investigated various techniques over the years. One suggested technique is to make changes in the ground plane which is called Defected Ground Structure (DGS) [132]. Other techniques are proposed by using an extra layer of a substrate, which is called the multilayer technique [104], or by using another structure above the patch which is called metamaterial [133], or by using multiple patches connected to an array [68], or by employing different periodic and non-periodic air holes in the substrate which is called PCs [12, 13, 14, 15, 64, 66, 125, 134, 135, 136].

The PBG structures are artificial periodic arrangements of a hollow air cylinder having a circular, hexagonal, triangular and elliptical shape which can be implanted in the dielectric substrate material. These structures can open a band gap, which is a frequency range for which the propagation of electromagnetic waves is prevented. There are different types such as 1D, 2D, or 3D structures, depending on their periodic arrangements. The hollow PBG structures which are 2D square lattices are mostly used, by surrounding the patch antenna with a square lattice of small metal pads through the ground plane, a substantial suppression of surface waves excited in the dielectric substrate can be noticed, which enhances the antenna radiation characteristics [137]. Another solution to those surface waves is to design a shorted annular structure in the radiator that provides a better surface waves reduction in comparison with the metallic patch [61, 92, 137, 138]. There are several transmission windows across the THz frequency band where the patch loss is comparatively small, one of these windows exists around 0.65 THz, where THz transmission could be established at this low loss frequency to enhance the wireless link reliability.

Previously, a silicon substance was employed as a substrate for a microstrip patch antenna design by Temmar et al. [125] which obtained a gain of 9.17 dB and bandwidth of 56 GHz at a resonance frequency of 0.63 THz. Also, an enhanced flexible THz microstrip patch antenna based on the modified silicon-air PC was reported in



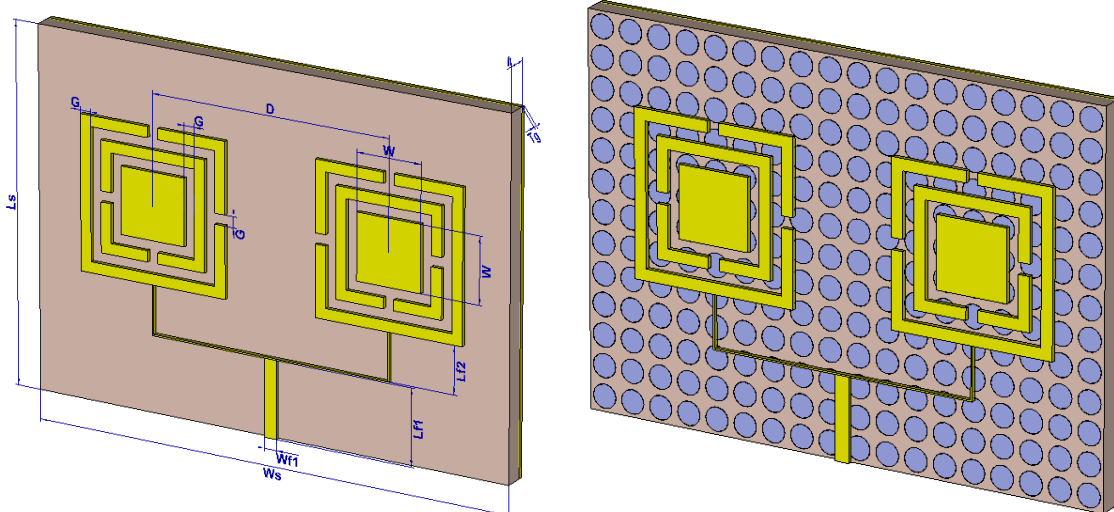
[135], which obtained a gain of 9.75  $dB$  and bandwidth of 47 GHz at a resonance frequency of 0.607 THz. In addition, Hocini et al. [134] designed a single microstrip patch antenna based on periodic and non-periodic PCs embedded in a polyimide substrate around 0.65 THz and showed promising results compared to the conventional one, where the gain and radiation efficiency were 8.95  $dB$ , 9.19  $dB$ , 89.31 % and 90.84 %, respectively, and the bandwidth was greater than 230 GHz. Subsequently, various THz microstrip antennas with different kinds of patches based on PCs for applications in the detection of explosives, wireless communications and characterizing materials have been reported in [117, 139, 140, 141]. However, it is noticed that the performance of the mentioned antennas is still with low gain and narrow bandwidth which limits their applications. To resolve these issues, two novel microstrip patch antenna array structures are designed and studied with different substrates based on PCs for a high gain, larger bandwidth and high radiation characteristics around 0.65 THz. This chapter is organized as the following: In Section 2.2, the performance of the proposed 1x2 microstrip patch antenna array based on PCs and the homogeneous substrates is analyzed around 0.65 THz. In Section 2.3, the performance of the proposed 2x2 microstrip patch antenna array is analyzed around 0.65 THz and it is being studied for different substrates including homogeneous, periodic and non-periodic PCs substrates. Finally, the summary of this chapter is done in Section 2.4.

## 2.2 Design and Analysis of a novel 1x2 Microstrip Patch Antenna Array based on Photonic Crystals

In this section, a novel microstrip patch antenna array is designed in the frequency range of 0.58-0.72 THz based on PCs substrate. The substrate is made of air cylinders embedded in a silicon dielectric material with high relative permittivity and electrical conductivity of 11.9 and 0.00025  $S/m$ , respectively. The air holes have a lattice

constant and the same radius of  $65.94 \mu m$  and  $26.38 \mu m$ , respectively, and the same thickness as the substrate thickness at  $47.1 \mu m$ . Hence, the dimensions of the square unit cell are  $65.94 \times 65.94 \mu m^2$ . The patch is made by using two ring resonators separated by two annular slots of width  $25.93 \mu m$ , each ring is opened loop in two different sides by creating a gap distance of  $25.93 \mu m$ . The dimensions of the inner resonating patch are  $159.90 \times 159.90 \mu m^2$  which is not directly coupled to the feed line. Hence, the antenna array is made by using two similar patches which can be fed by using the corporate feed technique [79]. The corporate feed technique is often utilized for compact array designs, this type of feed technique leads to constructional simplicity. However, due to feed radiation and feed resistive loss, unwanted radiation can be created which is called spurious radiation. In practice, experimental investigations have highlighted this problem in [142, 143], which is found that spurious radiation has a noticeable effect on the antenna array radiation pattern. The feed line is designed to distribute the power in equal parts and achieve the input impedance of  $50 \Omega$ . The width of the feed line  $W_{f1}$  is given by the formula [144]:

$$W_{f1} = \exp\left(\frac{Z_0}{87\sqrt{\epsilon_r + 1.41}}\right) \frac{0.8}{5.98h} \tag{2.1}$$



(a) Based on the homogeneous substrate. (b) Based on the PBG substrate.

**Figure 2.1** – The geometry of the proposed microstrip patch antenna array.

where  $Z_0$  is the impedance of the feed line,  $h$  and  $\epsilon_r$  are the height and the dielectric constant of the substrate material, respectively. Finally, the various geometrical parameters of the proposed antenna array based on **PCs** are shown in Table 2.1, while the structure is shown in Fig.2.1 below.

**Table 2.1** – Parameters of the proposed antenna array based on **PCs**.

Parameter	value ( $\mu m$ )
Length and width of outer ring	367.37
Length and Width of inner ring	263.64
Length and width of square patch ( $W$ )	159.90
Gap in outer and inner ring ( $G$ )	25.93
Annular slot width ( $G$ )	25.93
Substrate thickness ( $h$ )	47.1
Ground thickness ( $T_g$ )	10
Lattice constant ( $a$ )	65.94
Substrate width ( $W_s$ )	18 x $a$
Substrate length ( $L_s$ )	13 x $a$
Cylinder radius ( $r$ )	26.38
Length of feed line ( $L_{fl}$ )	115
Width of feed line ( $W_f$ )	30
Length of feed line ( $L_f$ )	185.08
Distance between the two resonator ( $D$ )	594.64

The simulation has been performed in the frequency range of 0.58-0.72 THz by using two different simulators, **CST** Microwave Studio based on **FIT** and Ansys **HFSS** based on **FEM** in order to check the accuracy of the proposed antenna array, and then the performance of the designed microstrip patch antenna array based on **PCs** and the homogeneous substrate is analyzed in terms of return loss ( $S_{11}$ ), bandwidth (GHz), **VSWR**, gain (dB), directivity (dBi), and radiation efficiency (%). To see the effect of **PCs** on the antenna array performance and to make a comparison, the same antenna array that is mounted on the homogeneous substrate has been used.

Fig.2.2 shows the magnitudes of the scattering parameter  $S_{11}$  for the proposed antenna array based on the homogeneous substrate and the **PBG** substrate structure using **CST** Microwave Studio and Ansys **HFSS**, which indicates that the antenna array based on the homogeneous substrate in the case of **CST** Microwave Studio resonates at the frequency of 0.606 THz with a return loss ( $S_{11} \leq -10$  dB) of -20.49

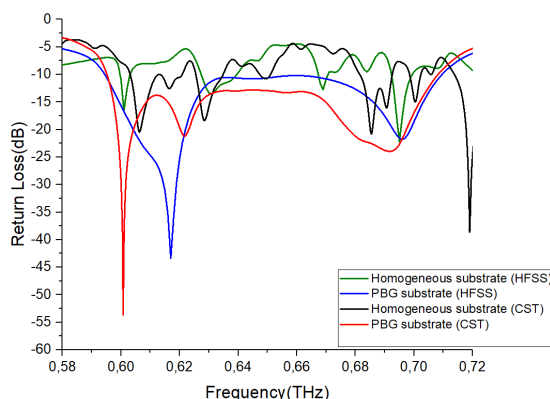


**Figure 2.2** – The magnitudes of the  $S_{11}$  parameter of the designed antenna array based on the homogeneous and the PBG substrates using CST Microwave Studio and Ansys HFSS.

$dB$  and narrow bandwidth of 9.78 GHz. Whereas, in the case of Ansys HFSS this antenna array resonates at the frequency of 0.601 THz with a return loss ( $S_{11} \leq -10$  dB) of  $-16.60$  dB and narrow bandwidth of 3.45 GHz. However, the same antenna array that is mounted on the PBG substrate resonates at the frequency of 0.601 THz with a deeper return loss ( $S_{11} \leq -10$  dB) of  $-53.66$  dB, and exhibits a larger bandwidth of 113.01 GHz in the case of CST Microwave Studio. Whereas, in the case of Ansys HFSS this antenna array resonates at the frequency of 0.617 THz with a minimal return loss ( $S_{11} \leq -10$  dB) of  $-43.4$  dB, and exhibits a larger bandwidth of 115.2 GHz. Due to the strong surface waves in the homogeneous substrate, the proposed antenna array showed a deteriorated performance like narrow bandwidth, however, after employing the PBG substrate huge enhancements in the performance were noticed.

Fig.2.3 shows the Voltage Standing Wave Ratio (VSWR) of the designed antenna array based on the PBG and the homogeneous substrates at their resonated frequencies using CST Microwave Studio and Ansys HFSS. In the case of the homogeneous substrate, the values of VSWR are 1.21 and 1.34 obtained by CST Microwave Studio and Ansys HFSS, respectively. However, the values of VSWR are close to unity for the case of the PBG substrate of 1.004 and 1.014 obtained by CST Microwave Studio and Ansys HFSS, respectively. The achieved values of VSWR are less than

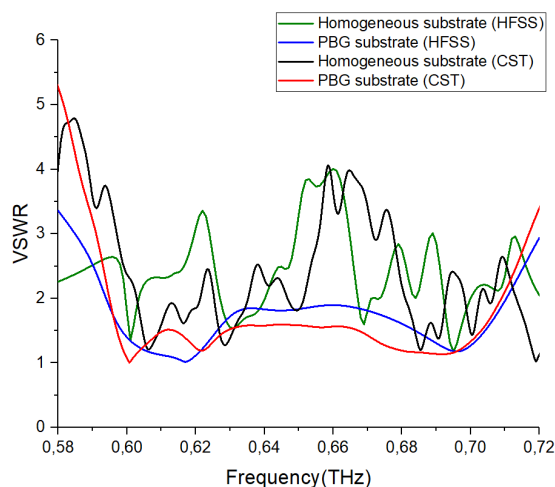


**Figure 2.3** – VSWR performance of the designed antenna array based on the homogeneous and the PBG substrates using CST Microwave Studio and Ansys HFSS.

2, which satisfied and validated the condition for perfect impedance matching. The obtained results by these two different simulators are comparable, however, the small discrepancies between the two simulation results are due to the different simulation techniques.

Fig 2.4 shows the input impedance characteristic of the proposed antenna array based on the homogeneous and PBG substrates using CST, which defines impedance matching between the input signal and the feed line. The value of the input impedance should be around  $50 \Omega$  in real and around  $0 \Omega$  in imaginary to properly match the input signal and the feed line. At their resonant frequencies, the input impedance is  $67.40 \Omega$  in the real part and  $-0.27 \Omega$  in the imaginary part in the case of the homogenous substrate and  $78.46 \Omega$  in the real part and  $9.1 \Omega$  in the imaginary part in the case of the PBG substrate.

For next-generation wireless communication systems, the gain and radiation efficiency of an antenna array are very crucial parameters in comparison with others because of the increased energy loss of the wave in propagation. From Fig.2.5 and Fig.2.6 by using CST Microwave Studio, it is observed that the antenna array based on the PBG substrate achieves a high gain of  $11.60 \text{ dB}$  and radiation efficiency of  $86.75 \%$ , compared to  $5.87 \text{ dB}$  and  $73.62 \%$ , respectively, for the antenna array based

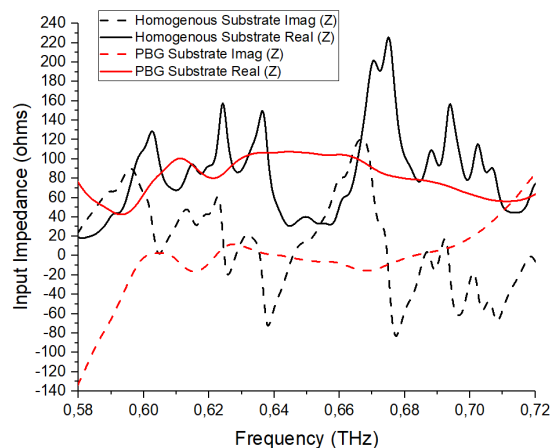


**Figure 2.4** – The input impedance characteristics of the proposed antenna array.

on the homogeneous substrate.

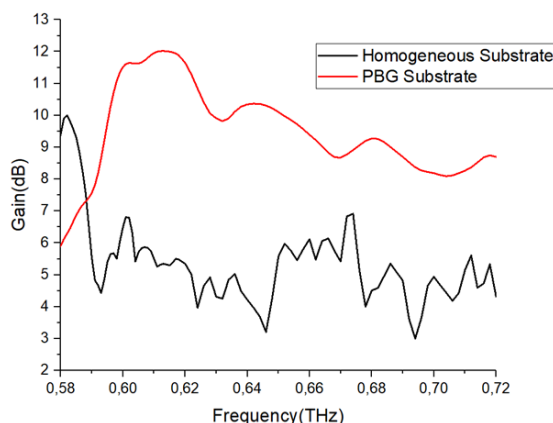


**Figure 2.5** – Gain performance of the designed antenna array based on the homogeneous and the **PBG** substrates.

The **2D** and **3D** far-field radiation patterns of the proposed antenna array are shown in Fig.2.7 and Fig.2.8 by using **CST** Microwave Studio, respectively. Fig.2.7 shows the **2D** polar plots of the radiation patterns for both antenna arrays at their resonance frequencies in the plane containing the solid angle at which the maximum radiation was achieved. The maximum radiation occurs at  $\phi=90^\circ$  in the case of the **PBG** substrate, where the maximum directivity was achieved at  $\theta=17^\circ$  with the value of 12.21 *dBi*. Whereas, the maximum radiation occurs at  $\phi=0^\circ$  in the case of the homogeneous substrate, where the maximum directivity was achieved at  $\theta=0^\circ$  with

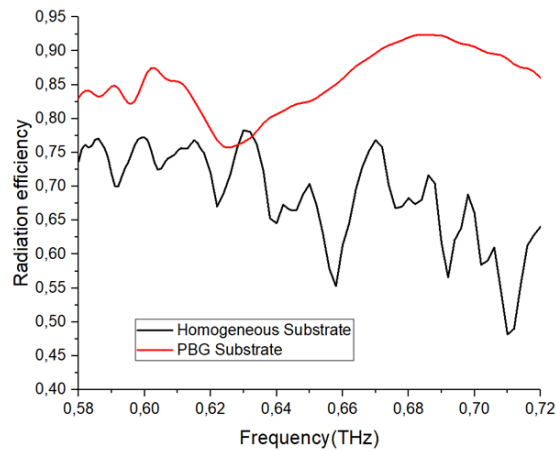


**Figure 2.6** – Radiation efficiency performance of the designed antenna array based on the homogeneous and the PBG substrates.

the value of 7.18 *dBi*. After employing the PBG substrate, the side lobes are decreased at some angles and the directivity increased a lot from 7.18 *dBi* to 12.21 *dBi*, which means that the antenna array based on the PBG performed better than the antenna array that is based on the homogeneous substrate at the maximum radiation.

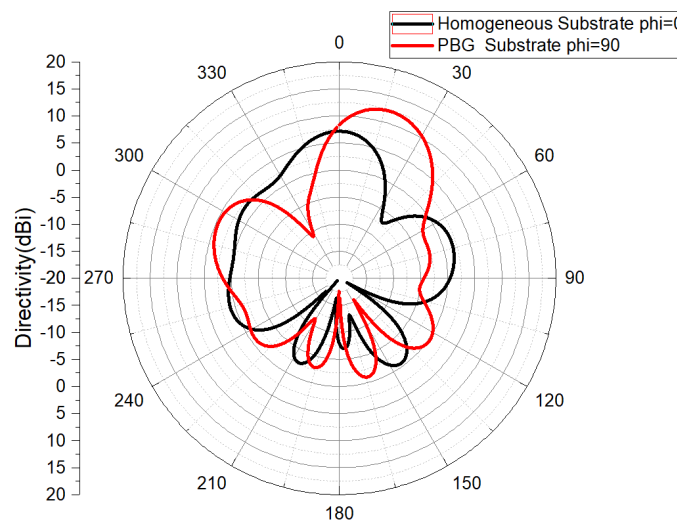


**Figure 2.7** – Polar plots of the directivity for the proposed antenna array.

The surface current of the proposed antenna array based on the PBG and the homogeneous substrates at their resonance frequencies with the phase of 120 is presented in Fig.2.9. It is clearly noticed that the surface current is distributed over the



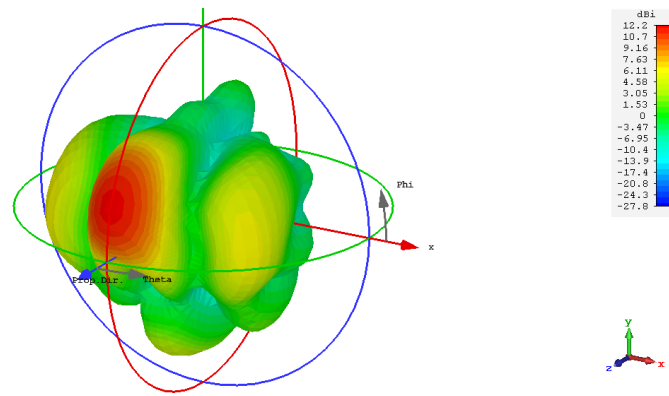
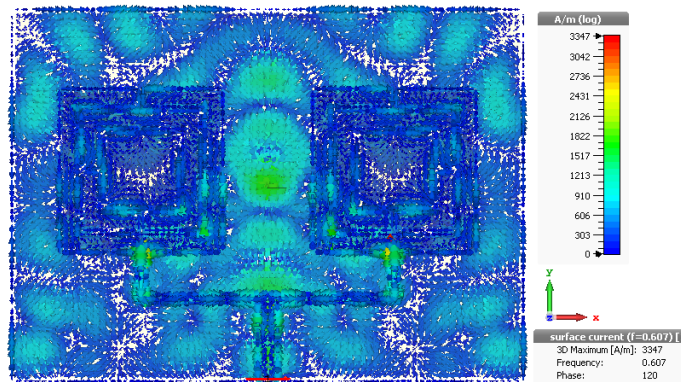
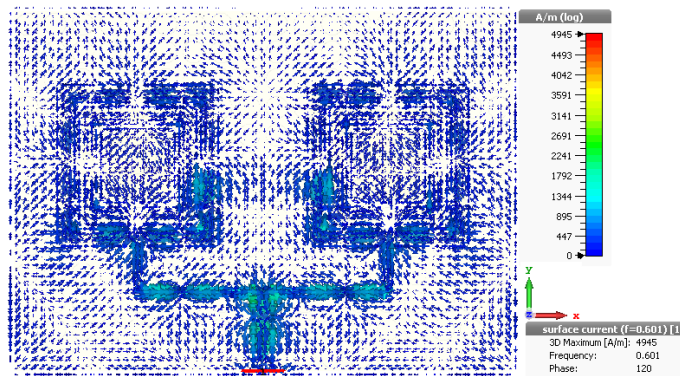


**Figure 2.8** – 3D radiation pattern of the directivity of the proposed antenna array based on the PBG substrate with maximum directivity of 12.21 dBi.



(a) Based on the homogeneous substrate.



(b) Based on the PBG substrate.

**Figure 2.9** – Surface current distribution of the proposed antenna array.

substrate surfaces and the radiated patches since the simulated silicon substrate is a lossy dielectric. The transmitted power from the feed line is dispatched through the radiated patches and then into outer space (air), where most of the power in the



substrate is radiated. The advantage of using a PBG substrate is maintained as most of the power is radiated, moreover, a significant reduction in the reflected power from the antenna-air edge interfaces is achieved.

Thus, considering the obtained results, there were remarkable enhancements in the performance of the proposed antenna array after employing the PBG substrate instead of the homogeneous substrate in terms of return loss, bandwidth, VSWR, gain, directivity and radiation efficiency. These enhancements in the performance are due to the reduction of the excitation of the surface waves which are modes of propagation supported by a grounded substrate. The surface wave excitation occurs because the lowest  $TM_0$  surface wave mode has a zero frequency cut-off, where the cut-off frequencies for the different surface wave modes are expressed by [145]:

$$f_c = \frac{n}{4h\sqrt{\epsilon_0\mu_0}\sqrt{\epsilon_r\mu_r - 1}} \quad (2.2)$$

where  $n = 0, 2, 4, \dots$  for TM modes,  $n = 1, 3, 5, \dots$  for TE modes and  $h$  is the dielectric thickness. By decreasing the dielectric permittivity, less energy is coupled into the surface waves and thus reducing the magnitude of the surface waves which improves the antenna array radiation characteristics. The reduction of the dielectric permittivity is due to the utilization of the PBG by creating a discontinuity in the air-substrate interface surface.

Finally, the performance of the proposed antenna array is compared to previously reported designs in Table 2.2. The proposed antenna array that is designed based on the PBG substrate, which achieved a high gain of 11.60 dB and exhibited a larger bandwidth of 113.01 GHz is compared with the results of existing antennas in the literature that offer the gain and bandwidth of 9.17 dB and 56 GHz, respectively [125]. 9.75 dB and 47 GHz, respectively [135]. 3.8 dB and 310 GHz, respectively [139]. 7.3 dB [140], 5.09 dB and 50 GHz [141], respectively. 7.94 dB and 36.23 GHz, respectively [117]. In addition, the proposed antenna array is compared to the work in [146] which offers a gain of 19.2 dB, a narrower bandwidth of less than 1 GHz with a very larger size. For such advantages, the THz devices demand miniaturization for

**Table 2.2** – Comparison of the proposed designed antenna array and previously reported designs.

	Antenna size ( $\mu m^2$ )	$f_r$ (THz)	$S_{11}$ (dB)	BW (GHz)	Gain (dB)	D (dBi)	Rad.Eff (%)
[125]	500 x 500	0.63	-64.04	56	9.17	9.58	91.08
[135]	500 x 500	0.607	-67.20	47	9.75	10.22	89.79
[139]	950 x 950	0.96	-13.05	310	3.8	-	-
[140]	500 x 500	0.67	-24	-	7.3	-	-
[141]	433.2 x 208.98	0.75	-35	50	5.09	5.71	86.58
[117]	800 x 600	0.6308	-44.71	36.23	7.94	8.612	85.71
[146]	12500 x 27000	0.1	-	< 1	19.2	-	-
Homogeneous Substrate	1186.92 x 857.22	0.607	-20.49	9.78	5.84	7.18	73.62
PBG Substrate	1186.92 x 857.22	0.601	-53.66	113.01	11.60	12.21	86.75

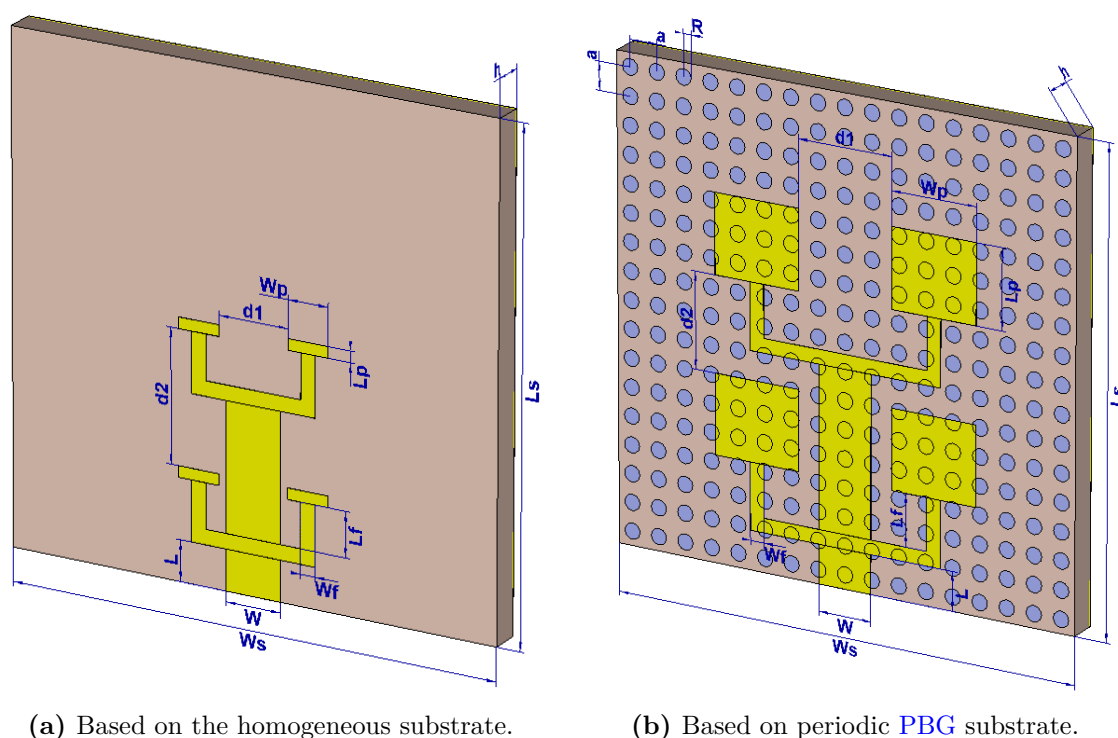
which the proposed antenna array is the best suited. This comparison indicates that the proposed antenna array presented herein is favorable, and may have applications in sensing and next-generation wireless communication systems technologies. Furthermore, this type of antenna is a standing wave antenna, which is a good candidate for integrated SoC applications in THz.

## 2.3 Design and Analysis of a novel 2x2 Microstrip Patch Antenna Array Based on Periodic and Non-Periodic Photonic Crystals Substrate

### 2.3.1 Design and Analysis of a 2x2 Microstrip Patch Antenna Array Based on Periodic Photonic Crystals Substrate

In this subsection, two antenna arrays are designed and simulated using two EM simulators CST Microwave Studio and Ansys HFSS, antenna array 1 and antenna array 0 as a 2x2 microstrip patch antenna array based on periodic PBG substrate and homogeneous substrate, respectively as shown in Fig.2.10. The antenna array

1 is designed based on a 2D PCs substrate whose host material is PTFE ( $\epsilon_r=2.08$ ,  $\tan \delta =0.0004$ ) of thickness  $135.62 \mu m$ . However, the air cylinders of a radius of  $37.80 \mu m$  and a period of  $131.64 \mu m$  are embedded in the host substrate. Hence, the dimensions of the square unit cell are  $131.64 \times 131.64 \mu m^2$ . The substrate of the microstrip antenna plays a very important role in achieving desirable electrical and physical characteristics. The aim of using the PBG substrate is to reduce the surface waves that are found in the substrate of antenna array 0 by either reducing the effective permittivity or thickness of the substance. Therefore, the width  $W_p$  and length  $L_p$  of the patch were initially computed using Eqs.(1.6), (1.7) and (1.8) [101].



(a) Based on the homogeneous substrate. (b) Based on periodic PBG substrate.

**Figure 2.10** – The geometry of the proposed 2x2 microstrip patch antenna array.

With the design of the single element patch complete, the expansion to a 2x2 array requires a feed network to connect all radiating patches to a single input. In the microstrip array, elements can be fed by a single line or multiple lines in a feed network arrangement. Therefore, feeding methods are classified as series feed network, corporate feed network and corporate-series feed network [78, 147]. In this work, a

corporate feed network was chosen. The feeding line width  $W$  is computed as [148]:

$$W = \frac{7.475h}{e^x} - 1.25t \quad (2.3)$$

where

$$x = \frac{Z_0\sqrt{\epsilon_r + 1.41}}{87}$$

$h$  and  $t$  are the thickness of the substrate and the patch, respectively.  $Z_0$  is the characteristic impedance of the microstrip transmission line of  $50 \Omega$ , and  $\epsilon_r$  is the dielectric constant. The feeding lines lengths  $L$  and  $L_f$  provide impedance transformation and phase matching on the patches, respectively, which can be calculated by the following formulas [148]:

$$L = (2P + 1) \times \frac{\lambda}{4} \quad (2.4)$$

$$L_f = (2Q + 1) \times \frac{\lambda}{2} + 2\Delta l \quad (2.5)$$

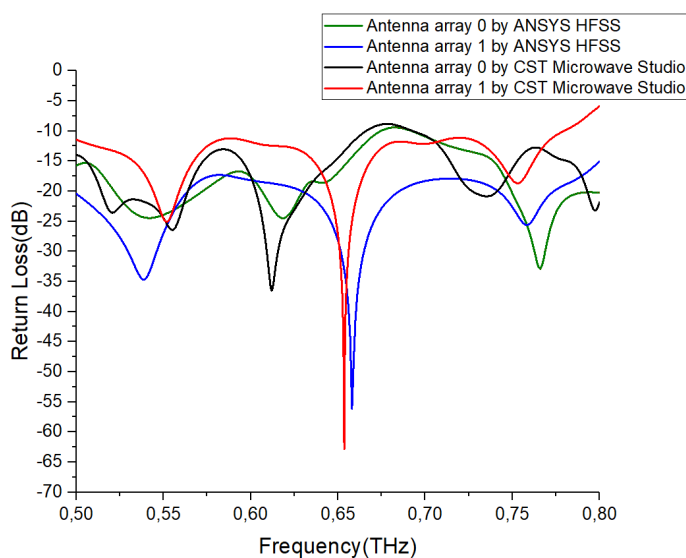
where  $P$  and  $Q$  are non-negative integers (in our design we chose  $P = Q = 1$ ). Then, optimization of the calculated values is performed. Finally, The dimensions of antenna array 0 and antenna array 1 are presented in Table 2.3. The thickness of the employed metal was  $0.5 \mu m$ .

Fig.2.12 shows the magnitudes of the scattering parameter  $S_{11}$  for both antenna arrays 0 and 1 using two simulators. It reveals that antenna array 0 that is designed based on the homogeneous substrate in the case of CST Microwave Studio simulation resonates at the frequency of 0.612 THz with a return loss of  $-36.49 dB$  and bandwidth greater than 166 GHz, whereas, in the case of Ansys HFSS simulation, the resonance frequency is 0.618 THz with a return loss of  $-24.48 dB$  and bandwidth greater than 174 GHz. The relative errors are 29 % and 4.8 % in the return loss and bandwidth, respectively with a difference of 6 GHz in the resonance frequency. After employing the periodic PBG substrate, improvements in the return loss and bandwidth are noticed where the resonance frequency gets closer to the desired frequency of 0.65 THz. So, in the case of CST Microwave Studio simulation, antenna array 1 resonates at the frequency of 0.654 THz with a minimal return loss of  $-62.87 dB$  and bandwidth

**Table 2.3** – Parameter values for antenna array 0 based on the homogeneous substrate and antenna array 1 based on periodic PBG substrate.

Parameter	Value ( $\mu m$ )	
	Antenna array 0	Antenna array 1
Patch width ( $W_p$ )	185	409.91
Patch length ( $L_p$ )	50	372.68
Distance between patches ( $d_1$ )	318.50	455.59
Distance between patches ( $d_2$ )	587.40	444.20
Substrate thickness ( $h$ )		135.62
Lattice constant ( $a$ )		131.64
Substrate width ( $W_s$ )		17 x $a$
Substrate length ( $L_s$ )		17 x $a$
Cylinder radius ( $R$ )		37.80
Feed line width ( $W$ )		252.52
Feed line length ( $L$ )		181.36
Feed line width ( $W_f$ )		67
Feed line length ( $L_f$ )	243.76	200

greater than 280 GHz, whereas, in the case of Ansys HFSS simulation, the resonance frequency is 0.658 THz with a minimal return loss of -56.12 dB and bandwidth larger than 300 GHz. The relative errors are 10.73 % and 7.1 % in the return loss and bandwidth, respectively with a difference of 4 GHz in the resonance frequency.



**Figure 2.11** – Magnitudes of the scattering parameter  $S_{11}$  of the designed antenna array based on homogeneous and periodic PBG substrates using CST Microwave Studio and Ansys HFSS.

**VSWR** should be in the range between 1 and 2. Fig.2.12 shows the **VSWR** performance of the designed antenna arrays 0 and 1 using **CST Microwave Studio** and Ansys **HFSS** at their resonant frequencies. It is noticed that antenna array 0 obtained a **VSWR** value of 1.0304 in the case of **CST Microwave Studio** and 1.127 in the case of Ansys **HFSS**, whereas, antenna array 1 obtained a **VSWR** value of 1.0014 in the case of **CST Microwave Studio** and 1.0031 in the case of Ansys **HFSS**. The obtained values of **VSWR** are less than 2 and very close to the ideal value of 1, which satisfied and validated the condition for perfect impedance matching.

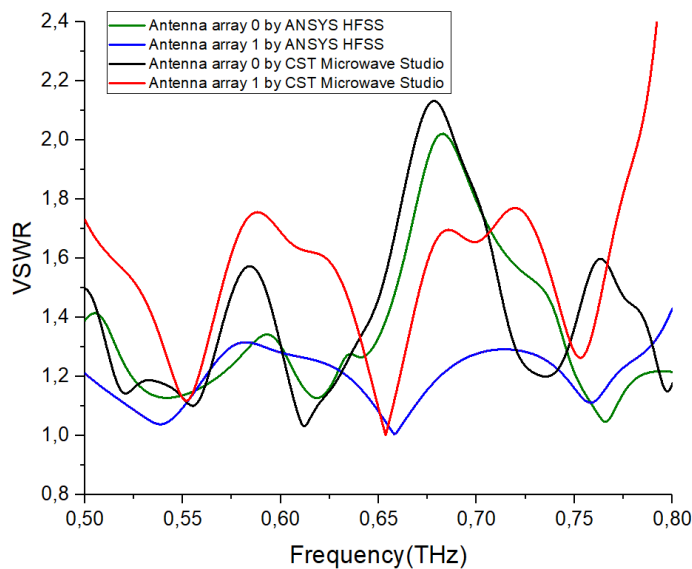


**Figure 2.12** – **VSWR** performance of the designed antenna arrays 0 and 1 using **CST Microwave Studio** and Ansys **HFSS**.

The gain and radiation efficiency are essential characteristics of the antenna’s compression, especially for this frequency band. The obtained results indicated that the gain and radiation efficiency were clearly enhanced for antenna array 1 that is designed based on periodic **PBG** substrate with values of 13.12 *dB* and 92.15 %, respectively. Whereas, antenna array 0 that is designed based on the homogeneous substrate achieved 6.68 *dB* and 90.13%, respectively using **CST Microwave Studio**.

Fig.2.13 shows the **2D** far-field radiation patterns for both antenna arrays 0 and 1 at their resonant frequencies in the planes containing the solid angle at which the

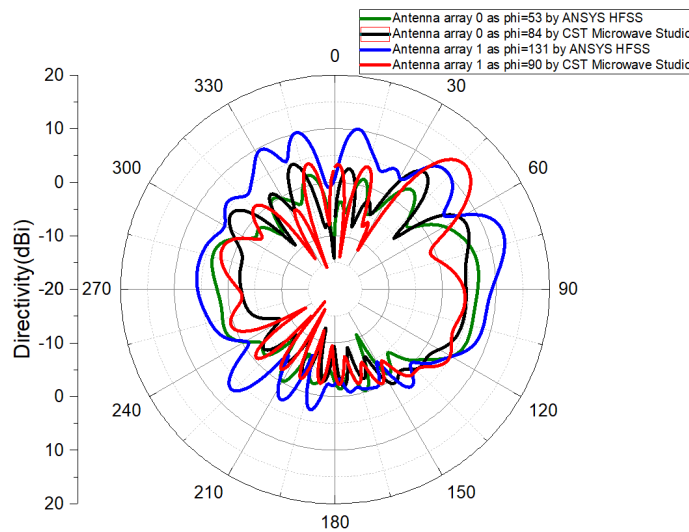
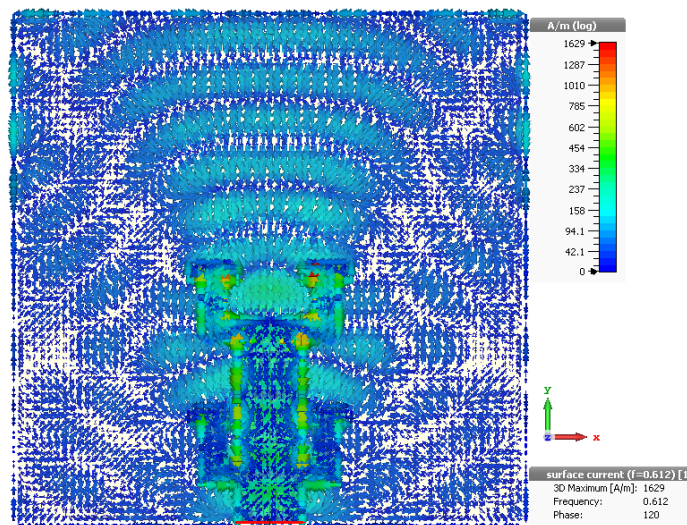


**Figure 2.13** – Polar plots of the radiation patterns for antenna arrays 0 and 1 at their resonance frequencies using CST Microwave Studio and Ansys HFSS.

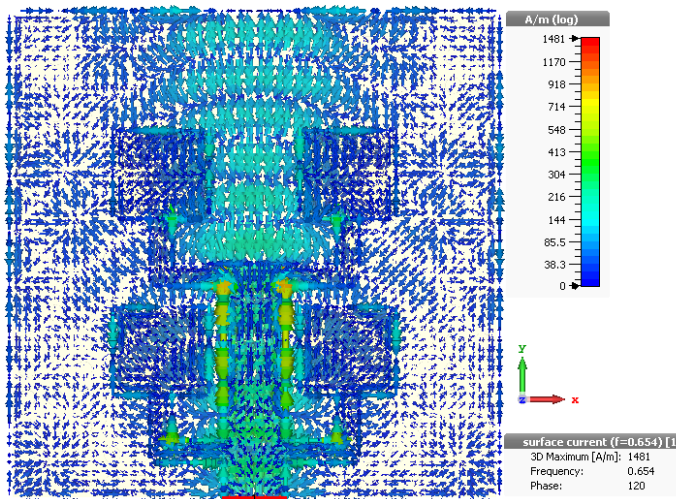
maximum radiation was achieved using CST Microwave Studio and Ansys HFSS. It is clear from the simulated radiation pattern that the directivity has increased a lot after employing PBG substrate with smaller side lobes effects at some angles compared to the homogeneous substrate. Therefore, the maximum radiation in the pattern of antenna array 0 occurs at  $\phi=84^\circ$ ,  $\theta = 37^\circ$  with a maximum directivity of 7.48 dBi in the case of CST Microwave Studio and at  $\phi=53^\circ$ ,  $\theta = 80^\circ$  with a maximum directivity of 7 dBi in the case of Ansys HFSS. However, the maximum radiation for antenna array 1 occurs at  $\phi = 90^\circ$ ,  $\theta=45^\circ$  with a maximum directivity of 13.50 dBi in the case of CST Microwave Studio and at  $\phi = 131^\circ$ ,  $\theta=72^\circ$  with a maximum directivity of 13.10 dBi in the case of Ansys HFSS.

Fig.2.14 shows the surface current of antenna array 0 based on the homogeneous substrate and antenna array 1 based on PBG substrate at their resonance frequencies with the phase of 120 using CST Microwave Studio. It is clearly noticed that the transmitted power from the feed line is dispatched through the patches and then into outer space (air), where most of the power in the substrate is radiated. The advantage of using a PBG substrate is maintained as most of the power is radiated, moreover, a significant reduction in the reflected power from the antenna-air edge interfaces is achieved.





(a) Antenna array 0.



(b) Antenna array 1.

**Figure 2.14** – Surface current distribution.

The results obtained by these two different simulators showed close agreement between various electrical parameters. The small discrepancies between the two simulation results are due to the different simulation techniques. Hence, antenna array 1 outperformed antenna array 0 in terms of return loss, bandwidth, VSWR, gain, radiation efficiency and directivity. This improvement is due to the use of the PBG substrate, which suppresses the surface waves propagating along the surface of the substrate and reflects most of the electromagnetic wave energy radiated to the substrate significantly. Thus, the PBG substrate is an effective technique for improving

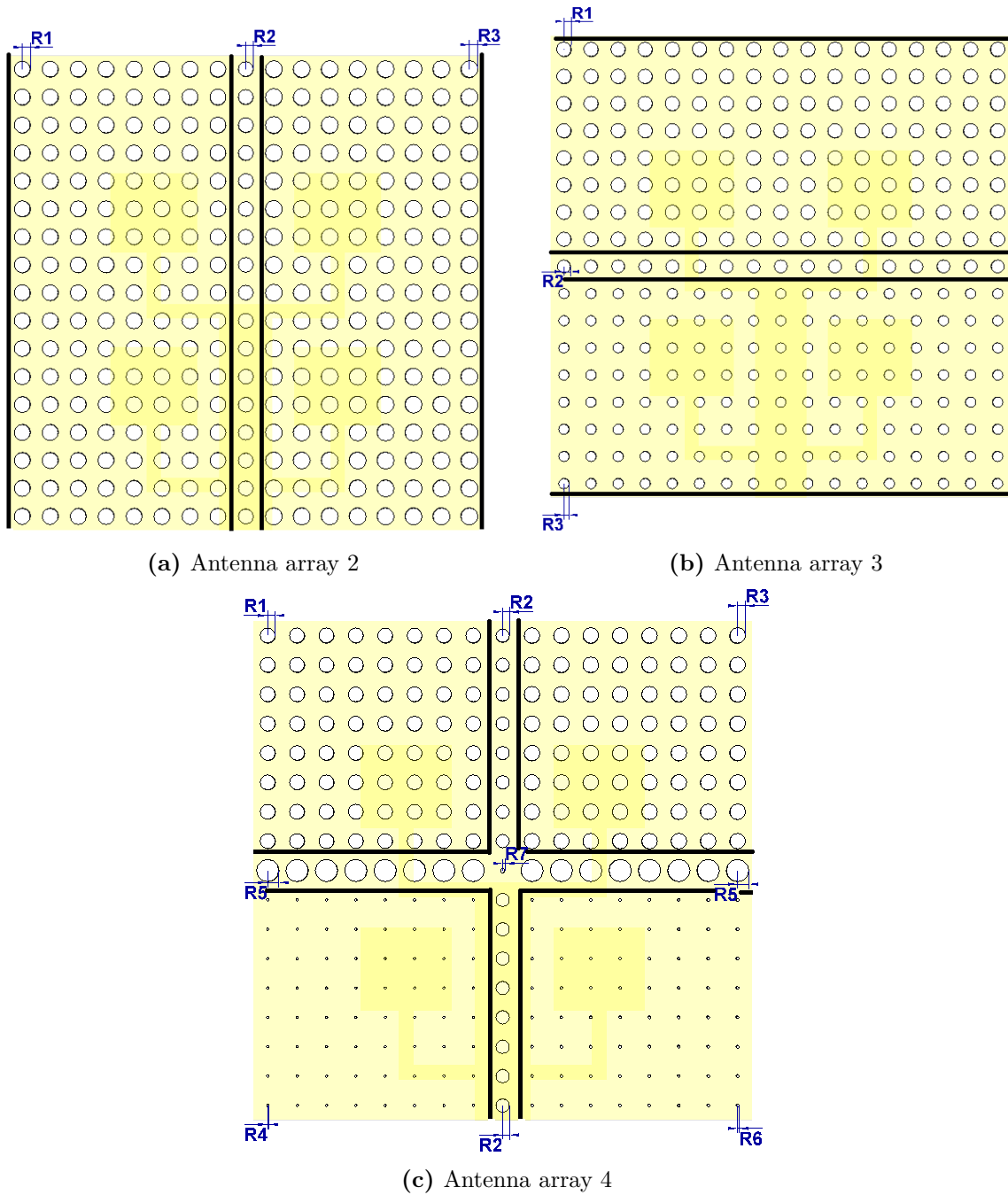


the antenna array performance.

### 2.3.2 Design and Analysis of a 2×2 Microstrip Patch Antenna Array Based on Non-periodic Photonic Crystals Substrate

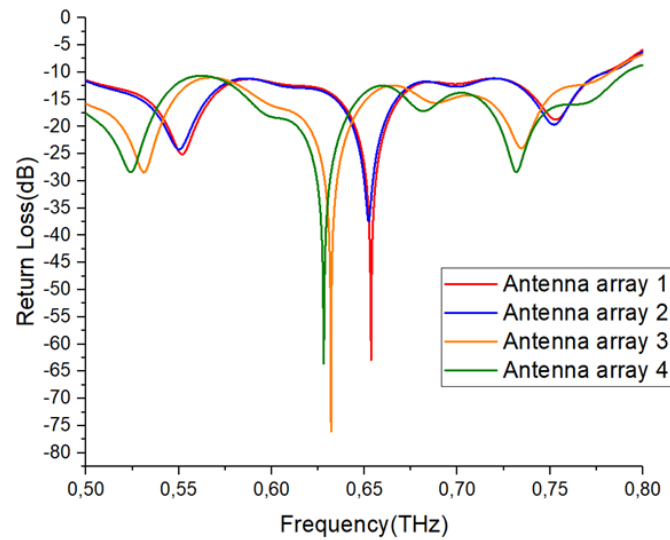
Previously, the performance of the conventional antenna array based on the homogeneous substrate was enhanced after using periodic PCs. In this subsection, the performance of antenna array 1 is investigated by using non-periodic PCs. The non-periodic PCs substrate means arranging the different radii of air holes into the dielectric or using the different distances between the centers of each air hole which can be arranged in a square lattice and triangular lattice. This technique has been experienced by many researchers [13, 134, 135] to enhance the bandwidth, gain and radiation efficiency of an antenna. Therefore, three antenna arrays based on the structure of antenna array 1 were designed, however, the air cylinders in the substrate were divided into several sets of air holes. Each set of air holes had a different radius, as shown in Fig.2.15. Where, Fig.2.15a shows antenna array 2 with three sets of air holes, Fig.2.15b shows antenna array 3 with three sets of air holes, Fig.2.15c shows antenna array 4 with seven sets of air holes. For better performance, the radii of the air holes for each set are optimized and summarized as follows: In antenna array 2,  $R_1=37.8 \mu m$ ,  $R_2= 35 \mu m$  and  $R_3= 40 \mu m$ . In antenna array 3,  $R_1=35 \mu m$ ,  $R_2= 31.5 \mu m$  and  $R_3= 25 \mu m$ . In antenna array 4,  $R_1=33.5 \mu m$ ,  $R_2= 30$ ,  $R_3=35 \mu m$ ,  $R_4= 5$ ,  $R_5= 50 \mu m$ ,  $R_6= 6 \mu m$  and  $R_7= 10 \mu m$ .

Fig.2.16 shows the magnitudes of the scattering parameter  $S_{11}$  of the designed antenna arrays 2,3, and 4 compared to antenna array 1 using CST Microwave Studio. It is clear that all designed antenna arrays based on non-periodic PCs resonate around 0.65 THz. Starting by antenna array 2, which resonates at the frequency of 0.652 THz with a return loss of -37.35 dB and bandwidth larger than 280.4 GHz. Then, antenna array 3 resonates at the frequency of 0.632 THz with the smallest return loss in this design of -76.11 dB and bandwidth larger than 283 GHz. Finally, antenna



**Figure 2.15** – The geometry of the proposed antenna array based on non-periodic PCs substrate.

array 4 resonates at the frequency of 0.628 THz with a return loss of -63.62 THz and obtains the highest bandwidth among all designed antenna arrays, which is larger than 291 GHz. Thus, antenna arrays 3 and 4 performed better than antenna array 1



**Figure 2.16** – The magnitudes of the scattering parameter  $S_{11}$  of the designed antenna arrays based on periodic and non-periodic PCs using CST Microwave Studio.

in terms of return loss and bandwidth around 0.65 THz.

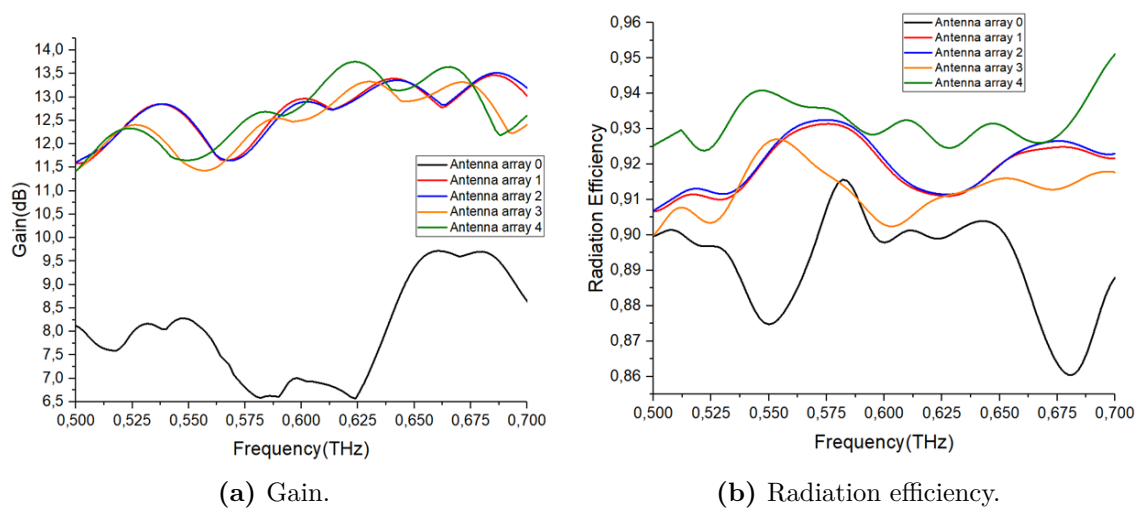


**Figure 2.17** – Gain and radiation efficiency performance of all designed antenna arrays in the frequency range 0.5-0.7 THz using CST Microwave Studio.

Fig.2.17 shows the gain and radiation efficiency of all designed antenna arrays in the frequency range of 0.5-0.7 THz including homogeneous, periodic and non-periodic PCs substrates, it is clear that antenna array 4 achieves the highest gain and radiation efficiency among all designed antenna arrays with the values of 13.70 dB and 92.45

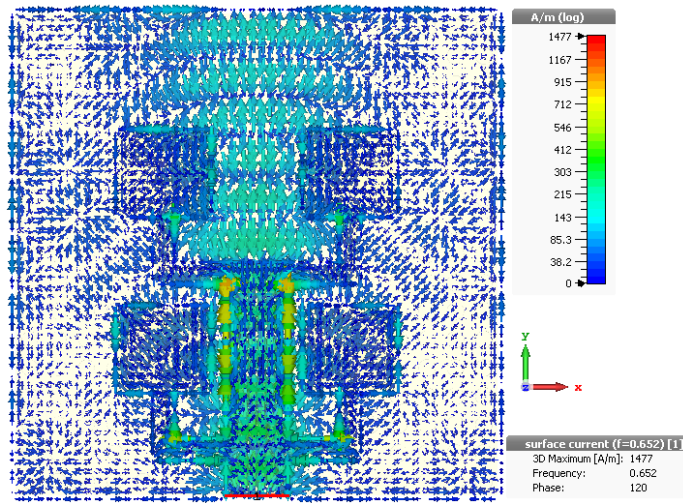
%, respectively. Then, antenna array 3 achieves 13.32 *dB* and 91.20 %, respectively. Finally, antenna array 2 achieves 13.20 *dB* and 92.10 %, respectively.

At the maximum radiation where  $\theta$  is  $45^\circ$  and  $\phi$  is  $90^\circ$ , the antenna array 4 achieved the maximum directivity between all designed antenna arrays with the value of 14.10 *dB**i*, then antenna arrays 3 and 2 achieved 13.80 *dB**i* and 13.60 *dB**i*, respectively. Thus, the gain and the directivity of the designed antenna arrays 4, 3 and 2 based on non-periodic **PCs** were improved compared to the gain and directivity that were achieved by antenna array 1 with periodic **PCs** and antenna array 0 with the homogeneous substrate.

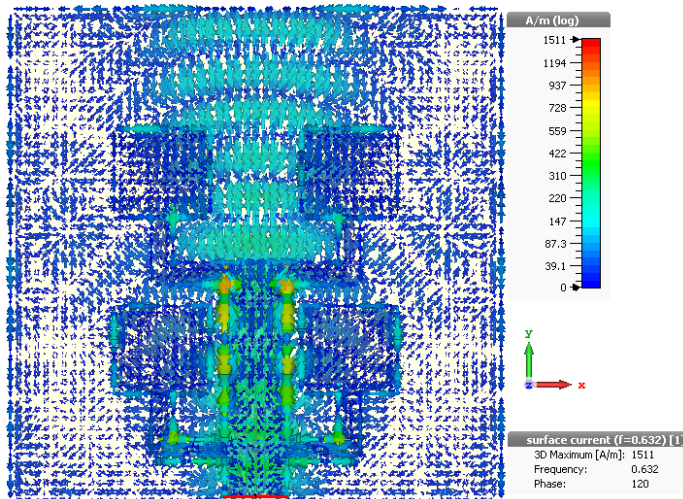
Fig.2.18 shows the surface current of antenna arrays 2, 3 and 4 based on non-periodic **PBG** at their resonance frequencies with the phase of 120 using **CST** Microwave Studio. It is clearly noticed that the transmitted power from the feed line is dispatched through the patches and then into outer space (air), where most of the power in the substrate is radiated. The advantage of using non-periodic **PBG** substrate is maintained as most of the power is radiated, moreover, a significant reduction in the reflected power from the antenna-air edge interfaces is achieved.

As the number of patch elements is increased to form an array, such as 16 elements (4x4 array) or 32 elements (4x8 array), much improvements in the performance like bandwidth, gain and directivity could be obtained, however, the size of the antenna becomes larger. So, complication increases for the feed network resulting in more power consumption, ohmic losses, mismatch losses and mutual coupling effects between the adjacent elements of an array [72, 88, 149]. Furthermore, an antenna with many numbers of radiating patches creates diffraction which can cause high side lobe level effects [150]. Hence, the performance of the microstrip patch antenna strongly depends on several factors such as the number of patches, feeding technique, the dielectric constant of the substrate, the type of substrate and its thickness.

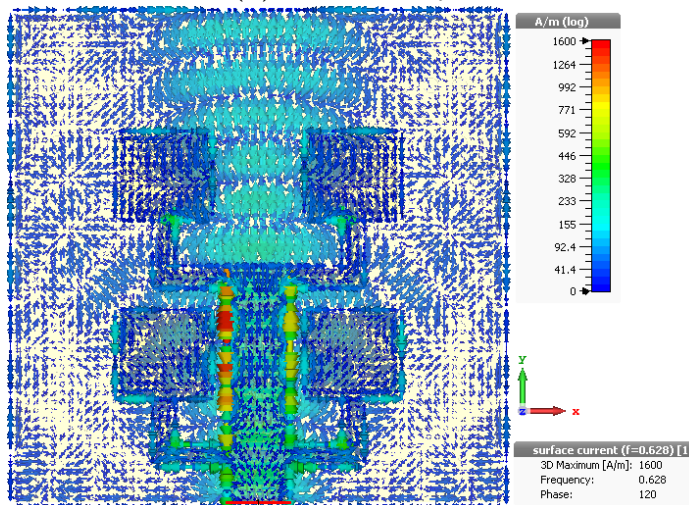
Generally, the **PBG** reduces the substrate absorption due to the existence of a non-transmission band of **PCs**, and by using a different radius of air holes more reduction of



(a) Antenna array 2



(b) Antenna array 3



(c) Antenna array 4

Figure 2.18 – Surface current distribution.

**Table 2.4** – Comparison of the proposed designed antenna arrays and previously reported designs.

	Antenna size ( $\mu m^2$ )	$f_r$ (THz)	$S_{11}$ (dB)	BW (GHz)	Gain (dB)	D (dBi)	Rad.Eff (%)
2x2 array [104]	2000 x 2000	0.6	-27.70	60	-	-	-
Periodic PBG [134]	600 x 600	0.63	-56.81	$\gg 230$	8.95	-	89.31
Non-periodic PBG [134]	600 x 600	0.61	-83.73	$\gg 230$	9.19	-	90.84
Non-periodic PBG [135]	500 x 500	0.607	-67.32	47	9.75	10.20	89.79
Antenna array 0	2237.88 x 2237.88	0.612	-36.49	$\gg 166$	6.86	7.48	90.13
Antenna array 1	2237.88 x 2237.88	0.654	-62.87	$\gg 280$	13.12	13.50	92.15
Antenna array 2	2237.88 x 2237.88	0.652	-37.35	$\gg 280.4$	13.20	13.60	92.10
Antenna array 3	2237.88 x 2237.88	0.632	-76.11	$\gg 283$	13.32	13.80	91.20
Antenna array 4	2237.88 x 2237.88	0.628	-63.62	$\gg 291$	13.70	14.10	92.45

the substrate absorption is created compared to the homogeneous and periodic PBG substrates. Finally, the radiation characteristics of the proposed antenna arrays are compared with those for previously reported antennas in Table 2.4. It is evident that the radiation performance of the proposed antenna arrays is significantly improved as compared to earlier reported researches because their resonance frequencies were close to 0.65 THz, which is a low atmospheric attenuation window in the THz range, and due to their electromagnetic characteristics, including high gain, high radiation efficiency, and wide bandwidth. These antenna arrays can be useful in next-generation wireless communication technologies and other interesting applications.



## 2.4 Summary

In this chapter, high gain novel microstrip patch antenna arrays were proposed and studied based on the PCs in THz, which can be employed for next-generation wireless communication technology and other interesting applications. To validate the accuracy of the proposed antenna arrays, two different simulation techniques are used, CST Microwave Studio based on FIT and Ansys HFSS based on FEM which showed close agreement between various electrical parameters. First, a 1x2 microstrip patch antenna array is designed based on a thick silicon substrate having a high relative permittivity and embedded air cylinder holes, and then the radiation characteristics of this antenna array are compared to the one that is mounted on the homogeneous substrate. For high radiation characteristics, the proposed antenna array resonated around 0.65 THz and showed remarkable enhancements. The simulated results indicated that the PBG substrate efficiently improved the characteristics of the conventional microstrip antenna array, which obtained enhancements of 161.88 %, 1055.52 %, 98.63 % and 17.83 % in the return loss, bandwidth, gain, and radiation efficiency, respectively, obtained by CST Microwave Studio. Next, a 2×2 microstrip patch antenna array was designed and analyzed around 0.65 THz based on different substrates including periodic PCs, non-periodic PCs and homogeneous substrates. The proposed antenna array was first designed based on periodic PCs substrate in order to enhance its performance around 0.65 THz, by suppressing undesirable surface waves that are found in the homogeneous substrate. The simulated results indicated that the periodic PCs substrate efficiently enhanced the characteristics of the conventional 2 × 2 microstrip patch antenna array. Finally, three different enhancements to the PCs substrate were described to improve the characteristics of the proposed antenna array. The simulated results showed that the return loss, bandwidth, gain and radiation efficiency were enhanced further by using non-periodic PCs, which was noticed in antenna array 4, which obtained a minimal return loss of -63.62 dB at a resonance frequency of 0.628 THz and a larger bandwidth greater than 291 GHz. The achieved gain and radiation efficiency were 13.70 dB and 92.45 %, respectively.

# Chapter 3

## Design and Analysis of Terahertz Microstrip Antenna Arrays Based on Modified Photonic Crystals

### 3.1 Introduction

Over the last decade, large demand for the development of miniaturized devices that are capable of transmitting and receiving the highest possible data rates at low power. The THz band plays a key role in the advancement of wireless communication technologies, which is the least explored communication band. This frequency band is located between microwave and mid-infrared and generally covers frequencies between 0.1 and 10 THz [151]. The benefits of the THz band include high spatial resolution, high-speed communications, ultra-wideband, high data rate transmission, and low power consumption [5, 106, 152, 153]. Because of its unique features, the THz band is promising applications in the fields of spectroscopy [154], space communication [155], object imaging [18], medical applications [156] and surveillance systems [114]. Unfortunately, there are certain emerging issues related to the THz band such as high path loss and signal attenuation due to water and molecular absorption in the air [157]. There are nine low-attenuation windows in the frequency range of 0.1–3



THz of the spectrum where the path loss is comparatively small, THz transmission could be established at these low-attenuation windows to enhance the wireless link reliability. One of these windows exists around 0.65 THz which has taken interest by many researchers in recent years [9].

The antenna is one of the important components in the THz band. Among various THz antennas, microstrip patch antennas which are good candidates for the THz applications, because of their cost effective, lightweight, easy to design and fabrication. These types of antennas are standing wave antennas, which are good candidates for use in THz integrated System-on-Chip (SoC) applications. On-chip antennas are an integral part of wireless sensor networks for data communication between ICs, which are the last barrier for the true SoC solution, omitting the demand for conventional 50  $\Omega$  interfaces, lossy RF interconnects, sophisticated packaging and therefore make congruent manufacture of cost effective in terms of packaging and compactness of the THz band compared to conventional packaging of an external antenna with transceivers [158, 159]. Unfortunately, the conventional patch antenna at higher substrate permittivities, thicknesses and operating frequencies suffers from some drawbacks such as low gain, low radiation performance and narrow bandwidth. The gain of patch antennas can be increased by using the array configurations. However, the mutual coupling between the adjacent elements of an array due to the excitation of surface waves is increased [88]. In addition, a factor that contributes to the degradation of the microstrip patch and striplines of various lengths at such high frequencies is called surface roughness, which increases the signal loss and dispersion due to the reduced effective conductivity of the metal [129, 130]. The reduction of the surface waves and the enhancement of antenna performance are experienced in this frequency band by many researchers. Commonly used approaches are multilayered substrate technique [104], Defected Ground Structures (DGS)[132], metamaterial technique [160], Epsilon-Near-Zero (ENZ) metamaterials[161], and Photonic Crystals (PCs) structures [14, 15, 16, 64, 66, 125, 134, 135, 138, 162, 163]. Therefore, a patch array design with PCs is definitely helpful in improving the performance of the patch antenna.

The PC structures are also known as PBG structures, which are artificial materials

made of periodic implants within a surrounding medium of a hollow air cylinder having circular, square, hexagonal, triangular, and elliptical shapes, which are implanted in the dielectric substrate material. These structures have been developed in which electromagnetic wave propagation in any direction is completely prevented for all frequencies within a stop band [58]. There are different structures types of PBG such as 1D, 2D, or 3D. 2D PCs have gained the most interest from many researchers, as they are much easier to fabricate and design compared to 3D PCs and have promising applications in planar waveguides, optical and microwave cloak [164, 165].

Ahmad et al. [166] proposed a novel shape antenna based on a PBG-based crystal polyimide substrate which obtained optimum performance with a gain of 9.45 dB and bandwidth of 29.79 GHz at a resonance frequency of 0.63 THz. Also, Kushwaha et al. [117] employed PCs and a polyimide substrate by designing a novel microstrip patch antenna in THz to obtain a gain of 7.934 dB, and a bandwidth of 36.25 GHz at a resonance frequency of 0.6308 THz. Moreover, Hocini et al. [134] investigated the perforated air cylinders embedded in a thick polyimide substrate by designing a microstrip patch antenna based on periodic and aperiodic PCs around 0.65 THz, which yielded the gain of 8.95 dB and 9.19 dB, respectively, whereas, the achieved bandwidth was greater than 230 GHz which is a really interesting result. Their antennas are suitable for applications in the detection of explosives and sensing, however, the gain is still low which can not be adequate to meet the challenges imposed by the high energy loss of this frequency band. In this chapter, another patch is added for improved gain and radiation characteristics. Therefore, a 1x2 microstrip patch antenna array with different patches including rectangular and circular is designed based on a thick polyimide substrate around 0.65 THz where the atmospheric path loss is relatively low, then the performance of this antenna array was investigated by using two different substrates, periodic and aperiodic PCs. This chapter is organized as the following: In Section 3.2, the effect of the periodic and aperiodic PCs on the performance of the 1x2 RMPA array is investigated. In Section 3.3, the effect of the PCs that include air cylinders and air cuboids holes on the performance of the 1x2 CMPA array is investigated. Finally, the summary of the chapter is given in Section

3.4.

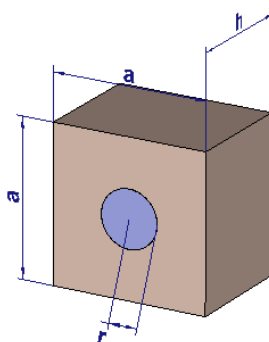
## 3.2 Design and Analysis of a 1x2 Rectangular Microstrip Patch Antenna Array Based on Modified Photonic Crystals Substrate

In this section, six THz rectangular microstrip patch antenna (RMPA) arrays based on different substrates, including homogeneous, periodic PCs and five new aperiodic PCs substrates are designed and studied in the frequency range of 0.5–0.8 THz. The proposed antenna arrays are mounted on a thick polyimide substrate where each of the modified PC substrates is divided into several sets of perforated air cylinder holes where each set has its particular radius. The simulation has been performed using CST Microwave Studio for the proposed antenna arrays which resonated around 0.65 THz and showed high radiation characteristics compared to the conventional antenna array.

### 3.2.1 Antenna Array Design Based on Periodic Photonic Crystals

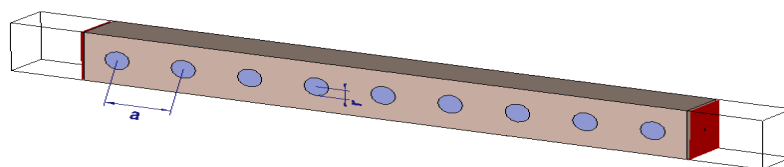
In this subsection, two different antennas are designed and simulated, antenna array 0 and antenna array 1 based on homogeneous and periodic PBG substrates, respectively. The host material of the unit cell is made of polyimide where  $\epsilon_r = 3.5$  and  $\tan \delta = 0.0027$ . Fig.3.1 shows the geometry of the square unit cell dielectric substrate material with an embedded air cylinder hole, where the width and length of the square unit cell are  $108.1 \mu m$ . At the center, an air cylinder hole of a radius of  $20 \mu m$  is embedded. The thickness of the substrate material and height of the air cylinder holes are equal to  $82.33 \mu m$ .

Fig.3.2 shows multiple concatenated duplicates of the air cylinder hole embedded dielectric substrate square unit cell. This 2D PC structure can be fabricated using



**Figure 3.1** – The geometry of the square unit cell.

lithographically fabricated using a custom-designed lithographic mask [167]. The simulations were performed in the frequency range of 0.5-0.8 THz to define the electrical properties of the substrate, therefore, the extracted real and imaginary parts of the dielectric permittivity are shown in Fig.3.3. Generally, the real and imaginary parts of an effective dielectric permittivity have the main role in determining the physical size of the antenna dimension. Therefore, it is important to mention that with the reduction in the effective dielectric permittivity of substrate material, the size of the antenna elements such as patch dimension may be increased [66, 101]. To design a substrate structure for the patch antenna array with resonance around 0.65 THz, the value of the effective permittivity is taken as 0.59, which is less than 1 because of the utilization of the PCs instead of the homogeneous substrate. They are artificial structures that enable different new properties compared to homogeneous materials. This kind of material also attains negative dielectric permittivity and magnetic permeability [168].



**Figure 3.2** – The geometry of the simulated PBG structure.

The proposed 1x2 microstrip patch antenna array consists of two symmetrical patch elements which are fed in parallel. The patch width  $W_p$  and length  $L_p$  are cal-

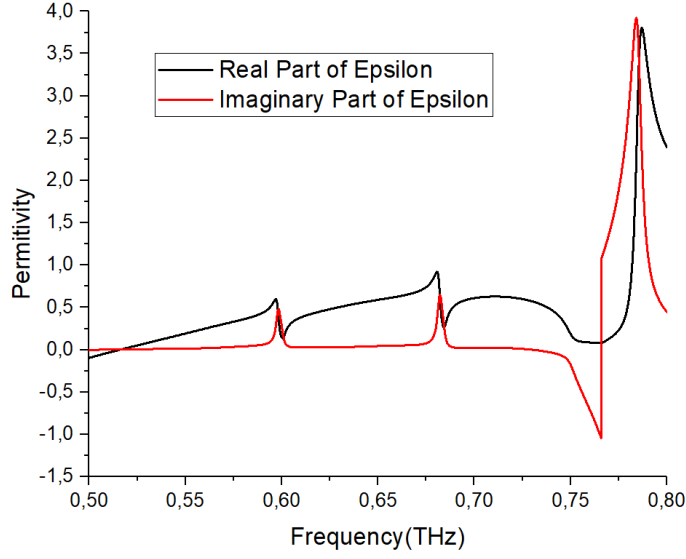


**Figure 3.3** – The relative permittivity of the designed PBG.

culated using Eqs.(1.6), (1.7) and (1.8) [101]. The feeding line width  $W_f$  is computed based on the total input impedance  $Z_a$  of the antenna, which in the current case of two patch elements fed in parallel, which is given as [169]:

$$Z_a = \frac{11.96\lambda_0}{W_p} \quad (3.1)$$

Finally,  $Z_a$  is matched with the standard  $50 \Omega$  impedance through feeding line length  $L_f$  with the characteristic impedance as  $Z_0$ .  $W_f$  is computed as [148]:

$$W_f = \frac{7.475h}{e^x} - 1.25t \quad (3.2)$$

where

$$Z_0 = \sqrt{Z_a \cdot 50}$$

and

$$x = \frac{Z_0 \sqrt{\epsilon_{eff} + 1.41}}{87}$$

$h$  and  $t$  are the substrate thickness and the ground plane thickness, respectively.

The feeding lines  $L_f$  and  $L_{f2}$  provide impedance transformation and phase match-

ing on the two patches in equal parts, respectively, which can be calculated by using the following formulas [169, 170]:

$$L_f = (2P + 1) \times \frac{\lambda}{4} \quad (3.3)$$

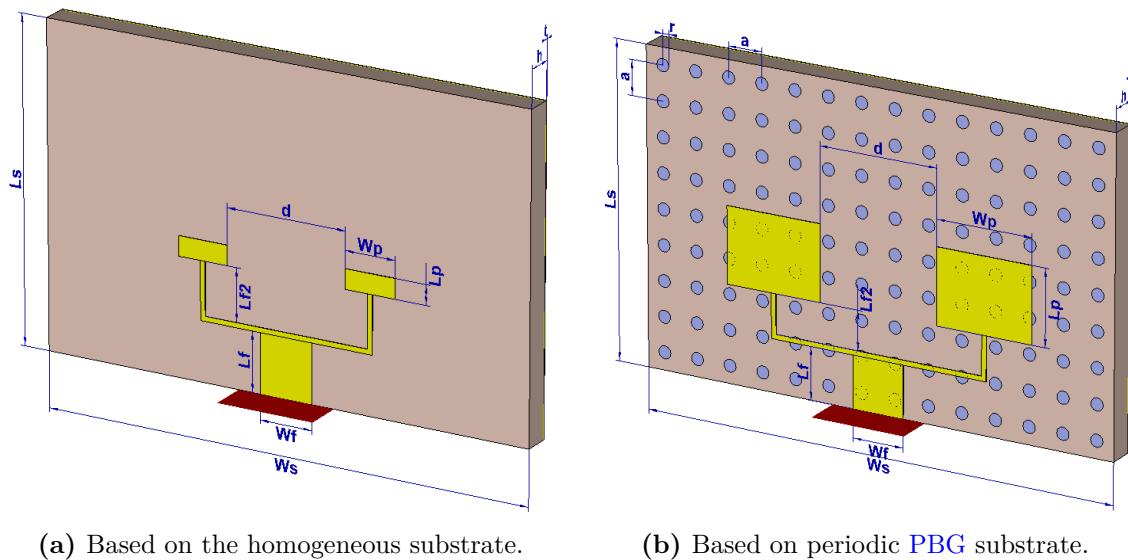
$$L_{f2} = (2Q + 1) \times \frac{\lambda}{2} + 2\Delta l \quad (3.4)$$

where  $P$  and  $Q$  are non-negative integers (in our design we chose  $P = Q = 1$ ).  $\lambda$  is the operating wavelengths and  $\Delta l$  is the patch length extension due to the fringing field effect [170].

At high frequencies, this type of feed structure tends to minimize the feed line lengths, however, in practice, it is found that the radiation from the feed network and feed resistive loss due to a number of discontinuities encountered in a typical antenna feed have a noticeable effect on the antenna array radiation pattern and lead to a mismatch in the input impedance by creating unwanted radiation, which is called spurious radiation [171]. Finally, the geometry of the proposed 1x2 RMPA array based on the homogeneous and periodic PBG substrate structure is shown in Fig.3.4, where the dimensions are obtained by using the optimization tools of CST Microwave Studio, which are presented in Table 3.1.

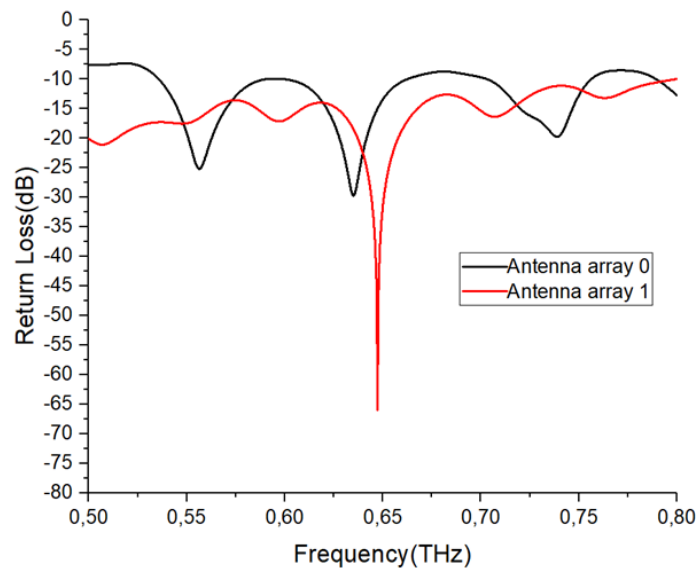
Among the methods of fabrication, one can say that the prototype can be fabricated using micro/nanofabrication processing technology. Therefore, the 2D PC structure can be fabricated using a lithographic method using a custom-designed lithographic mask [172], whereas, the 1x2 patch antenna array is generally fabricated by using the photo-lithographic method which includes the steps of UV exposure, developing, PCB etching process and assembling [173]. Finally, the experimental study can be performed by using VNA, or FTIR spectrometer, or the standard THz time-domain measurement system [14, 160].

Fig.3.5 shows the magnitudes of the scattering parameter  $S_{11}$  for the different antenna array configurations, which shows that antenna array 1 resonates at the frequency of 0.647 THz which is close to the desired frequency of 0.65 THz, with a



**Figure 3.4** – The geometry of the designed 1x2 RMPA array.

minimal return loss of  $-65.96$  dB and bandwidth greater than 299.29 GHz, whereas, antenna array 0 resonates at the frequency of 0.635 THz, with a return loss of  $-29.73$  dB and bandwidth of 62.81 GHz. Thus there was a remarkable enhancement in the antenna array performance after employing the PBG substrate.



**Figure 3.5** – Magnitudes of the scattering parameter  $S_{11}$  for antenna array 1 and antenna array 0.

**Table 3.1** – Parameter values for antenna array 0 based on a homogeneous substrate and antenna array 1 based on a periodic PBG substrate.

Parameter	Value ( $\mu m$ )	
	Antenna array 0	Antenna array 1
Patch width ( $W_p$ )	154	304.93
Patch length ( $L_p$ )	60	236.17
Distance between patches ( $d$ )	247	378.19
Substrate thickness ( $h$ )		82.33
Ground plane thickness ( $t$ )		1.3
Cylinder radius ( $r$ )		20
Lattice constant ( $a$ )		108.10
Substrate width ( $W_s$ )		14 x $a$
Substrate length ( $L_s$ )		9 x $a$
Feed line width ( $W_f$ )		161.8
Feed line length ( $L_f$ )	180	162.53
Feed line length ( $L_{f2}$ )	160	122.30

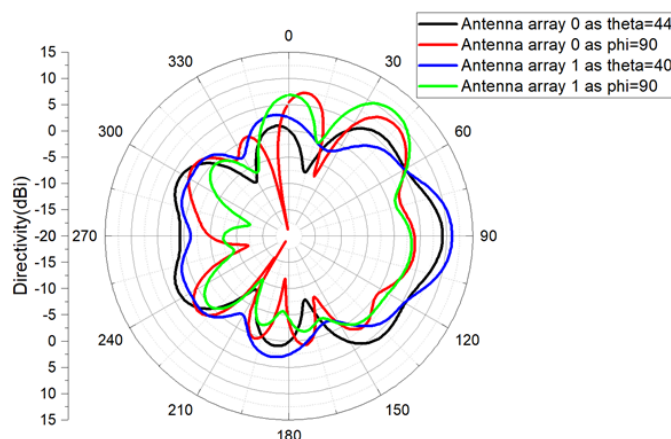
The gain and radiation efficiency of the antenna array must be taken into account, especially in the next-generation wireless communication systems for this frequency band. It is observed that the gain and radiation efficiency of the designed antenna array 1 based on periodic PCs substrate were enhanced with the values of 10.43 dB and 86.35 %, respectively. However, the antenna array 0 that is designed based on the homogeneous substrate obtained a gain of 8.47 dB and radiation efficiency of 84.21 %.

Fig.3.6 shows the 2D far-field radiation pattern for both antenna arrays 1 and 0 at their resonance frequencies in the planes containing the solid angle at which the maximum radiation was achieved. It is noticed that the main beam for both antenna arrays is tilted at some angle from the horizontal plane by the diffraction effects from the conductive small ground [174], with a high side lobe level. The effects of the high side lobe level are due to the diffraction of surface waves found at the edges of the antenna array substrates. Diffraction occurs whenever there is a sharp discontinuity in a radiating or reflecting surface, and because the antenna arrays have a number of elements all radiating, which creates diffraction. Hence, larger antennas have more side lobe level effects [150]. These effects were reduced after employing the PBG



substrate. Therefore, antenna array 1 achieved the maximum radiation at  $\theta = 40^\circ$ ,  $\phi=90^\circ$  with a maximum directivity of 11.1 *dBi*. However, the maximum radiation occurs at  $\theta = 44^\circ$ ,  $\phi=90^\circ$  for antenna array 0 with a maximum directivity of 9.24 *dBi*.

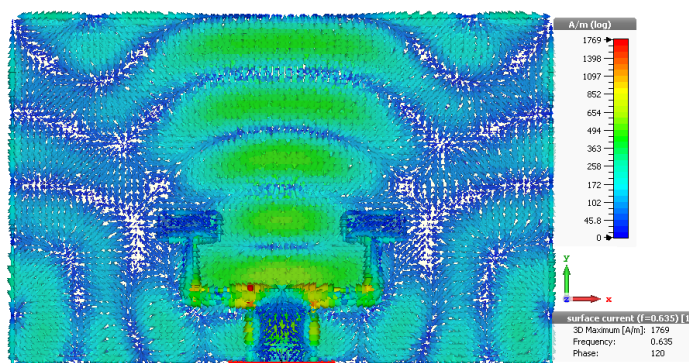
Fig.3.7 shows the surface current of antenna array 0 based on the homogeneous substrate and antenna array 1 based on PBG at their resonance frequencies with the phase of 120 using CST Microwave Studio. It is clearly noticed that the transmitted power from the feed line is dispatched through the patches and then into outer space (air), where most of the power in the substrate is radiated. The advantage of using a PBG substrate is maintained as most of the power is radiated, moreover, a significant reduction in the reflected power from the antenna-air edge interfaces is achieved. Thus, considering the obtained results, antenna array 1 outperformed antenna array 0.



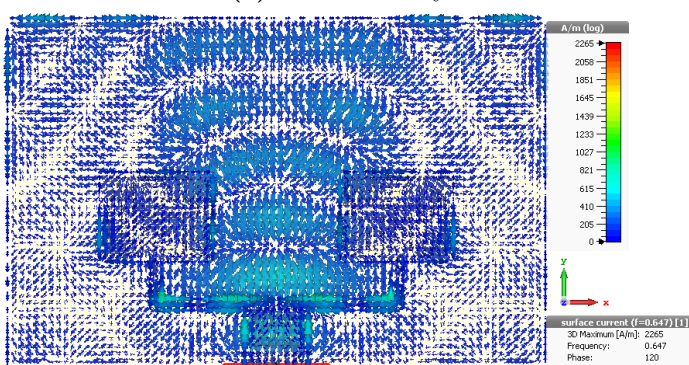
**Figure 3.6** – Polar plots of the radiation patterns for antenna array 0 and antenna array 1 at their resonance frequencies for the  $\theta$  and  $\phi$  planes, which define the solid angle of the maximum radiation.

### 3.2.2 Antenna Array Design Based on Aperiodic Photonic Crystals

The next step in this antenna array design is to analyze and enhance the performance of antenna array 1 and then compare it to the conventional antenna array based on



(a) Antenna array 0.



(b) Antenna array 1.

**Figure 3.7** – Current distribution.

the homogeneous substrate, therefore, five antenna arrays are designed based on the antenna array 1 structure with five different PC substrates by using optimized air holes radii in the substrate in order to distinguish the effect of different optimization choices such as air holes radii on the antenna array performance, furthermore, the non-transmission frequency band in the aperiodic PC will further reduce the substrate absorption and improve the radiation characteristics of the antenna array [14, 135]. Fig.3.8 shows the geometry of the proposed antenna arrays based on aperiodic PCs, where the air cylinder holes in the substrate are grouped into several sets, each set having its own radius. Fig.3.8a shows antenna array 2 with five sets of air holes, where each set contains similar air holes forming a ring. Fig.3.8b shows antenna array 3 with nine sets of air holes that are horizontally different. Fig.3.8c shows antenna array 4 with five sets of air holes, which are horizontally symmetrical to the center of the design. Fig.3.8d shows antenna array 5 with seven sets of air holes that are vertically

symmetrical to the center of the design. Finally, Fig.3.8e shows antenna array 6 with fourteen sets of air holes that are vertically different. The air cylinders holes radii of each geometry are optimized for the highest performance as summarized in Table 3.2.

**Table 3.2** – The optimized radii air cylinder holes of the proposed antenna arrays.

Radii ( $\mu m$ )	Antenna array				
	2	3	4	5	6
$R1$	26	26	25.11	38	39
$R2$	33	33	32.33	19.87	21.5
$R3$	33	33	25.11	31.87	40
$R4$	15	20.95	14.8	22.28	38
$R5$	29	29	28.39	25.91	20
$R6$	**	35	**	21.80	28
$R7$	**	38	**	18.14	20
$R8$	**	35	**	**	30.48
$R9$	**	25.11	**	**	12
$R10$	**	**	**	**	23.9
$R11$	**	**	**	**	36
$R12$	**	**	**	**	40
$R13$	**	**	**	**	24
$R14$	**	**	**	**	40

Fig.3.9 shows the magnitudes of the scattering parameter  $S_{11}$  of all proposed antenna arrays based on aperiodic PCs substrate and homogeneous substrate where they resonated close to the desired frequency of 0.65 THz within the range from 0.63 to 0.69 THz, where Fig.3.10 shows the gain and radiation efficiency of all designed antenna arrays in this study in the frequency range of 0.55-0.75 THz. It is noticed that the performance of the designed antenna arrays based on aperiodic PCs substrate improved compared to periodic PCs and homogeneous substrates in terms of the return loss, gain and radiation efficiency, however, the bandwidth remained closer to the maximum bandwidth of 299.29 GHz which was achieved by antenna array 1. Therefore, the obtained return loss, gain and radiation efficiency were -85.61 dB, 10.88 dB and 87.55 %, respectively, for antenna array 2. -71.54 dB, 11.28 dB and 89.24 %, respectively, for antenna array 3. -83.85 dB, 10.85 dB and 87.84 %, respectively, for antenna array 4. -91.18 dB, 11.16 dB and 86.11 %, respectively, for antenna array

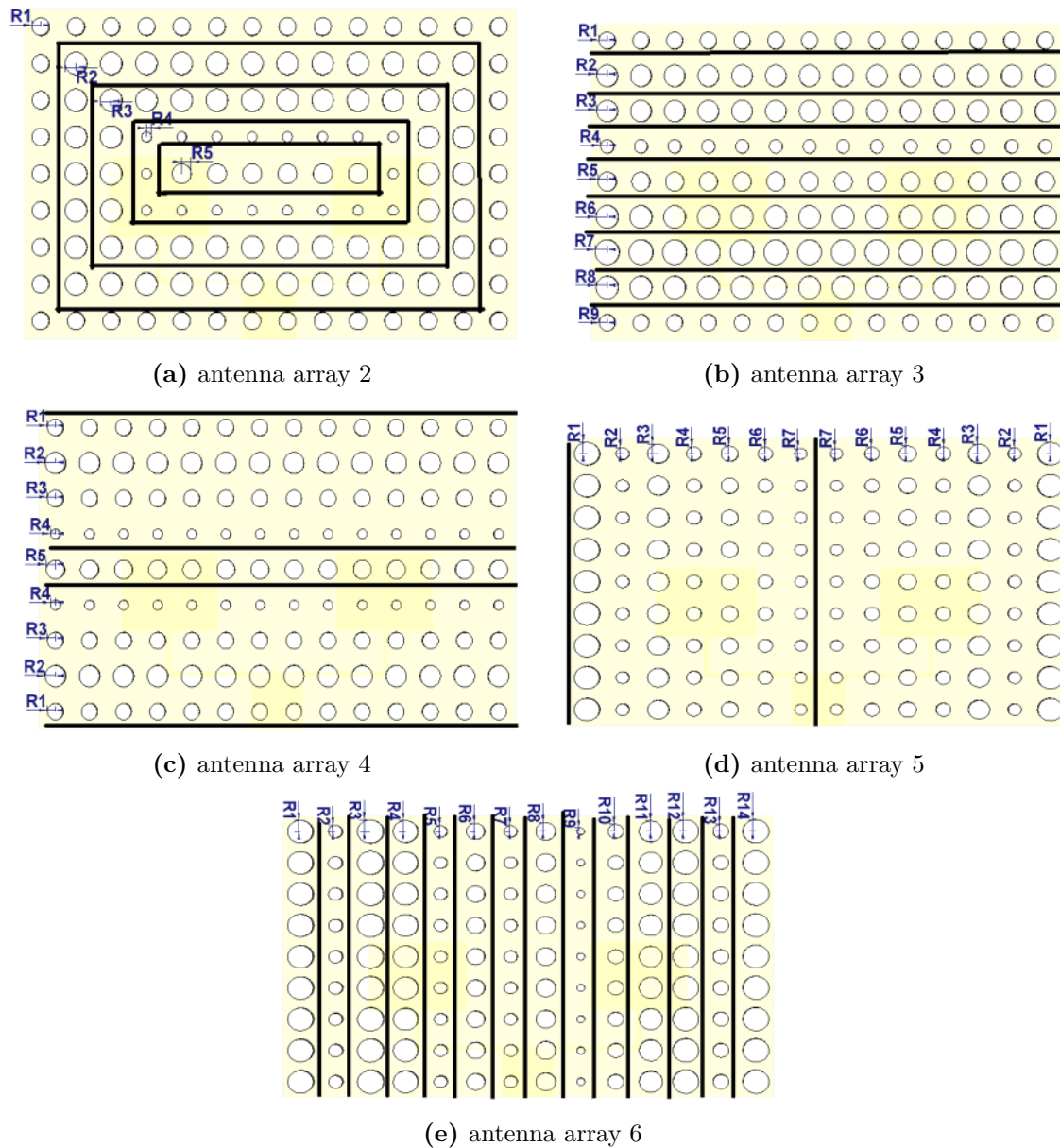


**Figure 3.8** – The geometry of the proposed antenna array based on an aperiodic PCs substrate.

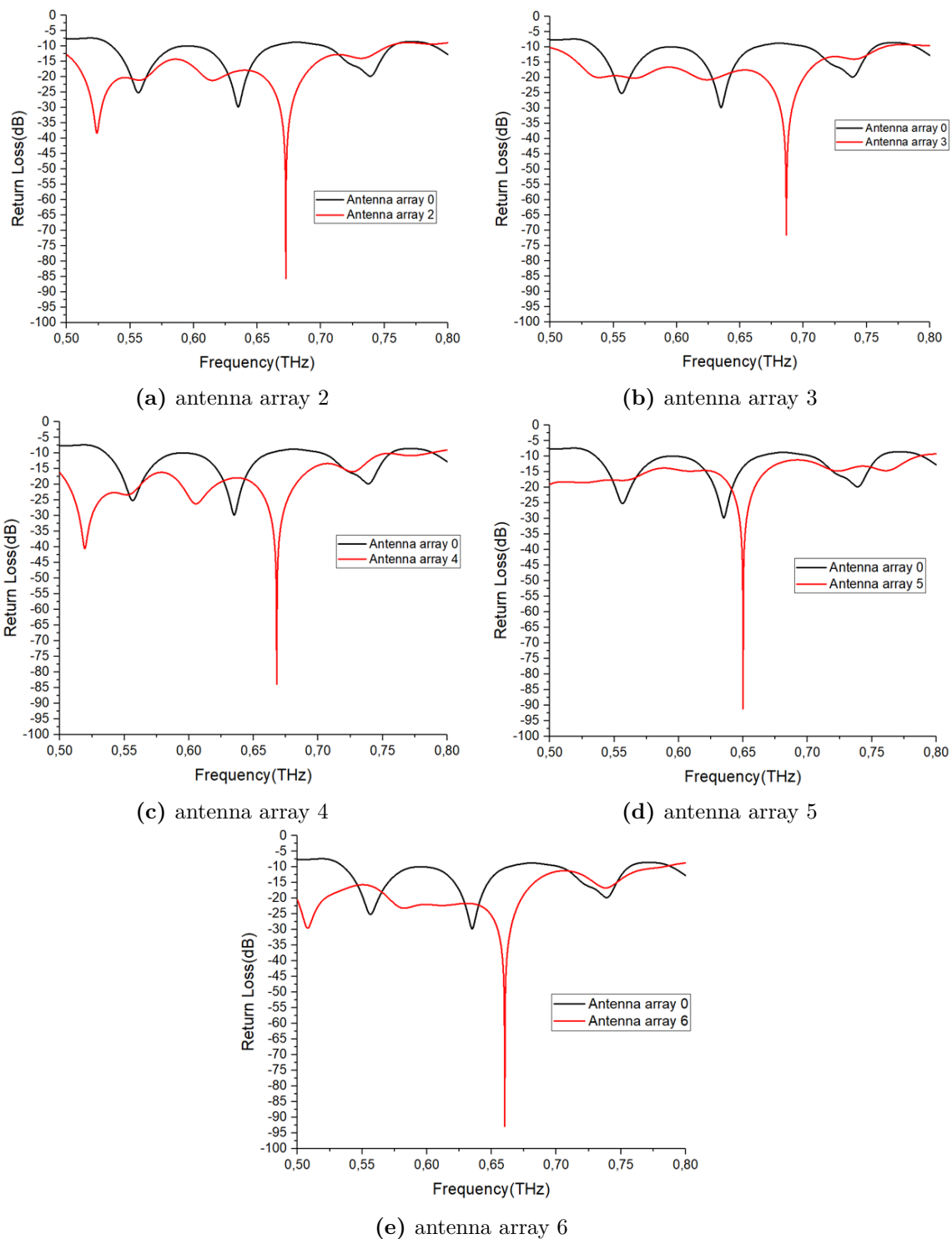
5.  $-92.89$  dB,  $11.77$  dB and  $87.63$  %, respectively, for antenna array 6. Whereas, the conventional antenna array based on the homogeneous substrate obtained  $-29.73$  dB,  $8.47$  dB and  $84.21$  %, respectively. It is obvious that the antenna array with more sets of optimized air holes radii, the high radiation characteristics achieved as found in antenna array 6 and antenna array 3. Hence, antenna array 6 achieved the

best performance among all the designed antenna arrays. According to the obtained results, it is clear that these five designed antenna arrays based on aperiodic PCs outperformed the conventional antenna array based on the homogeneous substrate in terms of return loss, bandwidth, gain and radiation efficiency.

**Table 3.3** – Comparison of the proposed designed antenna arrays and previously reported designs.

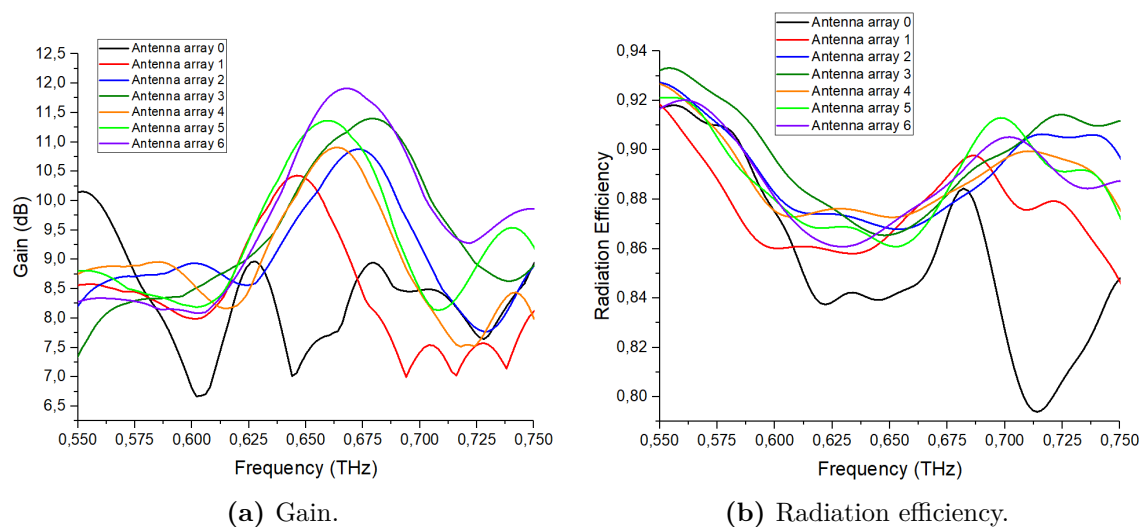
	Antenna size ( $\mu m^2$ )	$f_r$ (THz)	$S_{11}$ (dB)	BW (GHz)	Gain (dB)	D (dBi)	Rad.Eff (%)
[141]	433.2 x 208.98	0.75	-35	50	5.09	5.71	86.58
[175]	208 x 180	0.69	-64.16	26.7	6.793	6.914	85.78
[166]	700 x 660	0.63	-59.15	29.79	9.45	10.10	90.6
[176]	800 x 600	0.6308	-44.71	36.23	7.94	8.612	85.71
[134]	600 x 600	0.63	-56.81	$\gg 230$	8.95	-	89.31
[134]	600 x 600	0.61	-83.73	$\gg 230$	9.19	-	90.84
Antenna array 0	1513.4 x 972.9	0.635	-29.73	62.81	8.47	9.24	84.21
Antenna array 1	1513.4 x 972.9	0.647	-65.96	$\gg 299.29$	10.43	11.10	86.35
Antenna array 2	1513.4 x 972.9	0.673	-85.61	$\gg 253.51$	10.88	11.40	87.55
Antenna array 3	1513.4 x 972.9	0.687	-71.54	$\gg 263.40$	11.28	11.80	89.24
Antenna array 4	1513.4 x 972.9	0.668	-83.85	$\gg 286$	10.85	11.40	87.84
Antenna array 5	1513.4 x 972.9	0.65	-91.18	$\gg 286$	11.16	11.80	86.11
Antenna array 6	1513.4 x 972.9	0.66	-92.89	$\gg 282$	11.77	12.30	87.63

Fig.3.11 shows the 2D far-field radiation pattern for all designed antenna arrays based on aperiodic PCs substrate and the homogeneous substrate in the planes containing the solid angle at which the maximum radiation was achieved. The maximum radiation occurs at  $\theta = 40^\circ$ ,  $\phi=90^\circ$  for all antenna arrays that are designed based on aperiodic PCs. Therefore, antenna array 6 achieved the maximum directivity in this design with the value of 12.30 dBi, then antenna arrays 3 and 5 achieved the same directivity of 11.80 dBi. Finally, antenna arrays 2 and 4 achieved directivity of 11.50 dBi and 11.40 dBi, respectively, whereas, antenna array 0 achieved only 9.24 dBi.



**Figure 3.9** – Magnitudes of the scattering parameter  $S_{11}$  the proposed antenna arrays based on an aperiodic PCs substrate.





**Figure 3.10** – Gain and radiation efficiency of all proposed antenna arrays in the frequency range from 0.55-0.75 THz.

Also, The side lobes were greatest in the antenna array 0 compared to the other antenna arrays, however, the side lobes are reduced after applying the photonic crystal, as found in antenna array 3 and antenna array 5 as  $\theta = 40^\circ$  and  $\phi = 90^\circ$ , respectively.

The surface current of the proposed antenna arrays based on aperiodic PCs at their resonance frequencies with the phase of 120 is shown in Fig.3.12. The transmitted power from the feeder is dispatched through the radiated patches and then into outer space, in which most of the power in the substrate is radiated. The advantage of using an aperiodic PBG substrate is maintained as most of the power is radiated, moreover, a significant reduction in the reflected power from the antenna-air edge interfaces is achieved.

The simulated results showed the performance of the proposed antenna array improved after employing the PBG substrate in terms of the return loss, bandwidth, gain and radiation efficiency due to the suppression of the excitation of the surface waves found in the homogeneous substrate. The novelty of this study is the enhancement of the radiation characteristics of the antenna array by using optimized PC substrates, as illustrated in Fig.3.8, which provided extra performance with resonance frequencies close to the desired frequency of 0.65 THz. Hence, the proposed antenna arrays can

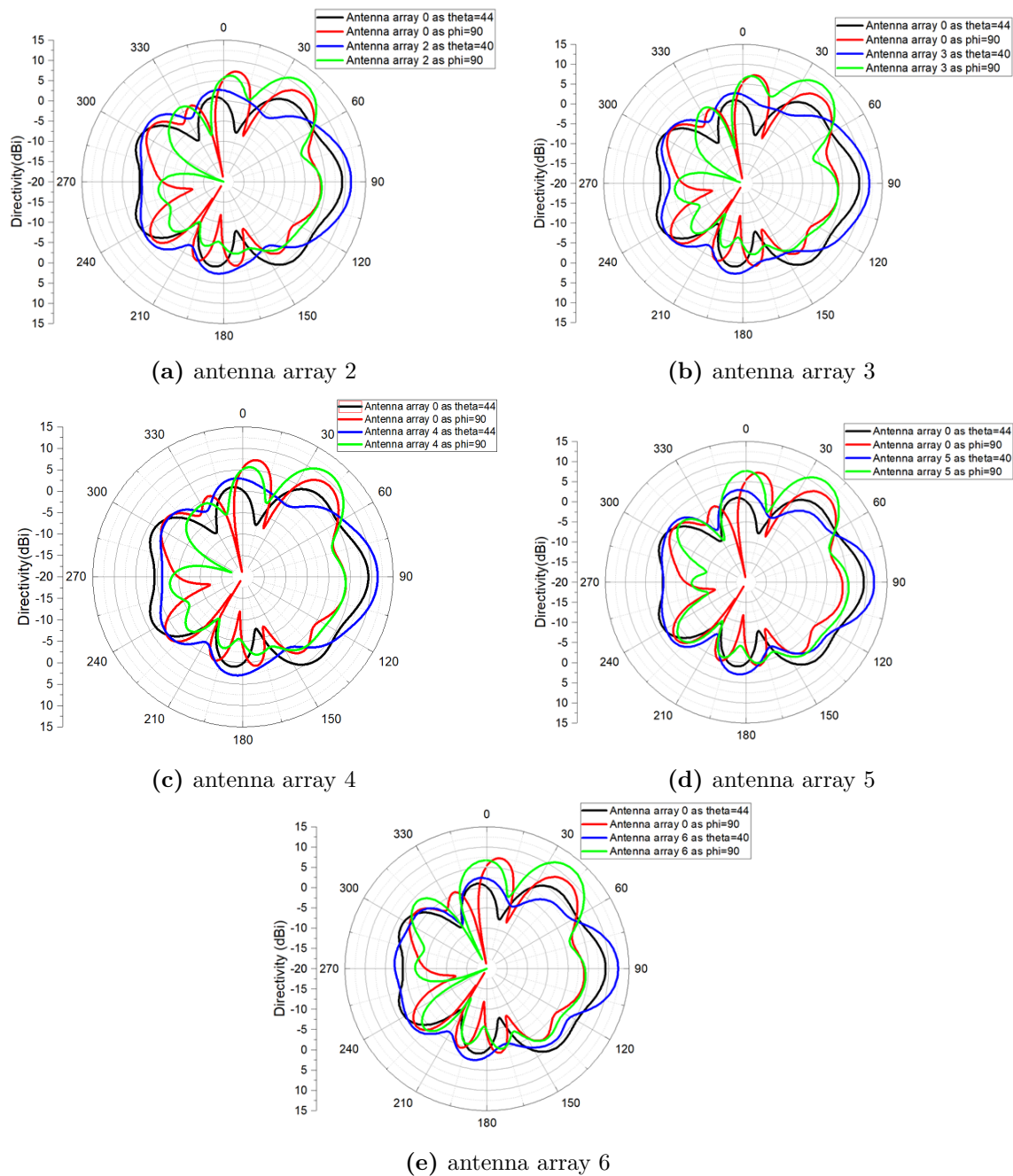


**Figure 3.11** – Polar plot of the proposed antenna arrays radiation patterns.

be useful in the next-generation wireless communication technologies such as imaging, sensing and detection, because of their high gain, very low return loss, larger bandwidth and most importantly their resonance frequencies were determined as close to 0.65 THz, where a low atmospheric attenuation window exists in the THz band. It



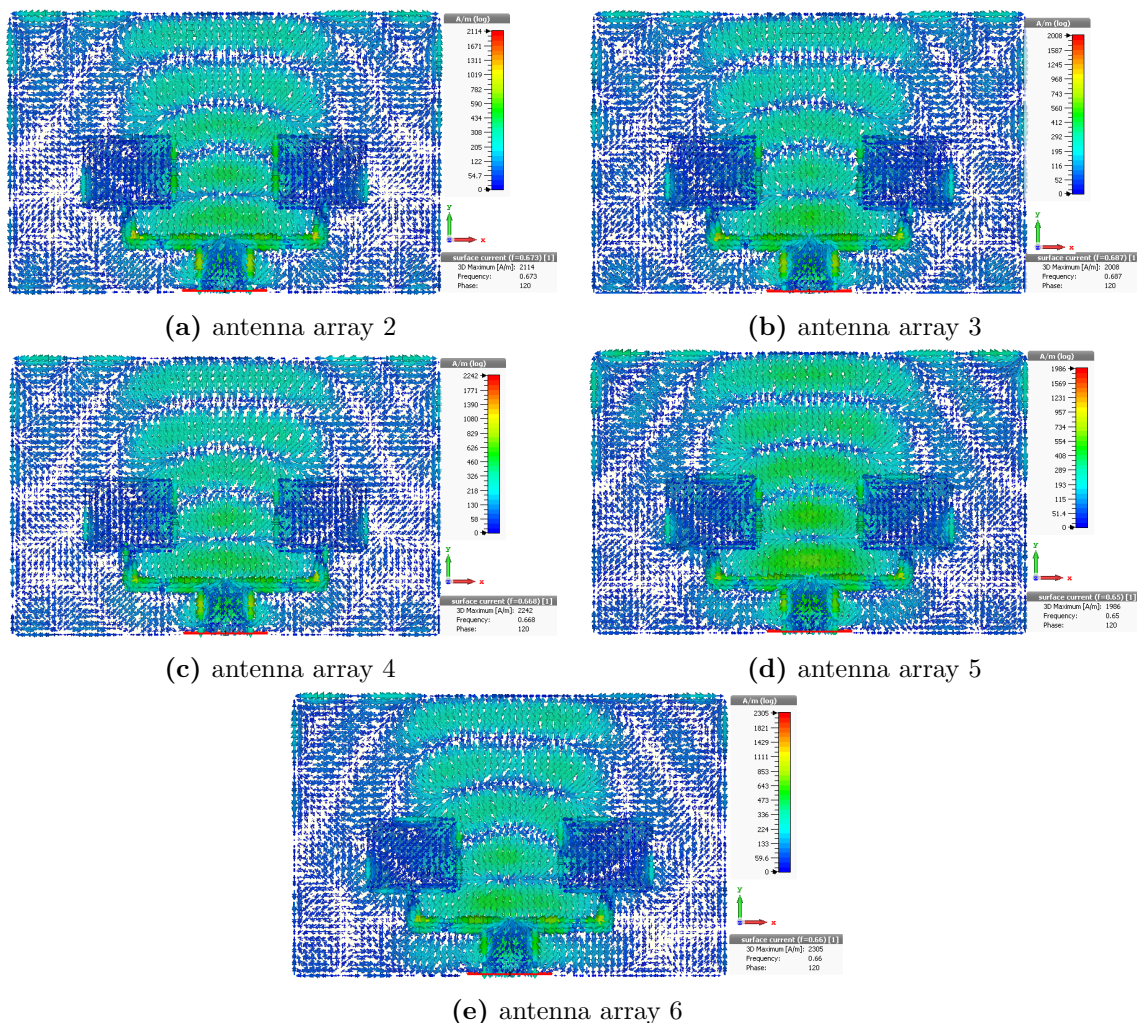


**Figure 3.12** – Current distribution.

could be worth interesting to observe that with the change in the air cylinder holes, the designed five antenna arrays performed better than the antenna array based on unmodified air cylinders holes in terms of return loss, gain and radiation efficiency, which can be found in antenna array 6, which achieved improvements of 212.45 %, more than 349 %, 39 % and 4.1 % in the return loss, bandwidth, gain and radiation efficiency, respectively, compared to the conventional antenna array based on the homogeneous substrate. Moreover, antenna array 6 achieved improvements of 40.83 %, 12.85 % and 1.48 % in the return loss, gain and radiation efficiency, respectively, compared to antenna array 1 based on an unmodified PC substrate.

Table 3.3 presents the overall radiation characteristics of the proposed antenna arrays in comparison with the existing designs. The highest gain and bandwidth in this study were 11.77 *dB* and greater than 299.29 GHz, respectively, which were achieved by antenna array 6 that is designed based on optimized PCs and antenna array 1 that is designed based on periodic PCs, respectively. These results show superior performance compared with the results of existing antennas in the literature that offer gain and bandwidth of 5.09 *dB* and 50 GHz [141], respectively. 6.793 *dB* and 26.7 GHz [175], respectively. 9.45 *dB* and 29.79 GHz [166], respectively. 7.94 *dB* and 36.23 GHz [117], respectively. 8.95 *dB*, 9.19 *dB* and greater than 230 GHz [134]. respectively. And most interestingly 8.47 *dB* and 62.81 GHz, respectively, for the conventional antenna array based on a homogeneous substrate. This comparison reveals that the proposed antenna arrays are favorable based on the requirements of the desired applications.

### 3.3 Design and Analysis of a 1x2 Circular Microstrip Patch Antenna Array Based on Modified Photonic Crystals Substrate

In this section, a high gain novel 1×2 CMPA array is proposed to operate around 0.65 THz based on different substrates. First, the effects of the PC have been investigated by using air cylinders holes and air cuboids holes embedded in a thick polyimide substrate. The simulation results showed that the best radiation characteristics were achieved when the air cuboids holes were employed. Next, a novel technique for the gain enhancement of the proposed antenna array is done by mixing the air cylinders holes with the air cuboids holes with a modified diameter value. This technique resulted in an enhancement in the gain.

### 3.3.1 Antenna Array Design Based on Cylindrical and Cuboid Photonic Crystal Substrate

In this subsection, a 1x2 microstrip patch antenna array is proposed which consists of two identical radiating patches which are circular in the shape of a radius  $195 \mu m$  designed with the parallel feed arrangement and separated by a distance of  $690 \mu m$ . The parallel or corporate feed has a single input port and multiple feed lines in parallel with the output port, each of these feed lines is terminated at an individual radiating patch [13]. Impedance matching techniques can be categorized into two broad categories i.e. Distributed Method and Lumped Element Method. Distributed Method can be done by structural modification via stubs and transformer, however, this method increases the size of the antenna and is not recommended for array systems. Lumped Element Method can be done by inserting a matching network i.e. inductor and capacitor, which is introduced to realize impedance matching between antenna array patches and feed structures [177]. The resonant input resistance of the edge-fed patch antenna array can be easily tuned to  $50 \Omega$ . Therefore, the width of the feed network  $W$  is given by [12]:

$$W = \exp\left(\frac{Z_c}{87\sqrt{\epsilon_r + 1.41}}\right) \frac{0.8}{5.98h} \quad (3.5)$$

where  $Z_c$  is the impedance of the feed line  $W$ ,  $\epsilon_r$ , and  $h$  are the dielectric constant and the height of the substrate material, respectively. The lengths  $L$  and  $L_f$  provide impedance transformation and phase matching on the radiated patches, respectively, which can be obtained using Eqs.(3.3) and (3.4).

The proposed antenna array structure is designed based on the PC substrate whose host material is also polyimide where  $\epsilon_r=3.5$  and  $\tan\delta=0.0027$  of thickness  $85 \mu m$ . However, the PC structure is made of air cylinders holes and air cuboids holes embedded in a polyimide dielectric material. The geometric configuration of the air cylinder hole and air cuboid hole embedded in the dielectric substrate unit cell is shown in Fig.3.13. The dimensions of the square unit cell for both the air cylinder hole and air cuboid hole are similar of  $109 \times 109 \mu m^2$  with a lattice constant and diameter

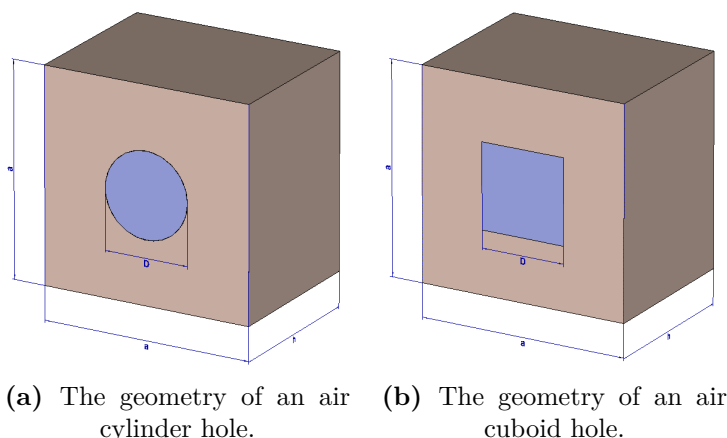
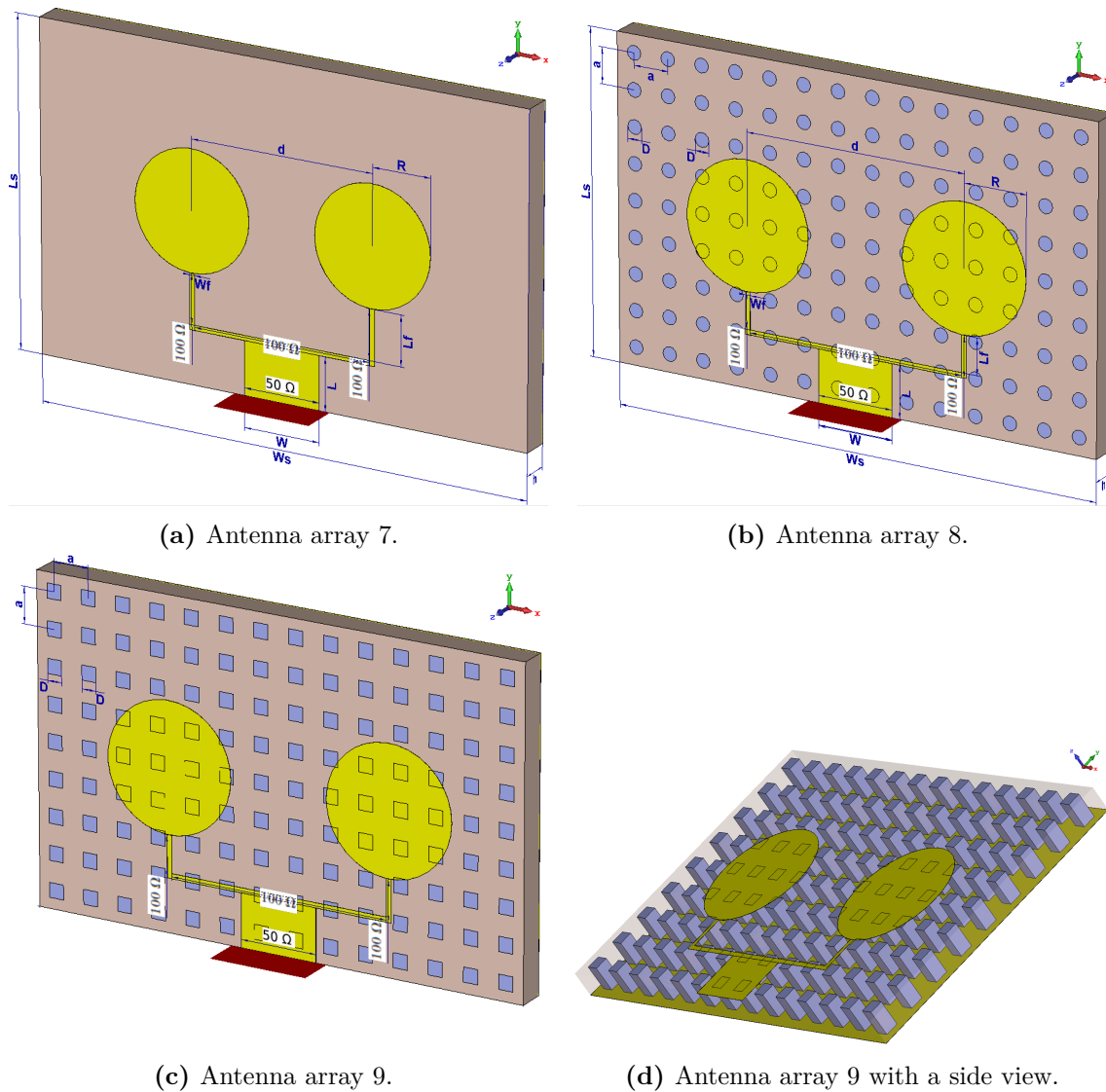


**Figure 3.13** – The geometry of the unit cell.

**Table 3.4** – Parameter values for antenna array 7 based on a homogeneous substrate, antenna array 8, and antenna array 9 based on a periodic PBG substrate.

Parameter	Value ( $\mu m$ )	
	Antenna array 0	Antenna arrays 1 and 2
Patch radius ( $R$ )	180	195
Distance between patches ( $d$ )	565	690
Substrate thickness ( $h$ )	85	85
Lattice constant ( $a$ )	**	109
Substrate width ( $W_s$ )	$14 \times a$	$14 \times a$
Substrate length ( $L_s$ )	$9 \times a$	$9 \times a$
Cylinder/Cuboids diameter ( $D$ )	**	44
Width of $50 \Omega$ microstrip line ( $W$ )	235	235
Length of $50 \Omega$ microstrip line ( $L$ )	160	160
Width of $100 \Omega$ line to the patch ( $W_f$ )	15	15
Length of $100 \Omega$ line to the patch ( $L_f$ )	150	111.4

of  $109 \mu m$  and  $44 \mu m$ , respectively, and a thickness of  $85 \mu m$ . Hence, the proposed 1x2 **CMPA** array structure is designed based on two different **PC** substrates, antenna array 8 is designed based on periodic air cylinders holes and antenna array 9 is designed based on periodic air cuboids holes. Antenna array 7, namely a conventional antenna array based on the homogeneous polyimide substrate, which is designed and simulated for comparison and analysis purposes. Fig.3.14 shows the structures of antenna array 7, antenna array 8, and antenna array 9 based on the homogeneous and periodic **PBG** substrates, respectively. The physical dimension of each element is shown in Table



(a) Antenna array 7.

(b) Antenna array 8.

(c) Antenna array 9.

(d) Antenna array 9 with a side view.

**Figure 3.14** – The geometry of the proposed antenna arrays based on the homogeneous and periodic PBG substrates.

3.4. The thickness of the employed metal was  $0.5 \mu m$ . The radiation characteristics of the proposed antenna arrays 7, 8, and 9 are investigated and analyzed around 0.65 THz using the CST Microwave Studio in terms of return loss, bandwidth, gain, directivity, and radiation efficiency.

Fig.3.15 shows the return loss versus the frequency for the different antenna array configurations, which indicates that antenna array 7 had a return loss of  $-20.75 dB$  at a resonance frequency of 0.63 THz and bandwidth greater than 194 GHz, whereas,

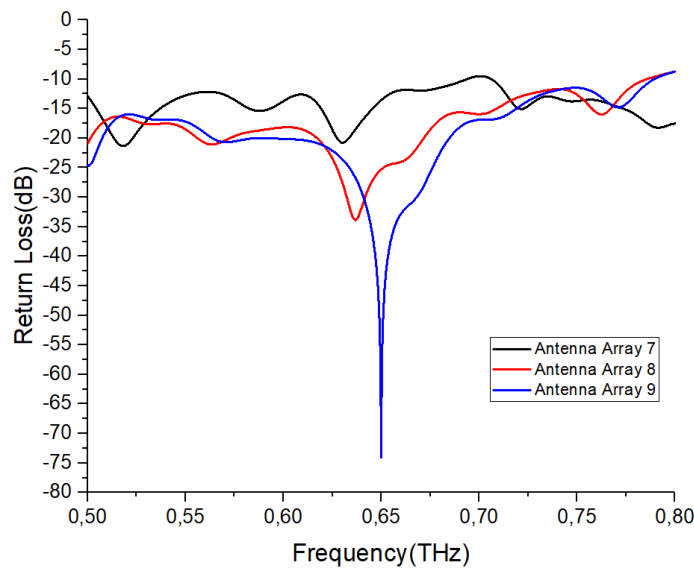


**Figure 3.15** – Return loss versus the frequency of the proposed antenna arrays.

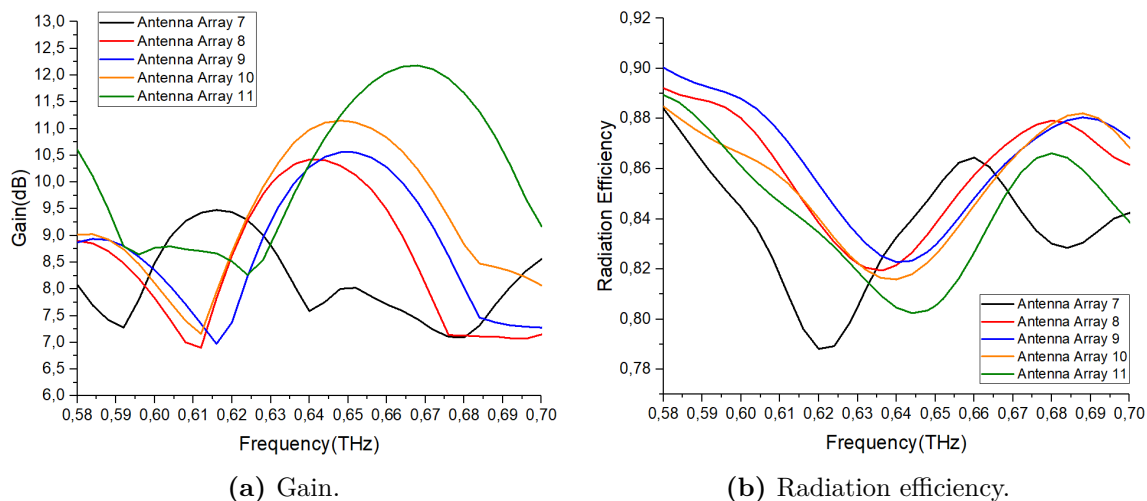


**Figure 3.16** – Gain and radiation efficiency of all proposed antenna arrays in the frequency range of 0.58-0.70 THz.

antenna array 8 achieved a return loss of  $-33.85\text{ dB}$  at a resonance frequency of  $0.637\text{ THz}$  and bandwidth greater than  $286\text{ GHz}$ . Finally, antenna array 9 resonated exactly at the frequency of  $0.65\text{ THz}$  with a minimal return loss of  $-74.10\text{ dB}$  and achieved the largest bandwidth which is greater than  $290\text{ GHz}$ . Thus, there was a noticeable improvement in the return loss and the bandwidth after employing the PC substrate.

The gain and radiation efficiency versus the frequency of all the designed antenna



arrays in the frequency range of 0.58-0.70 THz are shown the Fig.3.16a and Fig.3.16b, respectively. The results clearly showed that the gain and radiation efficiency were enhanced for antenna array 8 and antenna array 9 based on periodic PCs substrate. So, antenna array 9 achieved the maximum gain and radiation efficiency in this study with the values of 10.57 dB (20.11 %) and 82.96 %, respectively at 0.65 THz, then, antenna array 8 achieved a gain of 10.35 dB (17.61 %) and radiation efficiency of 81.96 % at 0.637 THz, compared to antenna array 7 based on a homogeneous substrate that obtained a gain of 8.80 dB and radiation efficiency of 80.55 % at 0.63 THz. It could be worth interesting to observe that antenna array 9 designed based on a circular patch with periodic air cuboids holes has achieved enhancement of 1.34 % and 12.34 % in the gain and return loss, respectively compared to antenna array 1 which is designed based on a rectangular patch with periodic air cylinders holes in Section 3.2.

Fig.3.17 shows the radiation pattern in dB for the proposed antenna arrays at their resonant frequencies in the plane containing the solid angle  $\theta$  at which the maximum radiation was achieved. The maximum radiation in the pattern of antenna array 7 occurred at  $\theta = 45^\circ$  with a directivity of 9.74 dBi. Then, the maximum radiation in the pattern of antenna array 8 occurred at  $\theta = 39^\circ$  with a directivity of 11.20 dBi. Finally, the maximum radiation in the pattern of antenna array 9 occurred at  $\theta = 40^\circ$  with maximum directivity in this study of 11.40 dBi. The directivity has increased a lot after employing the PC substrate, also it is noticed that the side lobes were reduced after employing PC substrate compared to the homogeneous substrate.

Fig.3.18 shows the surface current of antenna arrays 7, 8 and 9 at their resonance frequencies with the phase of 120 using CST Microwave Studio. It is clearly noticed that the transmitted power from the feed line is dispatched through the patches and then into outer space (air), where most of the power in the substrate is radiated. The advantage of using a PBG substrate is maintained as most of the power is radiated, moreover, a significant reduction in the reflected power from the antenna-air edge interfaces is achieved. Therefore, considering the obtained results, the performance of the proposed antenna array improved by using PCs. Also, it could be worth

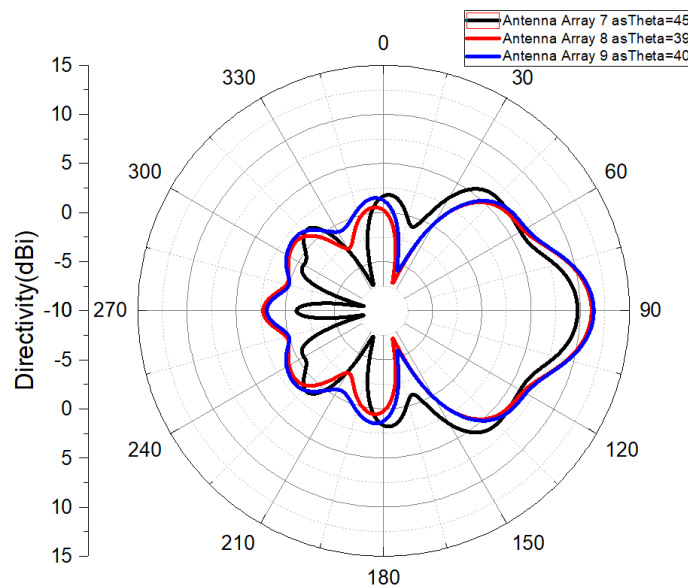
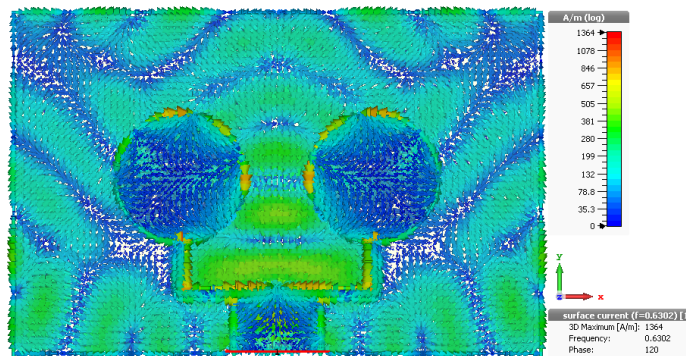


**Figure 3.17** – The radiation pattern of proposed antenna arrays based on the periodic PCs and the homogeneous substrate at their resonant frequencies for the  $\theta$  plane, which defines the solid angle of the maximum radiation.

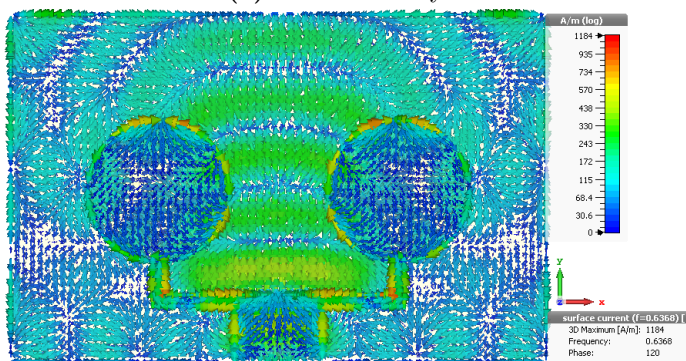
interesting to observe that by using air cuboids holes embedded in the substrate, an extra performance is observed compared to the air cylinders holes embedded in the substrate as found in antenna array 9 and antenna array 8, respectively, due to the reflection of electromagnetic waves falling in the non-transmission range.

For more clarity, the radiation characteristics of a single element patch such as return loss, bandwidth, gain, and radiation efficiency are shown in Fig.3.19. Antenna 8 is the single element patch of antenna array 8, which is designed based on periodic air cylinders holes. Antenna 9 is the single element patch of antenna array 9, which is designed based on periodic air cuboids holes. So, antenna 8 offers at a resonant frequency of 0.65 THz a return loss of  $-27.73$  dB, a bandwidth greater than 213 GHz, a gain of  $7.75$  dB, and radiation efficiency of 78.96 %. Whereas, antenna 9 offers at a resonant frequency of 0.656 THz a return loss of  $-31.42$  dB, a bandwidth greater than 209 GHz, a gain of  $7.92$  dB, and radiation efficiency of 79.32 %. Clearly, the performance of an array antenna outperforms a single element patch in terms of return loss, bandwidth, gain, and radiation efficiency.

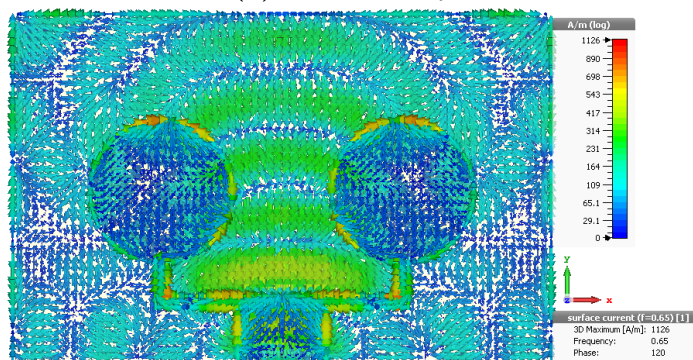




(a) Antenna array 7.



(b) Antenna array 8.

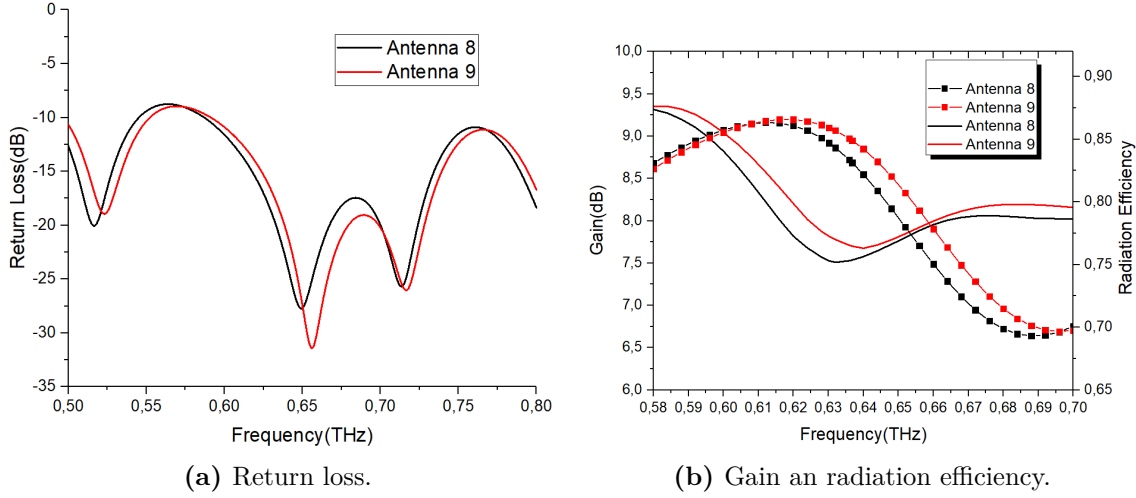


(c) Antenna array 9.

Figure 3.18 – Current distribution.

### 3.3.2 Antenna Array Performance Investigation

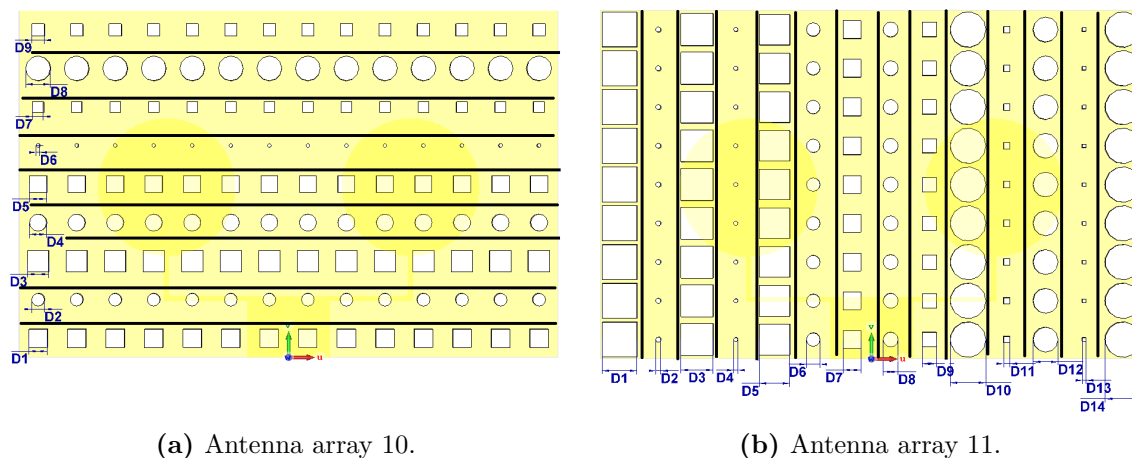
In this subsection, and in order to enhance the gain, two other antenna arrays were designed based on the structures of antenna array 8 and antenna array 9, but the substrate included mixed air cylinders holes and air cuboids holes at the same time which are divided into several sets, where each set of air cylinders holes and air cuboids holes



**Figure 3.19** – Single patch element performance based on PCs.

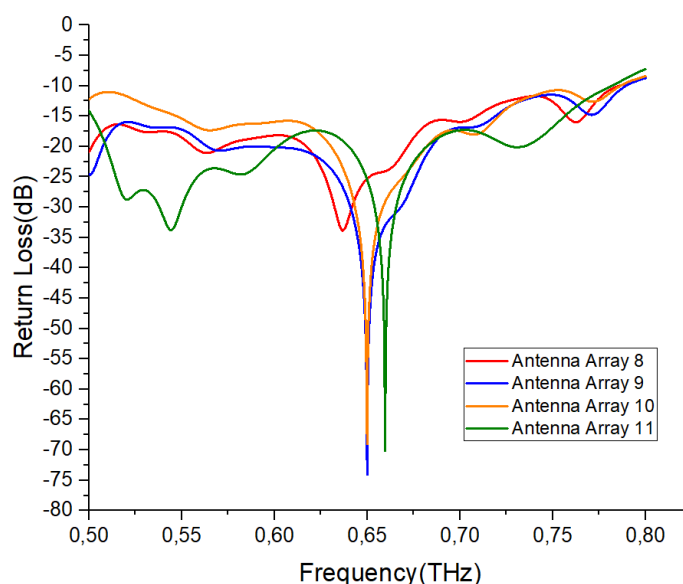
had different diameters, as shown in Fig.3.20. Therefore, Fig.3.20a shows antenna array 10 with five sets of air cuboids holes and four sets of air cylinders holes that are horizontally different, where the values of diameters are  $D_1=52 \mu m$ ,  $D_2=36 \mu m$ ,  $D_3=60 \mu m$ ,  $D_4=48.26 \mu m$ ,  $D_5=48 \mu m$ ,  $D_6=10 \mu m$ ,  $D_7=30 \mu m$ ,  $D_8=70 \mu m$ , and  $D_9=34 \mu m$ . Fig.3.20b shows antenna array 11 with seven sets of air cylinders holes and air cuboids holes that are vertically different, where the values of diameters are  $D_1=98 \mu m$ ,  $D_2=14 \mu m$ ,  $D_3=90 \mu m$ ,  $D_4=11.38 \mu m$ ,  $D_5=86 \mu m$ ,  $D_6=38 \mu m$ ,  $D_7=50 \mu m$ ,  $D_8=42 \mu m$ ,  $D_9=40 \mu m$ ,  $D_{10}=100 \mu m$ ,  $D_{11}=18 \mu m$ ,  $D_{12}=70 \mu m$ ,  $D_{13}=10 \mu m$ , and  $D_{14}=100 \mu m$ . The performance of antenna arrays 10 and 11 is compared to the performance of antenna arrays 8 and 9 in order to see the effect of non-periodic PC substrate on the gain and antenna array performance in the THz frequency band.

Fig.3.21 shows the return loss of the proposed antenna arrays based on the PCs versus the frequency, the resonant frequency is that frequency where most of the power fed goes to the radiated patch when the best impedance matching happens between the feed line and the radiated patch with very less power being reflected back. Antenna arrays 10 and 11 have almost the same resonance frequency due to the symmetrical structures with the same feeding method. Therefore, antenna array 10 resonated at the desired frequency of 0.65 THz with a minimal return loss of -69.04 dB, bandwidth greater than 287 GHz, and radiation efficiency of 82.56 %. Whereas,



**Figure 3.20** – Geometry of the proposed antenna arrays based on non-periodic PCs.

antenna array 11 resonated at 0.66 THz with a minimal return loss of  $-70.14$  dB, bandwidth greater than 282 GHz, and radiation efficiency of 82.52 %.



**Figure 3.21** – Return loss of the proposed antenna arrays based on PCs versus the frequency.

Fig.3.22 depicts the **VSWR** performance of the proposed antenna arrays. At their resonant frequencies, antenna array 7 obtained **VSWR** of 1.2. Whereas, antenna arrays 8, 9, 10, and 11 obtained the values of 1.042, 1.0004, 1.0007, and 1.0006, respectively. The achieved values of **VSWR** are less than 2, which satisfied the con-

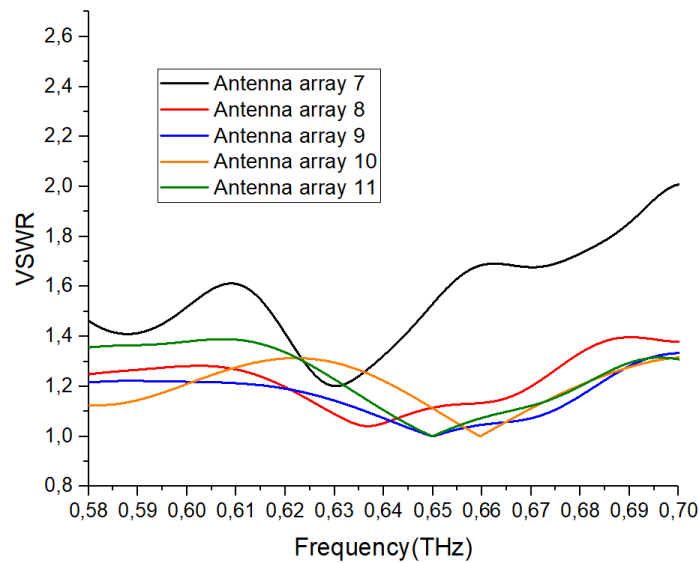


Figure 3.22 – VSWR of the proposed antenna arrays.

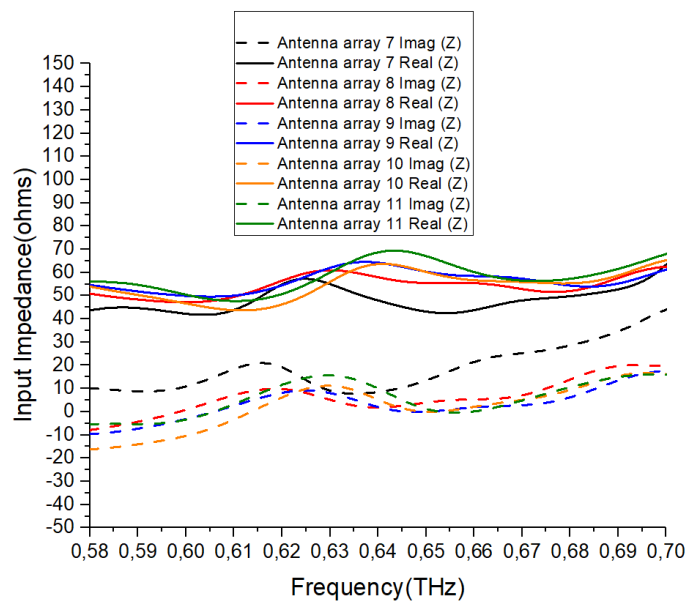


Figure 3.23 – The input impedance characteristics of the proposed antenna arrays.

dition for perfect impedance matching. The ideal value of VSWR should be equal to 1 which means 100 % power is accepted and zero reflection[139].

Fig.3.23 shows the input impedance characteristic of the proposed antenna arrays, which defines impedance matching between the input signal and the feed line. At their resonant frequencies, the input impedance of antenna arrays 7, 8, 9, 10 and 11 are

54.86  $\Omega$  in the real part and 9  $\Omega$  in the imaginary part, 59.28  $\Omega$  in the real part and 2.18  $\Omega$  in the imaginary part, 60.34  $\Omega$  in the real part and -0.02  $\Omega$  in the imaginary part, 60.27  $\Omega$  in the real part and -0.023  $\Omega$  in the imaginary part and 60.43  $\Omega$  in the real part and 0.011  $\Omega$  in the imaginary part, respectively. The value of the input impedance should be around 50  $\Omega$  in real and around 0  $\Omega$  in imaginary to properly match the input signal and the feed line [178].

There was a remarkable enhancement in the gain by using non-periodic PCs substrate compared to periodic PCs substrate and the homogeneous substrate. Thus, antenna array 10 achieved a gain of 11.14 dB with enhancements of 5.4 %, 7.63 % and 26.60 %, compared to antenna arrays 9, 8 and 7, respectively. Finally, antenna array 11 achieved the highest gain among all designed antenna arrays of 12.03 dB with enhancements of 13.81 %, 16.23 % and 36.70 % compared to antenna arrays 9, 8, and 7, respectively. The reason why antenna array 11 achieves the highest gain in this work, is because antenna array 11 has more sets of optimized air holes compared to antenna arrays 8, 9 and 10. Also, more sets of optimized air holes with different diameters create a discontinuity in the substrate which reduces the dielectric permittivity, thereby causing dielectric loss and conductor loss. These losses will definitely contribute to a drop in radiation efficiency. The radiation characteristics such as return loss, bandwidth, and radiation efficiency of antenna arrays 10 and 11 remained close to the maximum radiation characteristics that were achieved by antenna array 9, however, the gain was enhanced after employing non-periodic PCs substrate. It could be worth interesting to observe that antenna array 11 designed based on a circular patch with non-periodic PCs including mixed air cuboids holes and air cylinders holes has achieved an enhancement of 2.21 % in the gain compared to antenna array 6 which is designed based on a rectangular patch with non-periodic air cylinders holes in Section 3.2.

Fig.3.24 shows the effect on the gain with similar and different diameters for mixed air cylinders and air cuboids in antenna arrays 10 and 11, the value of the diameters has been varied from 10 to 90  $\mu m$ , clearly that the gain of antenna arrays 10 and 11 strongly depends on the diameters of the air cylinders and the air cuboids,

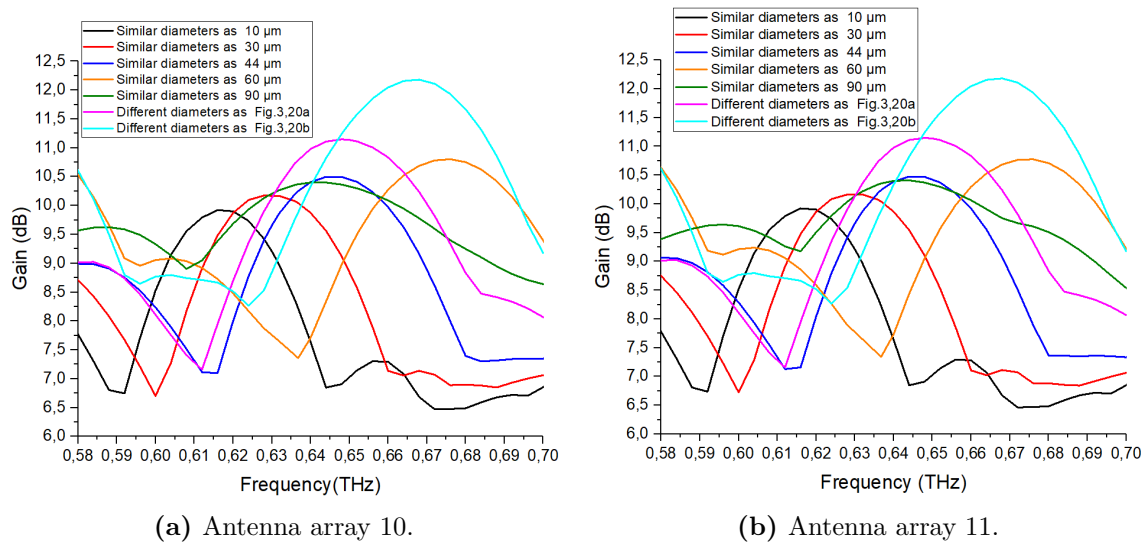


Figure 3.24 – Effect of diameters of the PCs on the gain.

furthermore, distinct diameters leads to higher gain.

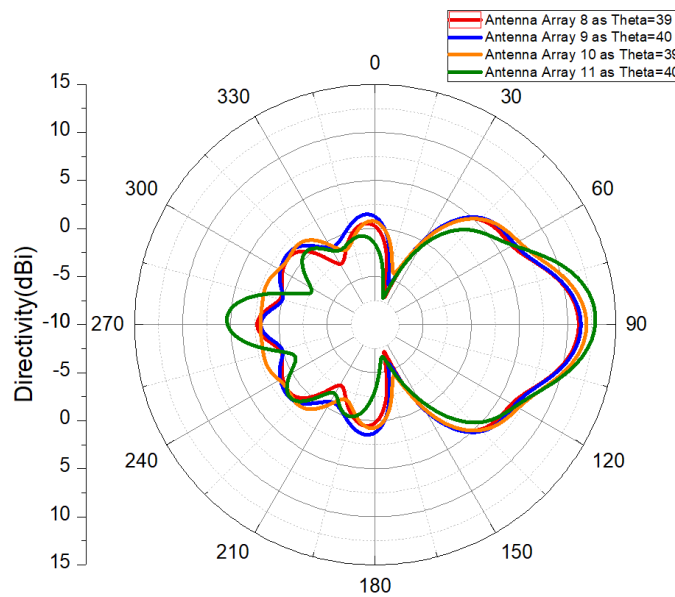
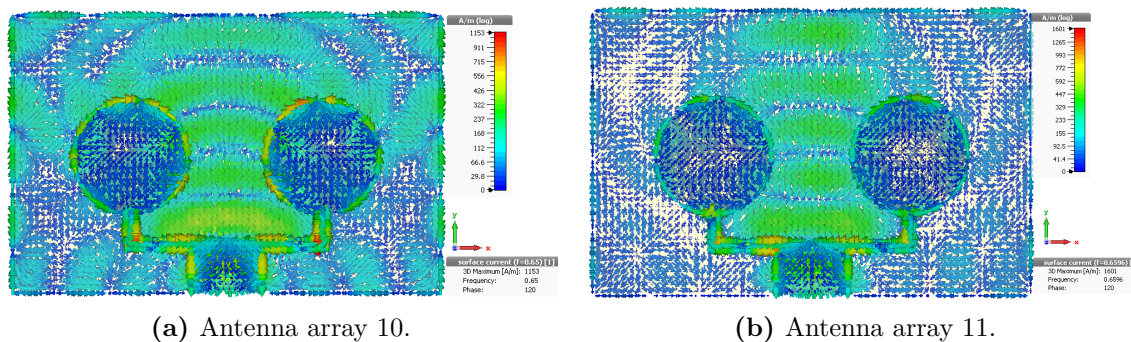


Figure 3.25 – The radiation pattern of the proposed antenna arrays based on periodic and non-periodic PCs at their resonant frequencies.

Since the gain and directivity are proportionally related, an enhancement in the directivity also is noticed. Therefore, the maximum directivity is achieved by antenna array 11 of 12.90 dBi where the maximum radiation in the pattern occurred at  $\theta=40^\circ$ , whereas, antenna array 10 achieved directivity of 12 dBi where the maximum



radiation in the pattern occurred at  $\theta = 39^\circ$ . The far-field radiation patterns are shown in Fig.3.25 for all designed antenna arrays based on PCs substrate.



**Figure 3.26** – Current distribution.

Fig. 3.26 shows the surface current of antenna arrays 10 and 11 at their resonance frequencies with the phase of 120 using CST Microwave Studio. It can be seen that the surface current distribution is sort of arrows, which is intense in the transmission line and radiated patches edges towards the direction of the y-plane where most of the power in the substrate is radiated. The surface current distribution is also presented in the substrate due to the fact that the simulated polyimide substrate is a lossy dielectric. The utilization of the periodic and non-periodic PC structures reduces the effective permittivity of the substrate which leads to a different variation of the surface current distribution. The advantage of using a PBG substrate is maintained as most of the power is radiated, moreover, a significant reduction in the reflected power from the antenna-air edge interfaces is achieved.

The simulation results indicated that the performance of the proposed antenna array based on the PC substrate containing air cylinders holes and air cuboids holes improved in terms of the return loss, bandwidth, gain, and radiation efficiency due to the suppression of the surface waves that are found in the conventional antenna array based on a homogeneous substrate. The novelty of this study is the enhancement of the antenna array gain by using mixed air cylinders holes and air cuboids holes embedded in the substrate as shown in Fig.3.20 causing more suppression of the undesirable excited surface waves in the substrate which enhances the gain. These results showed

**Table 3.5** – Comparison of the proposed designed antenna arrays and previously reported designs.

	Antenna size ( $\mu m^2$ )	$f_r$ (THz)	$S_{11}$ (dB)	BW (GHz)	Gain (dB)	D (dBi)	Rad.Eff (%)
[176]	800 x 600	0.6308	-44.71	36.23	7.94	8.612	85.71
[134]	600 x 600	0.63	-56.81	$\gg 230$	8.95	-	89.31
[134]	600 x 600	0.61	-83.73	$\gg 230$	9.19	-	90.84
[179]	600 x 300	0.472	-39	435	3.9	-	84
[166]	700 x 660	0.63	-59.15	29.79	9.45	9.99	90.6
[175]	208 x 180	0.69	-64.16	26.7	6.793	6.914	85.78
Antenna array 1	1513.4 x 972.9	0.647	-65.96	$\gg 299.29$	10.43	11.10	86.35
Antenna array 6	1513.4 x 972.9	0.66	-92.89	$\gg 282$	11.77	12.30	87.63
Antenna array 7	1526 x 981	0.63	-20.75	$\gg 194$	8.80	9.74	80.55
Antenna array 8	1526 x 981	0.637	-33.85	$\gg 286$	10.35 (17.61 %)	11.20	81.96
Antenna array 9	1526 x 981	0.65	-74.10	$\gg 290$	10.57 (20.11 %)	11.40	82.96
Antenna array 10	1526 x 981	0.65	-69.04	$\gg 287$	11.14 (26.60 %)	12	82.56
Antenna array 11	1526 x 981	0.66	-70.14	$\gg 282$	12.03 (36.70 %)	12.90	82.54

that the shape of the PC has an influence on the antenna array performance. The proposed antenna arrays based on periodic and non-periodic PC substrates exhibit larger bandwidth and higher gain with resonance frequencies close to the desired frequency of 0.65 THz as required for the next-generation wireless communication technologies and other interesting applications.

Table 3.5 presents the overall radiation characteristics of the proposed antenna arrays in comparison with previously reported works. The highest gain achieved in this study was 12.03 dB which shows superior performance compared with the results of existing antennas in the literature with the enhancements of 51.51 % [117], 34.41 % [134], 30.90 % [134], 208.46 % [179], 27.30 % [166], 77.10 % [175], and most interestingly 36.70 % compared to the antenna array 7 based on the homogeneous



substrate.

### 3.4 Summary

In this chapter, several THz microstrip patch antenna arrays based on optimized PC substrate are designed and analyzed around 0.65 THz to improve the performance of the conventional antenna array that is designed based on the homogeneous substrate by suppressing undesirable surface waves, which can be useful in the next-generation wireless communication technologies such as imaging, sensing and detection. First, six THz 1x2 RMPA arrays based on different substrates, including homogeneous, periodic PCs and five new aperiodic PCs substrates are analyzed. The simulated results demonstrated that the designed antenna arrays based on an optimized PC substrate structure exhibited excellent performance improvement, as compared to the homogeneous substrate in this frequency band. However, it could be worth interesting to observe that with the change in the air cylinder holes radii, the designed five antenna arrays performed better than the antenna array based on unmodified air cylinders holes radii in terms of return loss, gain and radiation efficiency, which can be found in antenna array 6, which achieved improvements of 212.45 %, more than 349 %, 39 % and 4.1 % in the return loss, bandwidth, gain and radiation efficiency, respectively, compared to the conventional antenna array based on the homogeneous substrate. Next, the effects of the PC have been investigated further by using air cylinders holes and air cuboids holes with a 1x2 CMPA array. The simulation results showed that the best radiation characteristics were achieved when the air cuboids holes were employed as found in antenna array 9 which achieved a minimal return loss of  $-74.10$  dB, bandwidth larger than 290 GHz, a gain of 10.57 dB, and radiation efficiency of 82.96 %. Finally, a novel technique for the gain enhancement of the proposed 1x2 CMPA is done by mixing the air cylinders holes with the air cuboids holes with a modified diameter value. This technique resulted in an enhancement in the gain as found in antenna array 11 which achieved a gain of 12.03 dB.

# Chapter 4

## Design and Analysis of MIMO System for Terahertz Indoor Communications

### 4.1 Introduction

In the long term, the conversion of carrier frequencies to the THz band enables the emergence of significant real-life technologies and is a key solution that provides a very wide bandwidth that can reach hundreds of GHz in order to meet the increasing demands of ultra-high data rate transmission in the communication link [180, 181]. High capacity channels have become a very important trend to keep pace with the rapid growth of numerous wireless technologies, however, the THz channel has distinct characteristics compared to the channel of lower band systems [182]. The transmission path loss, as well as molecular absorption loss are regarded as the main issue in the THz band, due to the high atmospheric attenuation [116]. To overcome the impact of these losses at THz frequencies while supporting high data rates, antennas should exhibit both high gain at the radiation angle with the lowest loss and wide bandwidth [1]. Besides the mentioned losses, the scattering and reflection of waves behaviors are also different from those in the GHz band [20, 183, 184]. The

surfaces of indoor objects at THz are regarded as rough surfaces instead of smooth surfaces because the traveling wavelength is comparable to the roughness of indoor surfaces such as plaster or wallpaper [185]. Furthermore, the environments change quite slowly for indoor communications due to slowly moving objects compared to THz waves through a certain time window. So, it is assumed that moving objects can be counted as static objects between the transmission antenna and the receiver antenna [136]. In most situations, the channel may be influenced by fading, therefore, these distinctive features guide new models to characterize the THz channel. The use of MIMO antenna methods for THz communications may minimize signal fading concerns in wireless networks, thereby increasing system capacity and building extra high-speed communication systems for practical indoor environment applications. However, the MIMO systems have main obstacles that include limited area, antenna size, isolation and spacing [159, 186]. Therefore, graphene-based directional antennas using the Photonic Crystals (PCs) substrate can be promising candidates to overcome such limitations [17, 77, 136, 144].

Graphene is an allotrope of carbon that consists of a single layer of atoms arranged in a two-dimensional honeycomb lattice nanostructure which initially was introduced in 2004 [187]. Graphene has outstanding physicochemical properties such as high thermal and electrical conductivity, high density, good biocompatibility, low electricity consumption, and high resistance, graphene is approximately 200 times stronger than steel [188, 189]. Due to the great properties mentioned above, graphene has applicability in numerous fields like medical sensors [190], biosensing [191], filters and absorbers [192]. In addition, graphene has been used in THz antennas to improve their radiation characteristics by changing the electrostatic voltage bias [193, 194, 195].

In THz communications, there are various types of antenna designs that are needed to adapt to the THz channel. Among them, Yagi-Uda [118], Bow-Tie [196], On-chip antenna [197], Horn antenna [198], MEMS antenna [199], Leaky wave antenna [200] and Lens antenna [201]. However, a complicated design procedure and a larger size are required for these mentioned antennas to function. For this aim, the microstrip patch antennas are becoming more ubiquitous as planar technology, because of their

various advantages, including low cost, lightweight, small size, design simplicity, and compatibility with integrated circuit technology [178, 202]. Despite their numerous advantages, the conventional patch antenna suffers from a number of drawbacks, such as narrow bandwidth, low gain, poor radiation performance, and surface wave excitation due to the substrate's high permittivity and comparatively huge thickness [88, 124, 203]. These drawbacks can be overcome by introducing the concept called PCs.

A PBG material, also known as a PC, is an artificial material made of periodic implants within a surrounding medium. The PC is a new class of periodic dielectric structures that has been developed in which electromagnetic wave propagation in any direction is completely forbidden for all frequencies within a stop band, these structures have promising applications such as transmission line for biosensing, optical gate, optical and microwave [164, 204]. Moreover, it is reported that these structures have been used in the THz antenna as a substrate for gain and radiation characteristics enhancement [12, 13, 14, 15, 16, 134, 135, 205, 206]. There are different types of PCs such as 1D, 2D, or 3D structures, depending on their periodic arrangements. Two-dimensional (2D) PCs have gained a lot of interest from many researchers in recent years, because they are much easier to fabricate compared to three-dimensional (3D) PCs [125, 207, 208], furthermore, characterizing PCs structures using a purely analytical approach is generally difficult because of their complexity. Therefore, full-wave simulators such as CST Microwave Studio, which is based on FIT have been used to analyze microstrip patch antennas based on the PCs substrate [209, 210, 211].

In this chapter, a novel MIMO indoor communication system was developed using a 1x2 microstrip patch antenna array based on the optimized PCs substrate with a graphene load in order to enlarge the channel capacity. The proposed MIMO antenna array was designed around 0.65 THz to offer a high gain to overcome the path losses. The remainder of this chapter is organized as follows: The interesting characteristics of the graphene load are described and investigated in Section 4.2. In Section 4.3, the design and the performance of the proposed 1x2 RMPA array based on the homogeneous substrate, PCs and optimized PCs with a graphene load substrates are

explained and investigated. Section 4.4 covered the investigation of the radiation characteristics of the designed MIMO antenna array based on the homogeneous, PCs and optimized PCs substrates with the graphene load as well as explained the application of the proposed MIMO antenna array in a normal indoor communication environment by calculating the total path loss and the channel capacity for different system configurations and spacings, and then compared the obtained results with other results in the literature. Finally, a summary of the work is given in Section 4.5.

## 4.2 Graphene Properties

Graphene is an allotrope of carbon composed of a single layer of atoms arranged in a 2D honeycomb lattice, which can conduct better electricity and heat incredibility than copper. The equivalent permittivity of the graphene monolayer is given by [212] as:

$$\epsilon = 1 + \frac{j\sigma_g\eta_0}{K_0\Delta} \quad (4.1)$$

where  $\sigma_g$  is the complex surface conductivity of graphene,  $\eta_0 = 377 \Omega$  is the intrinsic impedance in free space and  $K_0 = \frac{2\pi}{\lambda}$  is the wave number of the Surface Plasmon Polaritons (SPP) in the air.

Graphene has become a valuable and useful nanomaterial due to its exceptional properties such as high tensile strength, and electrical conductivity, it can conduct better electricity and heat incredibility than steel. The fabrication methods of graphene can be done by mechanical exfoliation, graphene oxide reduction synthesis, electrochemical exfoliation, Chemical Vapor Deposition (CVD), and vacuum arc discharge [213]. The total surface conductivity of graphene  $\sigma_g$  can be represented using the well-known Kubo's equations, and it consists of two terms, intra-band conductivity and inter-band conductivity [214]:

$$\sigma_g(\omega, \mu_c) = \sigma_{intra}(\omega, \mu_c) + \sigma_{inter}(\omega, \mu_c) \quad (4.2)$$

where

$$\sigma_{intra}(\omega, \mu_c) = \frac{je^2 K_B T}{\pi \hbar^2 (\omega + j/\tau)} \left( \frac{\mu_c}{K_B T} + 2 \ln(e^{-\frac{\mu_c}{K_B T}} + 1) \right) \quad (4.3)$$

$$\sigma_{inter}(\omega, \mu_c) \approx \frac{je^2}{4\pi \hbar^2} \ln \left( \frac{2|\mu_c| - (\omega + j/\tau)}{2|\mu_c| + (\omega + j/\tau)} \right) \quad (4.4)$$

where  $\mu_c$ = chemical potential,  $\omega$ =the angular frequency,  $T$ =temperature,  $\tau$ = relaxation time,  $\hbar$ =reduced Planck's constant,  $h$ = normal Planck's constant,  $K_B$ = Boltzmann's constant and  $e$ = electron charge. For the present work,  $e=1.6 \times 10^{-19}$  C,  $T=300$  K,  $\tau=1$  ps,  $K_B= 8.62$  eVK<sup>-1</sup>,  $\hbar=6.582 \times 10^{-16}$  eVs,  $\omega= 2\pi f$  and  $\mu_c$  is changing from 0 to 1.5 eV to check the conductivity behavior. So, the complex surface conductivity of monolayer graphene depends on the chemical potential  $\mu_c$  and the frequency  $f$ .

The total surface conductivity of graphene  $\sigma_g$  in Eq. (4.2) can be also represented as [215]:

$$\sigma_g(\omega, \mu_c) = \frac{je^2(\omega - 2j\tau)}{\pi \hbar^2} \times \left[ \frac{1}{(\omega - j2\tau)^2} \int_0^\infty \epsilon \left( \frac{\delta f_d(\epsilon)}{\delta \epsilon} - \frac{\delta f_d(-\epsilon)}{\delta \epsilon} \right) d\epsilon - \int_0^\infty \frac{(f_d(-\epsilon) - f_d(\epsilon)) d\epsilon}{(\omega - j2\tau)^2 - 4\left(\frac{\epsilon}{\pi}\right)^2} \right] \quad (4.5)$$

where  $f_d(\epsilon)$  is the Fermi–Dirac distribution which can be represented as [216]:

$$f_d(\epsilon) = \left( e^{\frac{\epsilon - \mu_c}{K_B T}} + 1 \right)^{-1} \quad (4.6)$$

In the THz band, the intraband conductivity dominates the value of total surface conductivity, whereas, the inter-band term has no significant effect on the total surface conductivity which can be ignored. Hence, the conductivity of graphene can be expressed by using only intra-band terms [214]. In addition, graphene carrier density  $n_s$  is described as follows [17]:

$$n_s = \frac{2K_B^2 T^2}{\pi \hbar^2 V_f^2} \left( e^{\frac{2\mu_c}{K_B T}} - 1 \right); \text{ For } \mu_c > K_B T \quad (4.7)$$

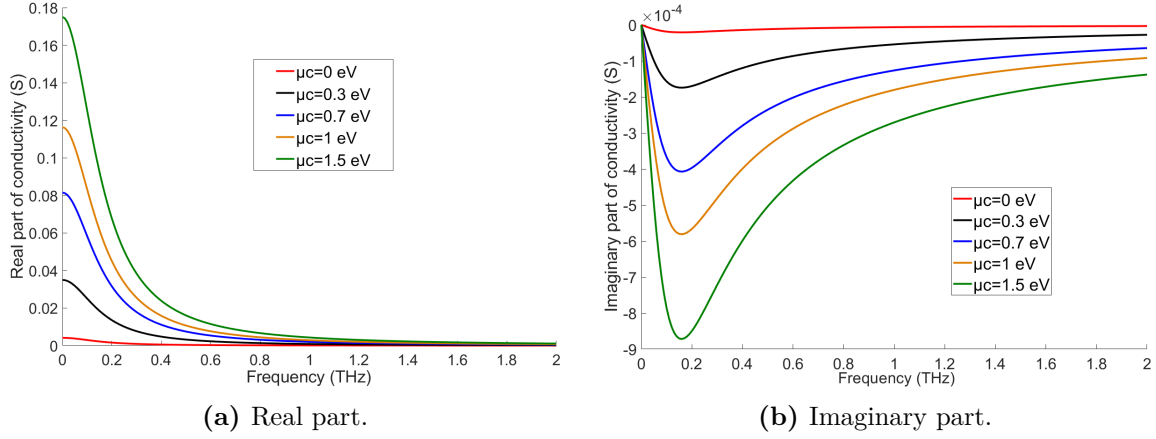


**Figure 4.1** – Intra-band conductivity of graphene.

or by [217] as:

$$n_s = \frac{2}{\pi \hbar^2 V_f^2} \int_0^\infty \epsilon [f_d(\epsilon) - f_d(\epsilon + 2\mu_c)] d\epsilon \quad (4.8)$$

where  $V_f$  is the Fermi velocity.

The chemical potential  $\mu_c$  is controlled by the carrier density  $n_s$ . The graphene conductivity can be easily inhibited by changing the chemical potential  $\mu_c$ . The chemical potential  $\mu_c$  can be changed via chemical doping or electrostatically biasing it. Fig.4.1 shows the effect of changing graphene chemical potential  $\mu_c$  on the real and imaginary parts of the intra-band conductivity. The real part of the intra-band conductivity is increased by increasing the chemical potential  $\mu_c$  resulting in a frequency shift, nevertheless, the imaginary part values of the intra-band conductivity approach to zero by increasing  $\mu_c$ . The shift in the frequency is called the chemical shift. In Nuclear Magnetic Resonance (NMR) spectroscopy, the chemical shift is related to the molecular structure or composition, therefore, a compound with a strong and higher conductivity such as graphene provides a frequency shift without changing the geometric dimensions [218].

The surface impedance of graphene for different chemical potentials in the frequency range of 0.4-1.1 THz is shown in Fig.4.2. It is seen that with the increase of the chemical potential  $\mu_c$ , the real impedance of the graphene decreased. Therefore, graphene can operate in two different modes, a high resistance mode when  $\mu_c = 0$  eV

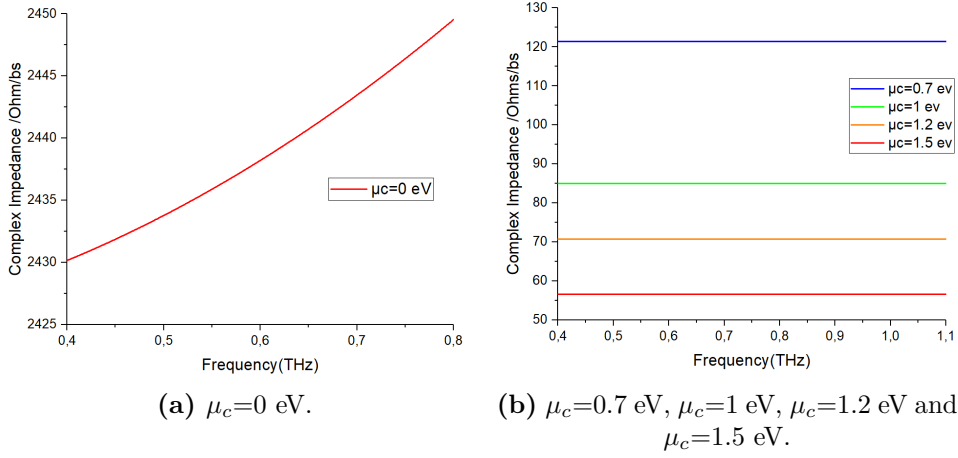


**Figure 4.2** – Properties of graphene.

and a low resistance mode when  $\mu_c = 1.5$  eV. When  $\mu_c = 0$  eV, graphene conductivity is almost 1000 times less than the conditions of  $\mu_c = 1.5$  eV [219].

### 4.3 Antenna Array Design Based on Periodic and Non-Periodic Photonic Crystals With a Graphene Load

Previously, various research works conducted on graphene-based antennas were presented aiming for THz band applications [16, 194, 220, 221, 222], among them, a 1x2 graphene antenna array which is designed to obtain a gain of 9 dB at 0.51 THz. In addition, Temmar et al. [136] investigated the characteristics of graphene by designing an antenna based on periodic and non-periodic PCs around 0.65 THz, which obtained interesting results at  $\mu_c = 1$  eV when the non-periodic PCs were used and obtained a gain of 8.92 dB and a bandwidth of 356 GHz. Unfortunately, all of the presented antennas showed very limited bandwidth and low gain, which restricts their application in THz. To resolve these problems, a 1x2 RMPA based on periodic and non-periodic PCs with a graphene load is proposed to offer an extra performance.

Antenna array 0, namely the conventional 1x2 RMPA array based on the homoge-



neous substrate, is designed and simulated for comparison purposes which is shown in Fig.4.3a. The proposed geometry structure of the 1x2 RMPA array based on periodic PCs with no graphene load is depicted in Fig.4.3b which is labeled as antenna array 1. By using the planar configuration, the size of the antenna becomes larger, so a large number of phase shifters is required. Also, complication increases for the design of the feed network resulting in more power consumption, ohmic losses, mismatch losses, mutual coupling effects between the adjacent elements of an array and high side lobe level effects. Hence, for such advantages, the linear configuration is commonly used by offering more simplicity [13]. The proposed antenna array consists of two symmetrical patch elements which are fed by the parallel feeding technique [13]. The patch width  $W_p$  and length  $L_p$  are  $360 \mu m$  and  $220 \mu m$ , respectively. This antenna array is mounted on a substrate with a dielectric constant of 2.91 and loss tangent of 0.0001 with a thickness  $h$  of  $80 \mu m$  that employs a periodic PBG. The air holes have a lattice constant and radius of  $127.95 \mu m$  and  $15 \mu m$ , respectively. Hence, the dimensions of the square unit cell are  $127.95 \times 127.95 \mu m^2$ . Finally, the width and length of the substrate are  $W_s=1279.50 \mu m$  and  $L_s=895.65 \mu m$ , respectively. Similarly, the ground is made up of a copper conductor with dimensions of  $1279.50 \times 895.65 \times 4.85 \mu m^3$ . The separation distance between both the patch structures is  $584.80 \mu m$ , which is equal to the operating wavelength  $\lambda$ , where  $\lambda$  is found based on Eq.(4.9) [134, 139]:

$$\lambda = \frac{\lambda_0}{\sqrt{\epsilon_{eff}}} \quad (4.9)$$

where  $\lambda_0$  is the free-space wavelength and  $\epsilon_{eff}$  is the effective permittivity. The extracted real and imaginary parts of the permittivity are presented in Fig.4.4 using CST Microwave Studio. In order to obtain the separation distance between both the patch structures and achieve a resonance around 0.65 THz, the effective permittivity value is taken as 0.756.

The feed network is designed to distribute the power in equal parts to achieve 50  $\Omega$  impedance. Hence, the width of the feed network  $W$  can be found using Eq.(3.5). The optimum values of  $W$ ,  $L$ ,  $W_f$  and  $L_f$  are  $109.23 \mu m$ ,  $204.47 \mu m$ ,  $6.6 \mu m$  and  $143$

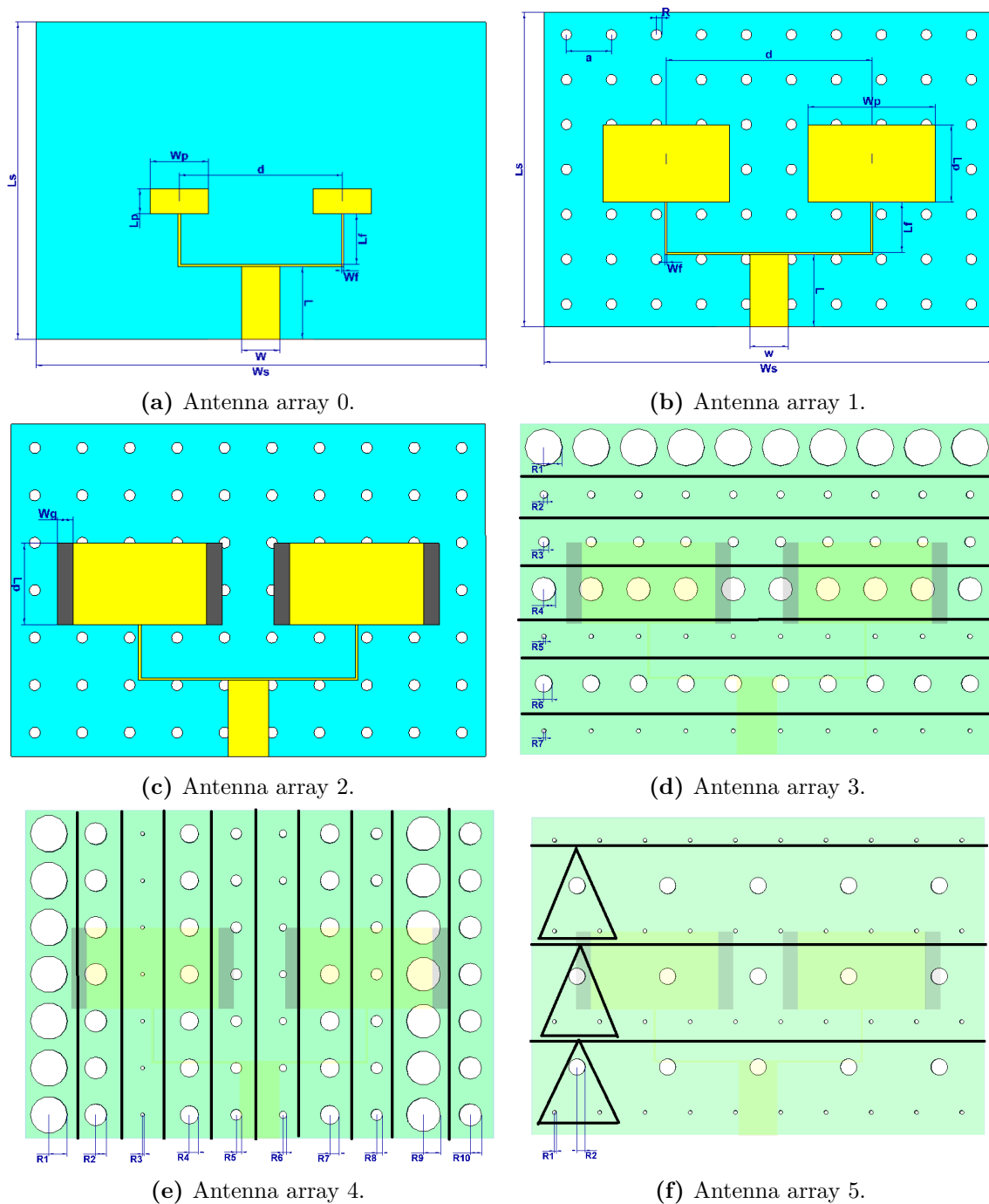


**Figure 4.3** – The geometry of the proposed 1x2 RMPA array based on the homogeneous substrate, periodic and non-periodic PCs with a graphene load.

$\mu m$ , respectively.

In order to investigate the performance of the proposed 1x2 RMPA array around

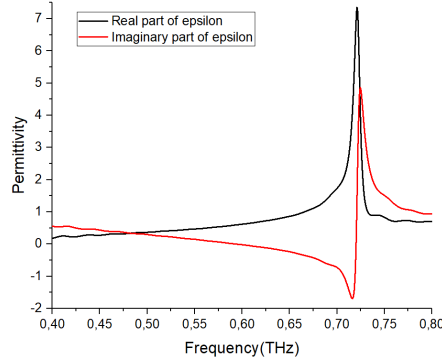


**Figure 4.4** – The effective permittivity of the designed PBG substrate.

0.65 THz, a graphene load is added to each side of the patch structure and is operated at  $\mu_c=1.5$  eV. Graphene-based nano-patch antennas for THz communications usually have a dimension on the order of microns. However, characterizing graphene using strictly analytical methods is generally difficult due to its complexity. Alternatively, full-wave simulators such as FIT in CST Microwave Studio have been used to analyze and model graphene, which enables fast and accurate analysis at high frequencies with different solvers. Therefore, graphene was modeled using a volumetric approach with an acceptable thickness of  $0.34$  nm for the graphene monolayer. This thickness was compatible with the chemical potential tuning of graphene [223, 224]. In antenna array 2, the graphene load had a width  $W_g$  of  $42.36$   $\mu m$  and a length similar to the length of the patch of  $L_p$   $220$   $\mu m$  as shown in Fig.4.3c.

Next, the performance of the proposed antenna array 2 at  $\mu_c=1.5$  eV is investigated further by employing non-periodic PCs substrate instead of periodic PCs substrate to enhance its radiation characteristics around 0.65 THz. The non-periodic PCs substrate technique has been investigated over the years by many researchers to enhance the microstrip patch antenna radiation features such that bandwidth and gain [13, 14, 16, 124, 134, 135], which can be made by using different radii of air holes into the dielectric or by using the different distances between the centers of each air hole forming a square lattice or triangular lattice. The utilized PC structures are made using 2D air cylinders embedded in the substrate consisting of lattices with various shapes. Traditionally, the five 2D Bravais lattice types include oblique,

square, hexagonal or triangular, primitive rectangular and centered rectangular lattices. These lattices combining simplicity and quasi-isotropy of their Brillouin zone, allow the opening of band gaps and lead to large absolute PBGs. Mostly, the microstrip patch antennas are implemented by using square or rectangular lattices, although the triangular lattice allows the use of fewer air gaps compared to a square lattice, but it may exhibit several advantages [225, 226]. Therefore, the proposed antenna array structure is designed and analyzed with three different PC substrate cases, where the air holes of the substrate are divided into different sets. Each set has its own radius. For the best radiation performance, the radii of the air holes are optimized.

In the case of the square lattice, two different antenna arrays are designed. Antenna array 3 is designed with seven sets of air holes that are horizontally symmetrical as shown in Fig.4.3d. The radii of the air holes are  $R_1=50 \mu m$ ,  $R_2=10 \mu m$ ,  $R_3=14 \mu m$ ,  $R_4=32 \mu m$ ,  $R_5=6 \mu m$ ,  $R_6=23 \mu m$ , and  $R_7= 5.4 \mu m$ . Antenna array 4 is designed with teen sets of air holes that are vertically symmetrical as shown in Fig.4.3e. The radii of the air holes are  $R_1=50 \mu m$ ,  $R_2=30 \mu m$ ,  $R_3=5 \mu m$ ,  $R_4=25 \mu m$ ,  $R_5=15 \mu m$ ,  $R_6=10 \mu m$ ,  $R_7= 26 \mu m$ ,  $R_8=15 \mu m$ ,  $R_9=46 \mu m$ , and  $R_{10}= 30.5 \mu m$ . In the case of the triangular lattice, Antenna array 5 is designed with three sets, each set contains a subset of three air that form a triangular lattice, two air holes are similar with a radius of  $R_1=5.4 \mu m$  and the third one with a value of  $R_2=23.1 \mu m$  as shown in Fig.4.3f.

The radiation characteristics such as return loss, bandwidth, gain, and directivity of the proposed 1x2 RMPA array based on the homogeneous substrate, periodic and non-periodic PCs with a graphene load are compared and presented in Fig.4.5. It is found that the resonance frequency, return loss, bandwidth and gain are 0.657 THz, -27.1 dB, 164 GHz and 9.25 dB, respectively for antenna array 0. 0.619 THz, -28.35 dB, 260 GHz and 10.95 dB, respectively for antenna array 1. 0.63 THz, -73.86 dB, 287 GHz and 11.11 dB, respectively for antenna array 2. 0.63 THz, -73.97 dB, greater than 415 GHz and 11.41 dB, respectively for antenna array 3. 0.636 THz, -75.9 dB, greater than 411 GHz and 11.53 dB, respectively for antenna array

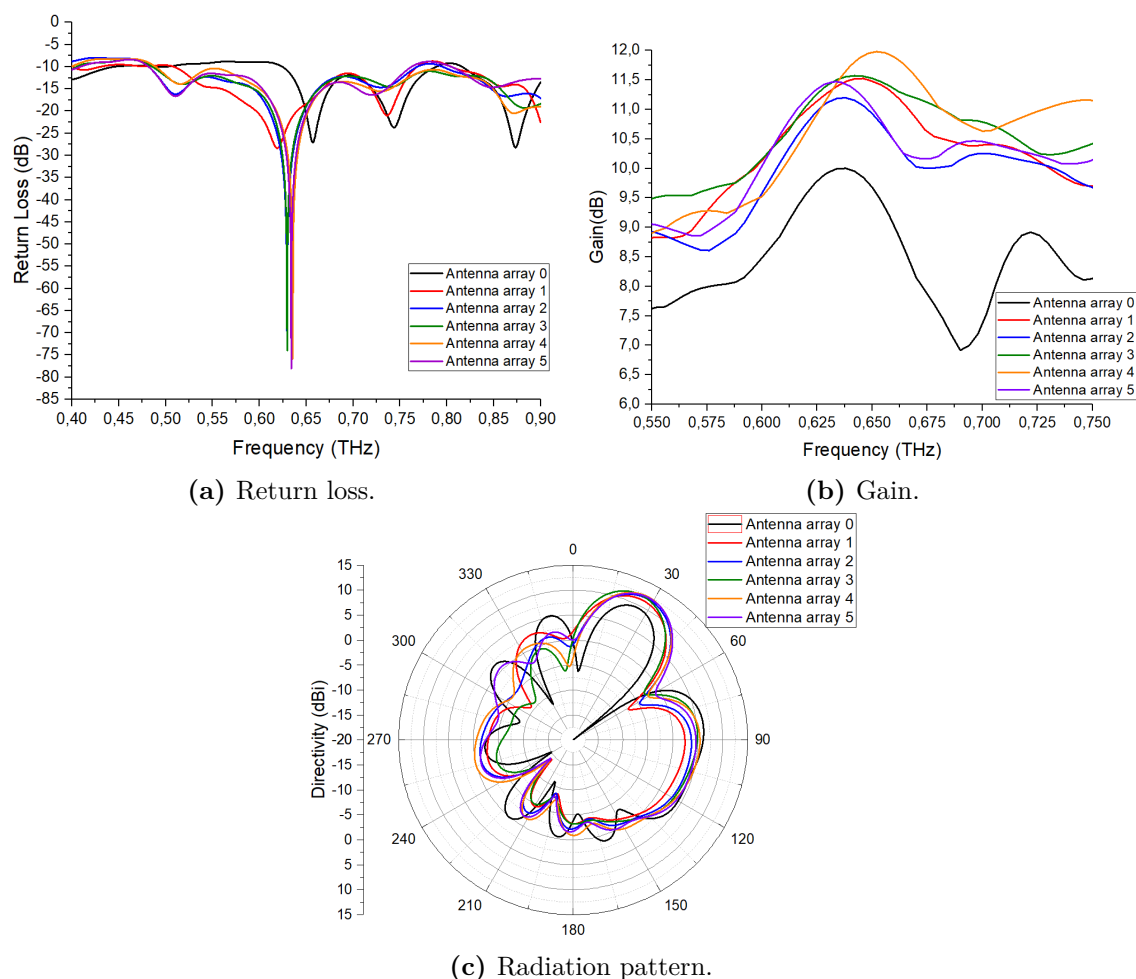


**Figure 4.5** – The radiation characteristics of the proposed 1x2 RMPA array based on the homogeneous substrate, periodic and non-periodic PCs with a graphene load.

4. 0.634 THz,  $-78.1$  dB, 281 GHz and  $11.47$  dB, respectively for antenna array 5. The maximum radiation in the pattern of all the designed antenna arrays occurs at  $\theta=25^\circ$  at their respective resonating frequencies which is the direction of maximum radiation. Therefore, the directivity of antenna arrays 0, 1, 2, 3, 4 and 5 is  $9.46$  dBi,  $11.50$  dBi,  $12$  dBi,  $12.10$  dBi,  $12.40$  dBi and  $12.30$  dBi, respectively.

According to the obtained results, antenna array 1 that is designed based on periodic PCs offered remarkable performance enhancements compared to the conventional antenna array, which achieved enhancements of 4.61 %, 58.54 %, 18.38 % and 21.56 % in the return loss, bandwidth, gain and directivity, respectively. However,

it could be worth interesting to observe that with the introduction of the graphene load at  $\mu_c=1.5$  eV, further enhancements in the performance were obtained as seen in antenna array 2, which obtained enhancements of 160.53 %, 10.38 %, 1.46 and 4.35 % in the return loss, bandwidth, gain and directivity, respectively as compared to antenna array 1 that is designed based on periodic PCs with no graphene load. After, employing non-periodic PCs with a graphene load at  $\mu_c=1.5$  eV, it was found remarkable enhancements in the antenna array bandwidth, gain and directivity. Therefore, antenna array 4 achieved the highest performance among all proposed antenna arrays, which obtained enhancements of 2.76 %, more than 43.21 %, 3.78 % and 3.33 % in the return loss, bandwidth, gain and directivity, respectively as compared to antenna array 2 that is designed based on periodic PCs with a graphene load.

**Table 4.1** – Comparison of the proposed designed antenna arrays and previously reported designs.

	Antenna size ( $\mu m^2$ )	$f_r$ (THz)	$S_{11}$ (dB)	BW (GHz)	Gain (dB)	D (dBi)
[134]	600 x 600	0.63	-56.81	$\gg 230$	8.95	-
[134]	600 x 600	0.61	-83.73	$\gg 230$	9.19	-
[222] 1x2 array	-	0.51	-35	-	9	-
[136]	1323 x 600	0.62	-	287	8.77	-
[136]	1323 x 600	0.62	-	356	8.92	-
[227]	1000 x 1000	0.6929	-41.65	22.47	10.43	-
[62]	1000 x 1000	0.852	-	34.3	8.248	8.789
[228]	1600 x 800	0.809	-	57.96	8.28	9.77
[105] 1x5 array	780 x 2900	0.6127	-14.75	8.34	10.3	10.70
[104] 2x2 array	2000 x 2000	0.6	-27.7	60	-	-
Antenna array 0	1279.50 x 895.65	0.657	-27.1	164	9.25	9.46
Antenna array 1	1279.50 x 895.65	0.619	-28.35	260	10.95	11.50
Antenna array 2	1279.50 x 895.65	0.63	-73.86	287	11.11	12
Antenna array 3	1279.50 x 895.65	0.63	-73.97	$\gg 415$	11.41	12.10
Antenna array 4	1279.50 x 895.65	0.636	-75.9	$\gg 411$	11.53	12.40
Antenna array 5	1279.50 x 895.65	0.634	-78.1	281	11.47	12.30

The simulations demonstrated that the performance of the proposed 1x2 RMPA array based on periodic PCs improved in terms of the return loss, bandwidth, gain and directivity after employing graphene. The highest radiation characteristics were achieved when  $\mu_c=1.5$  eV. The novel aspect of this study is the enhancement of the

performance of the 1x2 RMPA array by using the non-periodic PC substrate with a graphene load at  $\mu_c=1.5$  eV, as shown in Fig.4.3. The performance of the proposed antenna array was improved further by optimizing its air holes radii. In particular, three antenna array structures were examined. Their performance achieved interesting radiation characteristics at resonance frequencies close to the desired frequency of 0.65 THz, where a low atmospheric attenuation window exists in the THz band, which can be useful in sensing, imaging, detection and wireless communication technologies. The highest radiation characteristics were obtained by antenna array 4, because of its minimal return loss of  $-75.90$  dB, larger bandwidth which is greater than 411 GHz, higher gain and directivity of  $11.53$  dB and  $12.40$  dBi, respectively at a resonant frequency of 0.636 THz. Table 4.1 presents the overall radiation characteristics of the proposed antenna arrays compared with the previously reported researches. It is evident that the proposed THz antenna arrays designed based on PCs with a graphene load provided better output characteristics than other existing works.

## 4.4 MIMO System Design

### 4.4.1 MIMO Antenna Array Design and Analysis With a Graphene Load

In this subsection, the researcher designed and developed three different MIMO antenna arrays which are based on the structures of antenna arrays 0, 2 and 4 as discovered in the previous section 4.3. The MIMO antenna array structure is made by a copy of the antenna array structure, which is fed by another port where each port was fed separately, shifted by a distance ( $Dis$ ) of  $140 \mu m$  and rotated around its center. The separation distance ( $Dis$ ) was made to isolate both antenna arrays to reduce the effect of mutual coupling and correlation and also to avoid grating lobes. At each side of the radiator patches, a graphene load is added which was modeled using a volumetric approach with an acceptable thickness for the graphene monolayer. The graphene load had a width  $W_g$  of  $42.36 \mu m$ , a length similar to the length of the patch

of  $L_p$  220  $\mu m$  and a thickness of 0.34  $nm$  which was compatible with the chemical potential tuning of graphene. A change in the electrical conductivity of graphene leads to an increase in the gain of the MIMO antenna array compared to a simple MIMO antenna array. Therefore, the first MIMO antenna array was designed based on a homogeneous substrate which is labeled as MIMO antenna array 0 as shown in Fig.4.6. The second MIMO antenna array was designed based on the periodic PCs with  $\mu_c = 1.5$  eV which is labeled as MIMO antenna array 1 as shown in Fig.4.7. The third MIMO antenna array was designed based on the optimized PCs with  $\mu_c = 1.5$  eV which is labeled as MIMO antenna array 2 as shown in Fig.4.8.

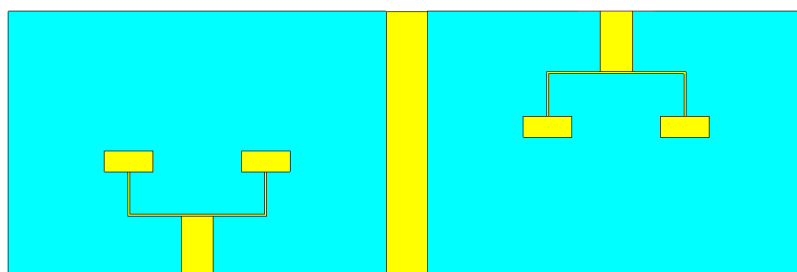


**Figure 4.6** – The geometry of the designed MIMO antenna array based on the homogeneous substrate.

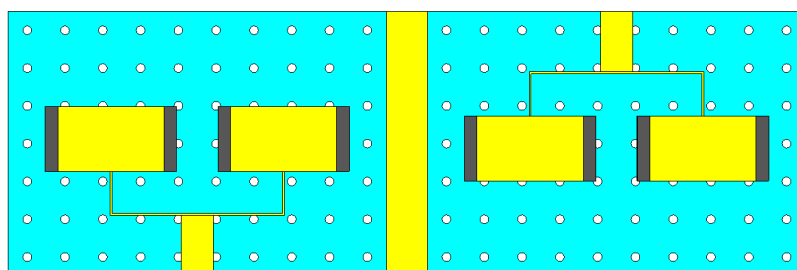


**Figure 4.7** – The geometry of the designed MIMO antenna array based on the periodic PCs with a graphene load.

The CST Microwave Studio software has been used to calculate the MIMO antenna array features. The scattering parameters  $S_{11}$ ,  $S_{21}$ ,  $S_{12}$ , and  $S_{22}$  were extracted for the MIMO antenna array based on the homogeneous substrate and for the MIMO antenna array based on the PCs with optimized PCs substrates, where the utilized chemical potential was 1.5 eV as shown in Fig.4.9. The resonance frequencies of the designed MIMO antenna arrays were observed at around 0.65 THz. Therefore, MIMO



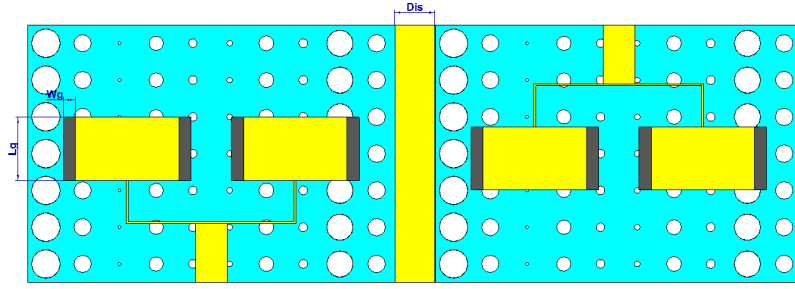


**Figure 4.8** – The geometry of the designed MIMO antenna array based on the optimized PCs with a graphene load.

antenna array 0 resonated at the frequency of 0.66 THz with a return loss of  $-25.27$  dB. Whereas, MIMO antenna arrays 1 and 2 resonated at the frequencies of 0.631 THz and 0.638 THz, respectively with return losses of  $-40.68$  dB and  $-41.30$  dB, respectively. The  $-10$  dB bandwidths were 174, 300, and greater than 614 GHz for MIMO antenna array 0, MIMO antenna array 1, and MIMO antenna array 2, respectively. Thus, employing the periodic PCs and the optimized PCs with a graphene load as seen in MIMO antenna arrays 1 and 2, respectively enlarged the bandwidth compared with MIMO antenna array 0, which was designed based on the homogeneous substrate, which is very important for high data transmission rates based on Shannon theorem [106].

Fig.4.10 displays the gain performance of the designed MIMO antenna arrays in the frequency range of 0.55-0.75 THz. Clearly, the gain was enhanced when the graphene load operated in the low resistance mode for both MIMO antenna arrays 1 and 2 due to the suppression of surface waves by the PCs substrate compared to the conventional MIMO antenna array. Therefore, at their resonating frequencies, MIMO antenna array 2 achieved the maximum gain with the value of 11.80 dB, whereas, MIMO antenna arrays 1 and 0 achieved 11.48 dB and 9.44 dB, respectively.

The radiation patterns of the designed MIMO antenna arrays are investigated with the corresponding resonance frequencies which can be revealed in Fig.4.11. The directivity of MIMO antenna array 0 was maximized at the incidence angles  $\theta$  of  $27^\circ$  and  $-27^\circ$  for port 1 and port 2, respectively with the value of 9.84 dBi at the resonance frequency of 0.66 THz. Whereas, the maximum directivity of MIMO antenna arrays

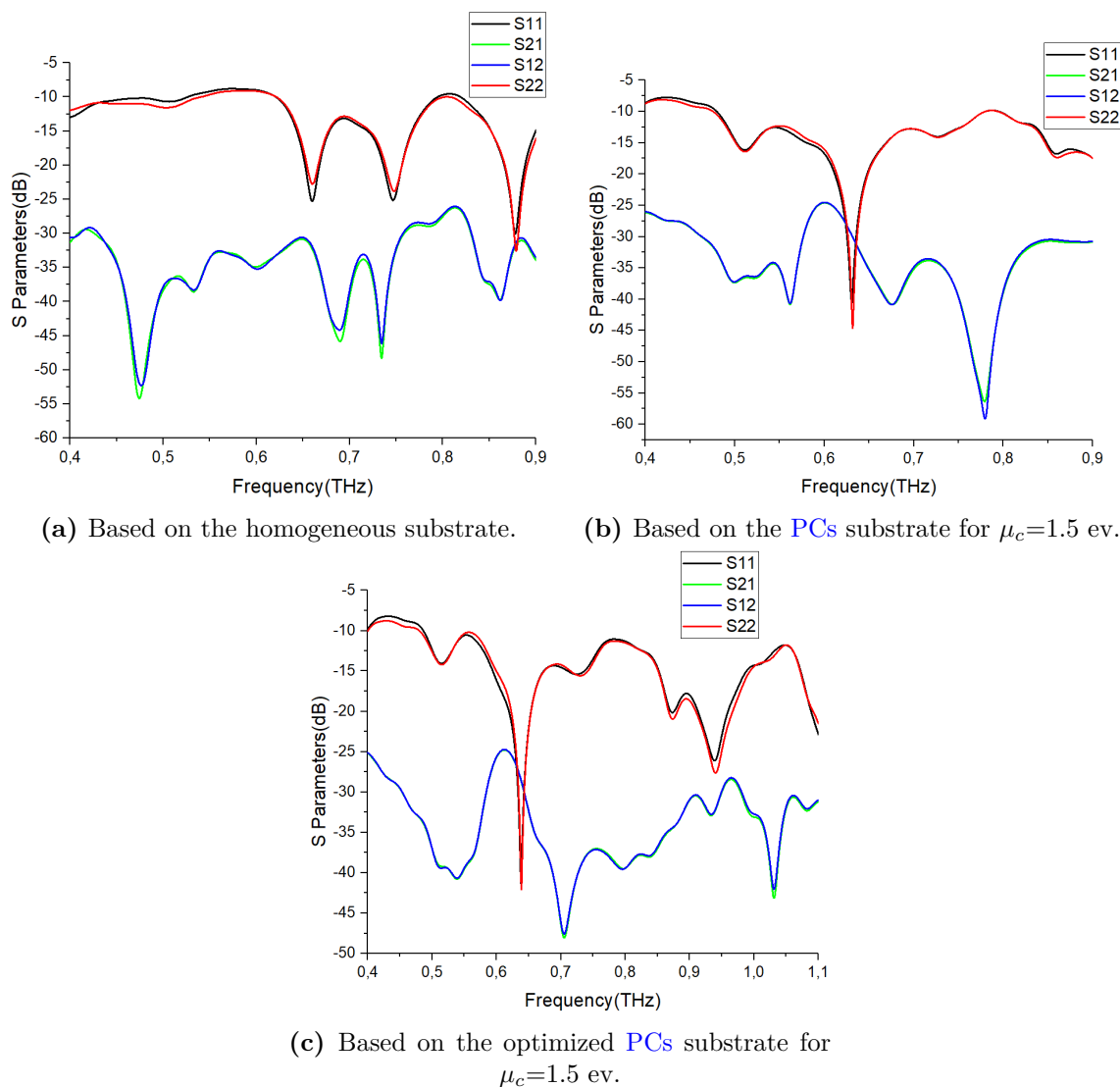


**Figure 4.9** – S Parameters of the designed MIMO antenna arrays.

1 and 2 was achieved at the incidence angles  $\theta$  of  $30^\circ$  and  $-30^\circ$  for port 1 and port 2, respectively with the values of  $12.40$  dBi and  $12.80$  dBi, respectively at resonating frequencies of  $0.631$  THz and  $0.638$  THz, respectively.

The 3D far-field radiation pattern for MIMO antenna array 2 is shown in Fig.4.12. The radiation characteristics such as return loss and gain of the designed MIMO antenna array based on the optimized PCs were investigated by changing the different chemical potentials ( $\mu_c = 0$  eV,  $0.7$  eV,  $1$  eV,  $1.2$  eV), then compared them to the case of  $\mu_c = 1.5$  eV. The results are presented in Fig.4.13 which confirm the previously

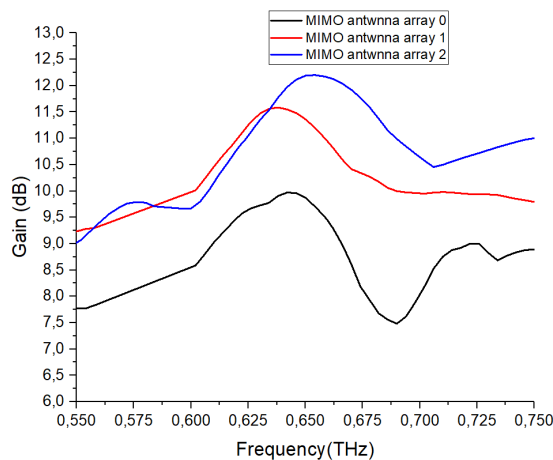


**Figure 4.10** – The gain performance of the designed MIMO antenna arrays.

obtained conclusions. The gain was slightly ameliorated by increasing the chemical potential of the graphene load from 0 eV to 1.5 eV, which corresponded to the low resistive mode of the graphene load, moreover, the introduction of the small graphene load widened the bandwidth.

#### 4.4.2 Losses and Terahertz Channel Capacity

THz band communication is considered as a key wireless technology. The THz channel model has been studied and discussed in several recent works because of its promising characteristics, alleviating the path loss limitations [136, 217, 229, 230, 231]. In order to get the capacity of the MIMO system, the total path loss in the THz band should be studied first. For the line of sight communication systems, losses are mainly due to free-space path loss which is contributed by two frequency-dependent terms: the spreading loss  $A_{spread}$  and the molecular absorption loss  $A_{abs}$ . In addition to the mentioned losses, the reflection loss  $A_{ref}$  which is due to the collision of waves with indoor rough surfaces. The surfaces of indoor objects, which can be considered as smooth surfaces at the GHz frequency, are now regarded as rough surfaces at the THz frequency band. The formulas for the spreading loss, molecular absorption loss, and reflection loss are defined as follows [12, 231]:

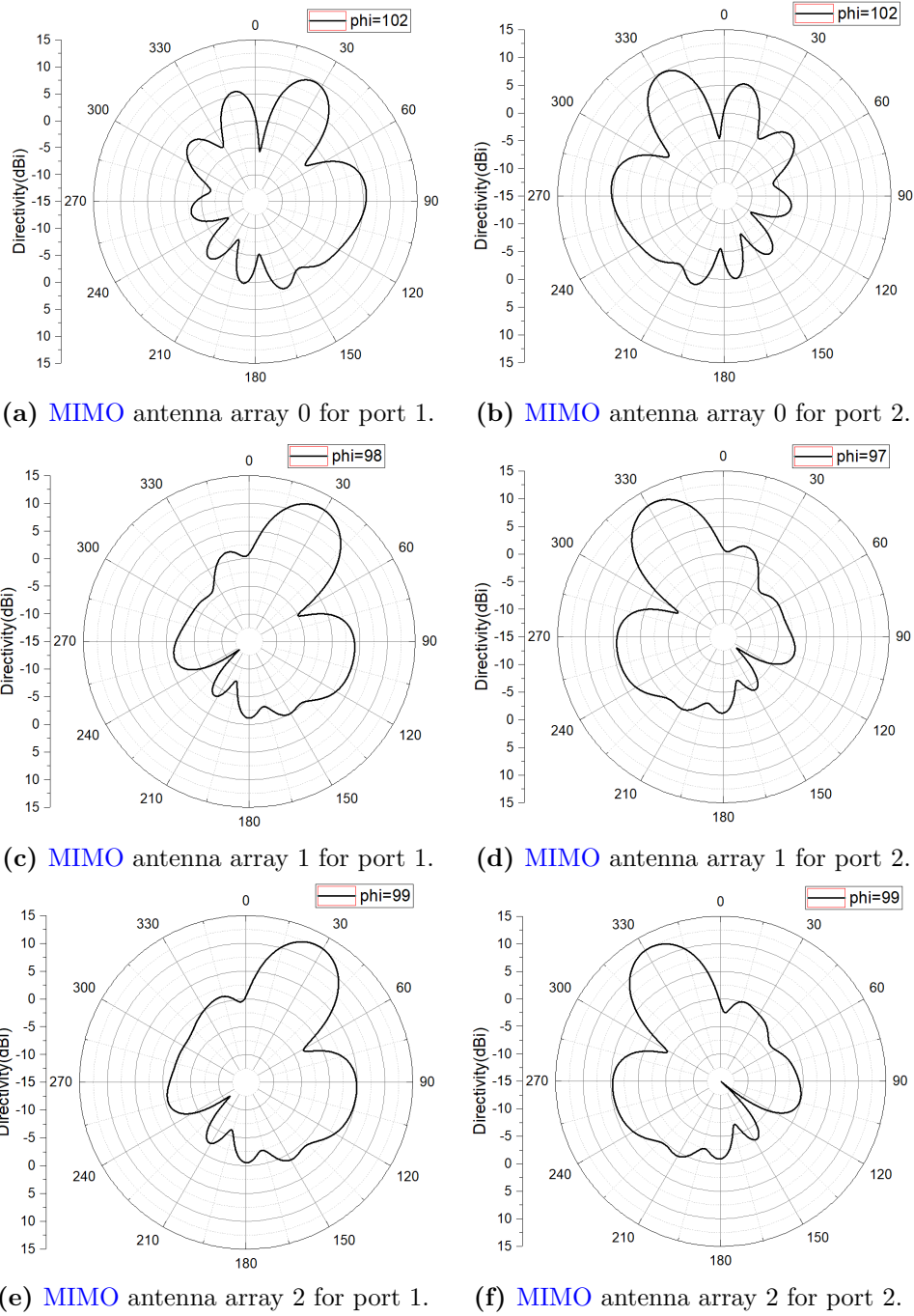


**Figure 4.11** – The far field radiation patterns of the designed MIMO antenna arrays.

$$A_{spread}(f, d) = 20 \log\left(\frac{4\pi fd}{c}\right) \quad (4.10)$$

$$A_{abs} = k(f)d10 \log_{10} e \quad (4.11)$$

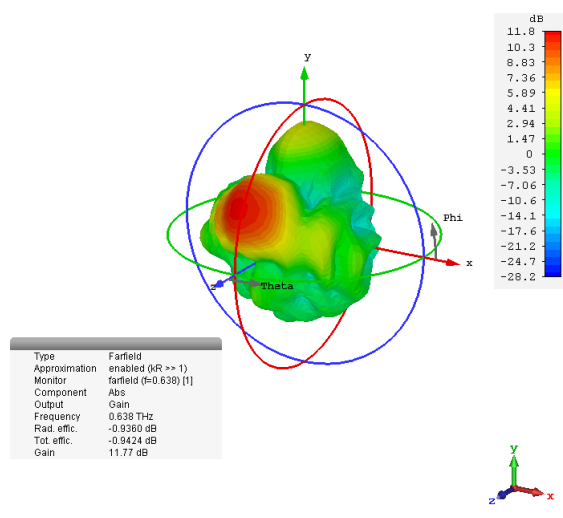


**Figure 4.12** – The 3D far-field radiation pattern of the designed MIMO antenna array 2.

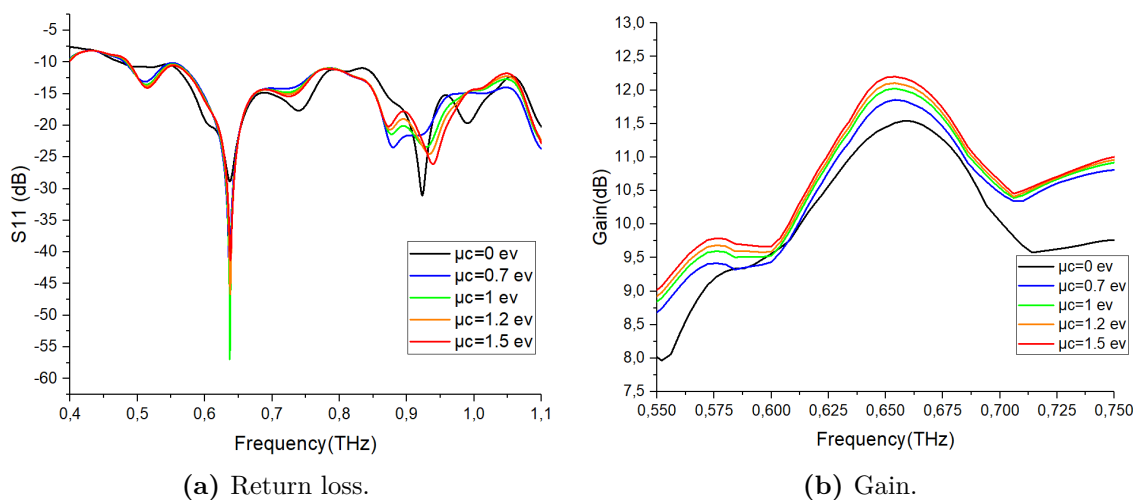


**Figure 4.13** – The performance of the designed MIMO antenna array based on the optimized PCs with different chemical potentials.

where  $A_{spread}$  is the spread loss in  $dB$ ,  $f$  is the operating frequency,  $d$  is the traveled distance and  $c$  is the speed of light.  $A_{abs}$  is the molecular absorption loss in  $dB$ ,  $K(f)$  is the medium absorption coefficient and equals the sum of weighted coefficients of each gas in the air. Since the total band is segmented into several transmission windows, the molecular absorption is very small and it can be ignored at the window

around 0.65 THz. The roughness factor  $\rho$  is given as follows:

$$\rho = e^{\frac{-g}{2}} \quad (4.12)$$

$$g = \left( \frac{2\pi\Delta(\cos(\theta_I) + \cos(\theta_O))}{\lambda} \right)^2 \quad (4.13)$$

where  $g$  represents the intensity of the surface variation,  $\Delta$  is the standard deviation coefficient of the surface roughness (88  $\mu m$  for plaster),  $\theta_I$  and  $\theta_O$  are the angles of incidence and reflection, respectively.

The gain matrix  $H$  comprises the gain between the  $i$ th transmit antenna and the  $j$ th receive antenna which is obtained from the following formula [232]:

$$h_{ij} = -A_{spread} - A_{abs} + \rho + G_T + G_R \quad (4.14)$$

where  $G_T$  and  $G_R$  are the transmitter and the receiver antenna gain at the angle of incidence  $\theta_I$  and the angle of reflection  $\theta_O$ , respectively. These angles were calculated for the length of the radiation path  $d_{ij}$  based on the scenario presented in Fig.4.14 using the following formulas [17, 217]:

$$\frac{Sp_i}{\cos(\theta_I)} + \frac{Sp_{ij}}{\cos(\theta_O)} = d_{ij} \quad (4.15)$$

$$Sp_i \tan(\theta_{I_i}) + Sp_{ij} \tan(\theta_{O_{ij}}) = L_{ij} \quad (4.16)$$

where  $Sp_i$  is the distance between the transmitter and the corresponding indoor wall,  $Sp_{ij}$  is the distance between the receiver  $j$  and indoor wall  $i$ ,  $L_{ij}$  is the horizontal distance between the transmitters and receivers and  $d_{ij}$  is the length of the radiation path between the  $i$ th transmit antenna and the  $j$ th receive antenna. Whereas,  $d_t$  and  $d_r$  are the spacings between the transmitters and between the receivers, respectively.

Finally, for the channel computation, a system with  $M$  transmit antennas and  $N$

receive antennas are considered, where the channel can be represented as an  $M \times N$  matrix. The time-invariant channel is described as:

$$y = Hx + w \quad (4.17)$$

where  $x$  is the transmit signal,  $y$  is the receive signal and  $w$  is the white Gaussian noise. The capacity is given by maintaining singular values  $\lambda_i$  for the gain matrix  $H$  as follows [232]:

$$C = \sum_{i=1}^{n_{min}} \log_2 \left( 1 + \frac{p_i \lambda_i^2}{N_0} \right) \quad b/s/Hz \quad (4.18)$$

where  $n_{min}$  is the rank of the matrix  $H$ ,  $p_i$  is the transmitting power from the  $i_{th}$  MIMO antenna array,  $\lambda_i$  is the singular value of the matrix  $H$  and  $N_0$  is the noise power spectral density which is taken as  $0.01 nW$ .

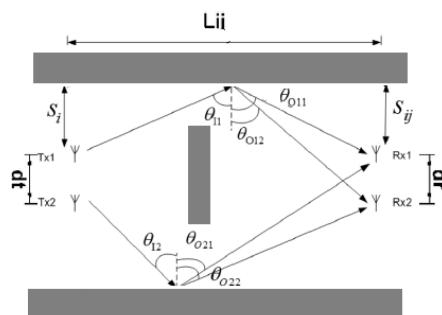
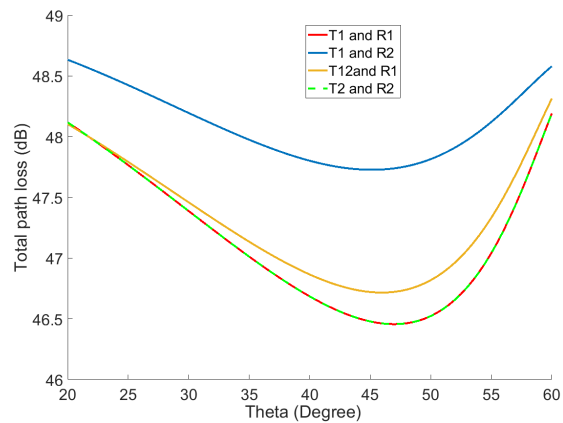


Figure 4.14 – A scenario based on the MIMO antenna array.

### 4.4.3 Results and Discussion

Now, channel capacity will be investigated for the defined scenario given in Fig.4.14. First, the total path loss that includes the spreading loss, molecular absorption loss, and reflection loss should be estimated. Therefore, it is important to have the main direction of the radiation pattern of the designed antennas towards the angle with the lowest total path losses. Hence, to calculate the channel capacity in this design, the



**Figure 4.15** – The total path loss with different incident angles for a 2x2 MIMO system configuration.

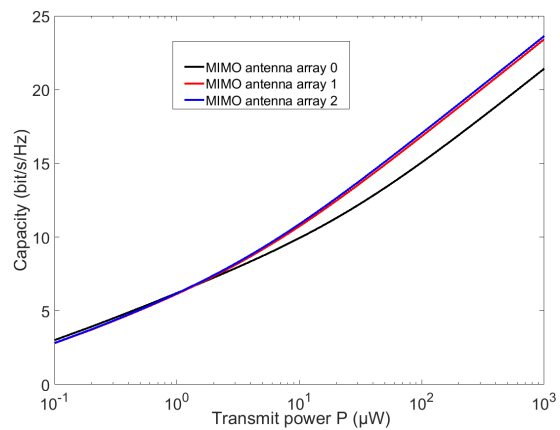


**Figure 4.16** – The capacity performance for a 2x2 MIMO system configuration based on MIMO antenna arrays 0, 1 and 2.

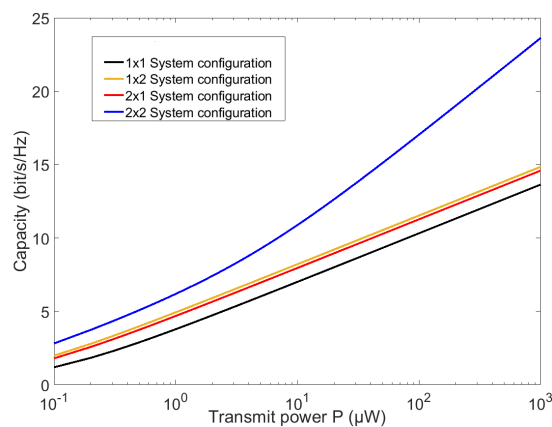


**Figure 4.17** – The capacity performance for different system configurations.



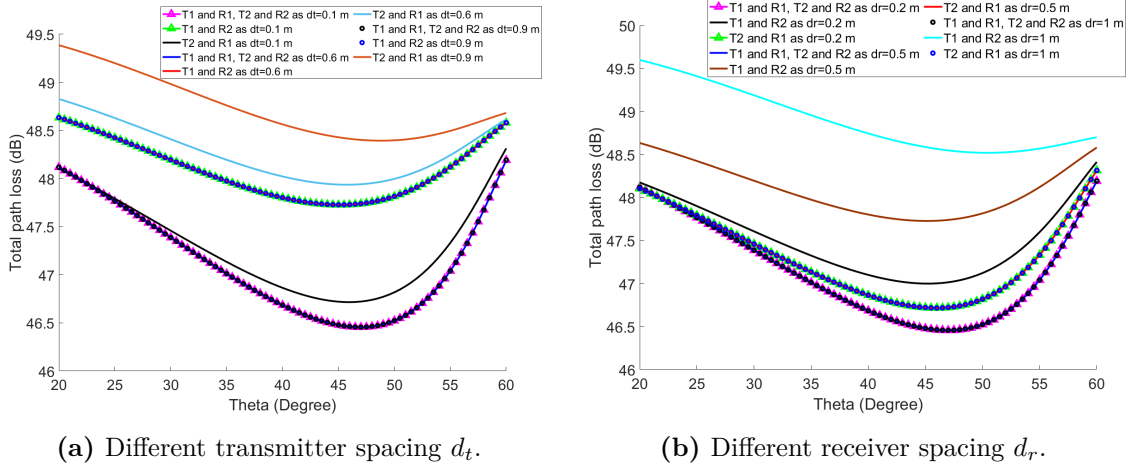


**Figure 4.18** – The total path loss of the proposed MIMO system (2x2 system configuration).

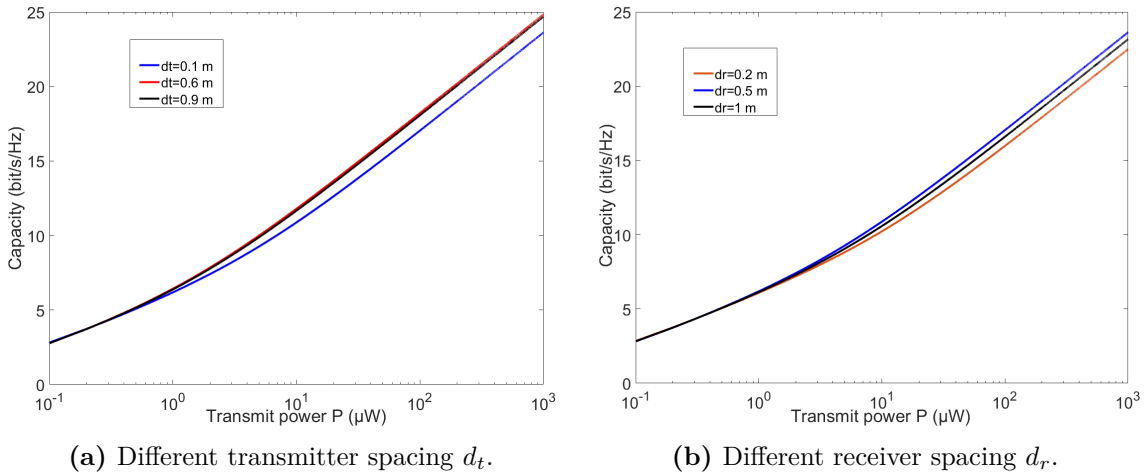


**Figure 4.19** – The capacity of the proposed MIMO system (2x2 system configuration).

gain that was achieved by the MIMO antenna arrays at the incidence angle with the lowest loss is considered. The total path loss versus the incidence angle of transmission for a MIMO (2x2 system configuration) is shown in Fig.4.15, where  $S_{p1}=1m$ ,  $S_{p11}=0.75m$ ,  $L_{ij}=2m$ ,  $d_t=0.1m$  and  $d_r=0.5m$ . For the first transmit antenna and the first receive antenna, which is equivalent to the case of the second transmit antenna and the second receive antenna, the best incidence angle was observed at  $47^\circ$  with a total path loss of  $46.46\text{ dB}$ . For the first transmit antenna and the second receive antenna, the best incidence angle was observed at  $45^\circ$  with a total path loss of  $47.73\text{ dB}$ . Whereas, for the second transmit antenna and the first receive antenna, the best

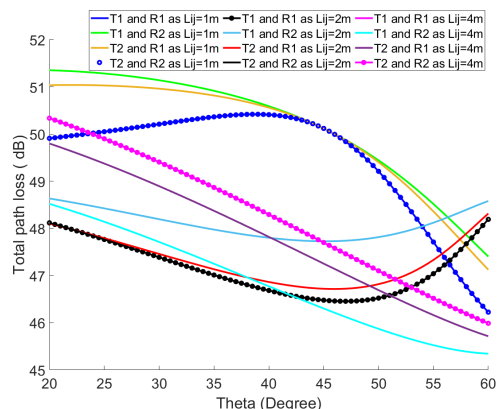


**Figure 4.20** – The total path loss of the proposed MIMO system (2x2 system configuration) for different  $L_{ij}$  values.

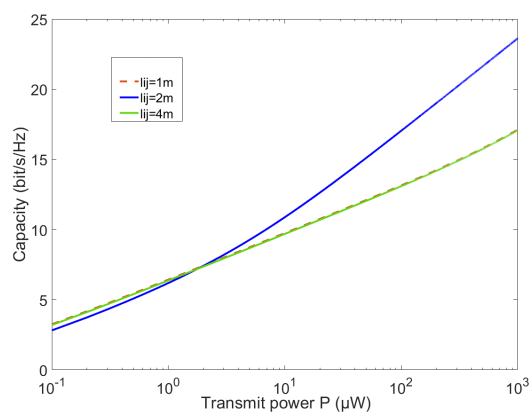


**Figure 4.21** – The capacity of the proposed MIMO system (2x2 system configuration) for different  $L_{ij}$  values.

incidence angle was observed also at  $45^\circ$  with a total path loss of  $46.72 \text{ dB}$ .

The channel capacity for the 2x2 MIMO system configuration with different transmit power is shown in Fig.4.16, the capacity was  $23.64$  and  $23.42 \text{ bit/s/Hz}$  for MIMO antenna arrays 2 and 1, respectively, compared with  $21.42 \text{ bit/s/Hz}$  for MIMO antenna array 0. Based on the obtained results, the capacity performance was enhanced when the PCs were employed as seen in MIMO antenna arrays 2 and 1. Therefore, a 2x2 system based on MIMO antenna array 2 has achieved the maximum capacity.

The capacity for different system configurations based on MIMO antenna array 2 comprising SISO (1x1), MISO (2x1) and SIMO (1x2) was investigated and compared to the 2x2 MIMO system configuration. The results are presented in Fig.4.17.

The capacities were 13.64, 14.59, and 14.85  $bit/s/Hz$  for **SISO**, **MISO** and **SIMO** system configurations, respectively compared to 23.64  $bit/s/Hz$  for the **MIMO** system configuration. Hence, an overall enhancement in the capacity performance was obtained with the **MIMO** system configuration compared to the **MISO**, **SIMO**, and **SISO** system configurations, respectively.

The effect of the distance between the transmitter antennas  $d_t$  and the receiver antennas  $d_r$  on the total path loss and the channel capacity in the **MIMO** system configuration using **MIMO** antenna array 2 were investigated by sweeping  $d_t$  from 0.1m to 0.3m and  $d_r$  from 0.2m to 1m, respectively. Fig.4.18 shows the total loss versus the incidence angle of transmission between each transmission antenna and receiver antenna. It is clear that the total path loss was increased by increasing the spacing between the transmitters and the receivers due to the added diversity scheme, moreover, a slight increase in the best incident angle of transmission was noticed. Fig.4.19a shows the capacities for different transmitter spacing as 23.64, 24.85, and 24.69  $bit/s/Hz$  at a transmission power of  $10^3\mu W$ . Whereas, Fig.4.19b shows the capacities for different receiver spacing as 22.5, 23.64, and 23.16  $bit/s/Hz$  at a transmission power of  $10^3\mu W$ . The results indicate that the capacity can be improved by varying the transmitter and the receiving spacing.

The impact of the horizontal distance between the transmitter antennas and the receiver antennas using **MIMO** antenna array 2 for the **MIMO** system configuration was investigated further by sweeping  $L_{ij}$  from 1m to 4m. The total path loss versus the incidence angle of transmission is shown in Fig.4.20. It is noticed that the total path loss was reduced when the horizontal distance was larger with a slight increase in the best incident angle of transmission. Fig.4.21 shows the capacities at a transmission power of  $10^3\mu W$  which were found as 17.13, 23.64, and 17.08  $bit/s/Hz$ , so, the capacity decreased by increasing the horizontal distance.

For the scenario presented in Fig.4.14, the maximum capacity was 23.64  $bit/s/Hz$  at a transmission power of  $10^3\mu W$  for the 2x2 system configuration using the **MIMO** antenna array based on the optimized **PCs**. For the same scenario, this capacity clearly is favorable compared to 11.5  $bit/s/Hz$  (enhancement of 105.57 %) by [231],

18.21 *bit/s/Hz* (enhancement of 29.82 %) by [136] and 22.3 *bit/s/Hz* (enhancement of 6.01 %) by [217]. This capacity can be improved further by using larger system scales or by manipulating the spacings and distances between the transmit and the receive antennas.

## 4.5 Summary

This chapter focused on channel capacity enhancement in THz communication systems, and to this end, the researcher developed and analyzed a novel MIMO system using a graphene-based 1x2 RMPA array through the use of different substrates, including homogeneous, periodic PCs and optimized PCs substrates. First, systematic analysis has been conducted on the graphene load conductivity by determining the operating modes related to its chemical potential. The employed graphene load operated in a low resistive mode where the chemical potential  $\mu_c$  is used as 1.5 eV. The targeted MIMO antenna arrays have been compared with their radiation characteristics such as return loss, bandwidth, and gain. The obtained results in CST simulations of the proposed graphene-based 1x2 patch antenna array using the optimized PCs substrate exhibited excellent performance improvements as compared to the homogeneous substrate and the periodic PCs substrate around 0.65 THz, which achieved a peak gain of 11.80 dB and broad bandwidth greater than 614 GHz. Next, an indoor communications environment based on the THz band was studied and analyzed where the scenario of a 2x2 MIMO system using the mentioned target MIMO antenna arrays was considered. The total path loss and channel capacity were numerically calculated. The obtained results showed that the proposed 2x2 MIMO system with the MIMO antenna array based on the optimized PCs substrate achieved the highest capacity and the lowest total loss compared to a simple MIMO antenna array based on a homogeneous substrate. The capacity was calculated as 23.64 *bit/s/Hz*, and this was a remarkable enhancement compared with previously reported studies. Finally, this capacity was investigated further for different system configurations and different spacings between the transmission and receiver antennas.

# General Conclusion

Initially, a literature review on the THz band is demonstrated by involving its potential impact, key characteristics and corresponding challenges. Next, the effect of the PCs was investigated by designing different THz antenna array configurations including 1x2, 1x4 and 2x8 RMPA arrays. The objective of this design was to enhance the radiation characteristics of these antenna arrays by suppressing undesirable surface waves that are found in the homogeneous substrate around 0.35 THz where there exists a low atmospheric attenuation window. The simulation was performed using CST and validated with the aid of HFSS. The main results showed that the designed antenna arrays based on the PBG substrate structure outperform the antenna arrays based on the homogeneous substrate in terms of return loss, bandwidth, gain and directivity. Therefore, the 1x2 RMPA array achieved improvements of 124.32 %, 591.03 %, 10.71 % and 7.75 %, respectively. The 1x4 RMPA array achieved improvements of 137.62 %, 454.46 %, 8.98 % and 8.93 %, respectively. Finally, the designed 2x8 RMPA array achieved the highest radiation characteristics and exhibited excellent performance improvement of 416.17 %, 961.39 %, 18.54 % and 19.02 %, respectively.

A novel 1x2 microstrip patch antenna array based on a silicon-air PC substrate is designed and analyzed around 0.65 THz, where a low loss atmospheric window exists in the THz band. The aim of this study was to improve its performance by suppressing undesirable surface waves that are found in the homogeneous substrate. The simulation was performed with the aid of two different simulation techniques, which indicated that the utilization of PBG substrate efficiently improved the radiation characteristics of the conventional microstrip antenna array, which obtained

enhancements of 161.88 %, 1055.52 %, 98.63 % and 17.83 % in the return loss, bandwidth, gain, and radiation efficiency, respectively. Next, a novel 2x2 microstrip patch antenna array is designed and analyzed around 0.65 THz based on different substrates including periodic, non-periodic PCs and homogeneous substrates. The simulation was performed also using two different simulation techniques and showed that the designed antenna array based on periodic PCs performed much better than the conventional antenna array, which obtained improvements of 72.29 %, 68.67 %, 91.25 % and 2.24 % in the return loss, bandwidth, gain, and radiation efficiency, respectively around 0.65 THz. Subsequently, three different enhancements to the PCs were made by introducing the non-periodic PCs. The simulated results showed that the return loss, bandwidth, gain and radiation efficiency were further improved using non-periodic PCs substrate compared to periodic PCs substrate as found in antenna array 4, which obtained improvements of 1.19 %, 3.93 %, 4.42 % and 0.33 %, respectively, in the return loss, bandwidth, gain, and radiation efficiency around 0.65 THz.

A variety of microstrip THz patch antenna arrays based on enhanced PCs were designed and analyzed around 0.65THz with the goal of minimizing the effect of surface waves found in the homogeneous substrate. First, six THz 1x2 RMPA arrays based on different substrates, including homogeneous, periodic PCs and five new aperiodic PCs substrates are studied. The obtained results showed that the designed antenna arrays based on periodic PCs substrate achieved much better radiation characteristics as compared to the homogeneous substrate around 0.65 THz with improvements of 121.86 %, more than 376.50 %, 23.14 % and 2.54 % in the return loss, bandwidth, gain and radiation efficiency, respectively. Later, it was found that aperiodic PCs substrate yields further performance improvements over periodic PCs substrate as found in antenna array 6, which achieved improvements of 40.83 %, 12.85 % and 1.48 % in the return loss, gain and radiation efficiency, respectively. Next, four THz 1x2 CMPA arrays with new PCs structures were introduced. These structures include air cylinders holes, air cuboids holes and mixed air cylinders holes with air cuboids holes with a modified diameter value. This novel technique demonstrated a significant improvement in the gain as found in antenna array 11 which achieved 12.03 dB ( 36.70

%) compared to the conventional 1x2 **CMPA** array which achieved 8.80 *dB*.

Finally, a novel **MIMO** system was developed using a graphene-based 1×2 **RMPA** array using different substrates, including homogeneous, periodic **PCs** and optimized **PCs** substrates. The obtained results in **CST** simulations of the proposed graphene-based 1×2 patch antenna array using the optimized **PCs** substrate exhibited excellent performance improvements as compared to the homogeneous substrate and the **PCs** substrate around 0.65 THz, which achieved a peak gain of 11.80 *dB* and broad bandwidth greater than 614 GHz. Later, a 2×2 **MIMO** system scenario was studied and analyzed using the aforementioned targeted **MIMO** antenna arrays by calculating the total path loss and the channel capacity. The capacity was compared with different schemes such as **MISO**, **SIMO** and **SISO**. The outcomes demonstrated that the proposed 2×2 **MIMO** system with a **MIMO** antenna array based on the optimized **PCs** substrate achieved the highest capacity of 23.64 *bit/s/Hz* in the highest transmit power compared to 23.42 *bit/s/Hz* and 21.42 *bit/s/Hz* obtained by the same 2×2 **MIMO** system using **MIMO** antenna array based on the periodic **PCs** and the homogeneous substrates, respectively. These results also showed a significant improvement compared to previously reported studies. Ultimately, an interesting improvement in the channel capacity was achieved by manipulating the geometric parameters of the indoor environment.

# Suggestions

As the research advances, there are some interesting suggestions about this thesis which can be highlighted as follows for the future:

1. Design of THz antenna array based on PCs in other low-attenuation windows in the frequency range of 0.99–1.09 THz, 1.21–1.41 THz, 1.42–1.59 THz, 1.92–2.04 THz, 2.05–2.15 THz, and 2.47–2.62 THz.
2. Design of larger THz array configuration based on PCs such as 8 elements (8x1 array), 16 elements (4x4 array), 32 elements (4x8 array) or 64 elements (8x8 array).
3. Design new PCs structures that improve further the antenna array radiation characteristics.
4. Design of new THz antenna arrays with different types of radiated patches based on PCs with graphene.
5. Design of different communication scenarios with larger system scales such as 4x4 and 8x8 for THz MIMO system implementation based on antenna arrays.



# Publications

## Journal Papers

1. **Mohamed Elamine Benlakehal**, Abdesselam Hocini, Djamel Khedrouche, Mohamed Nasr Eddine Temmar & Tayeb Ahmed Denidni, “Design and analysis of a  $2 \times 2$  microstrip patch antenna array based on periodic and non-periodic photonic crystals substrate in THz”. *Optical and Quantum Electronics*, volume 54, Article number: 190 (2022).
2. **Mohamed Elamine Benlakehal**, Abdesselam Hocini, Djamel Khedrouche, Mohamed Nasr Eddine Temmar & Tayeb Ahmed Denidni, “Design and analysis of novel microstrip patch antenna array based on photonic crystal in THz”. *Optical and Quantum Electronics*, volume 54, Article number: 297 (2022).
3. **Mohamed Elamine Benlakehal**, Abdesselam Hocini, Djamel Khedrouche, Mohamed Nasr Eddine Temmar & Tayeb Ahmed Denidni, “ Design and analysis of a  $1 \times 2$  microstrip patch antenna array based on periodic and aperiodic photonic crystals in terahertz”. *Optical and Quantum Electronics*, volume 54, Article number: 672 (2022).
4. **Mohamed Elamine Benlakehal**, Abdesselam Hocini, Djamel Khedrouche, Mohamed Nasr Eddine Temmar & Tayeb Ahmed Denidni, “ Design and analysis of MIMO system for THz communication using terahertz patch antenna array based on photonic crystals with graphene”. *Optical and Quantum Electronics*, volume 54, Article number: 693 (2022).
5. **Mohamed Elamine Benlakehal**, Abdesselam Hocini, Djamel Khedrouche, Mohamed Nasr Eddine Temmar, Tayeb Ahmed Denidni & Ibraheem Shayea, “ Design and analysis of a  $1 \times 2$  microstrip patch antenna array based on photonic crystals with a graphene load in THZ”. *Journal of Optics*, volume 52, pages 483–493 (2023).
6. **Mohamed Elamine Benlakehal**, Abdesselam Hocini, Djamel Khedrouche, Mohamed Nasr Eddine Temmar & Tayeb Ahmed Denidni, “ Gain enhancement of a novel  $1 \times 2$  microstrip patch antenna array based on cylindrical and cuboid photonic crystal substrate in THz”. *Analog Integrated Circuits and Signal Processing*, volume 114, pages 159–170 (2023).

7. **Mohamed Elamine Benlakehal**, Abdesselam Hocini, Djamel Khedrouche, Mohamed Nasr Eddine Temmar, Tayeb Ahmed Denidni & Ibraheem Shayea, “ Design and simulation of 1x2, 1x4 and 2x8 microstrip patch antenna arrays based on photonic crystals for improved gain performance in THz”. *Journal of Optics*. 53, 260–271 (2024).
8. **Mohamed Elamine Benlakehal**, Ibraheem Shayea, Ayman A. El-Saleh, Abdurraqeb Alhammadi, “ Design and simulation of high gain 2-element, 4-element and 16-element arrays of microstrip patch antenna for terahertz application based on photonic crystals”. *International Journal of Integrated Engineering*. (Accepted and waiting for production), 2024.

## International Communications

1. Ozan Emre Sabirli, **Mohamed Elamine Benlakehal**, Ibraheem Shayea, Ayman A. El-Saleh & Abdurraqeb Alhammadi, “ Network Core and Radio Access Network in 6G Communication Systems ”. *Multimedia University Engineering Conference 2023 (MECON 2023)*. #620 (1570925687).

# Bibliography

- [1] K. R. Jha and G. Singh, "Terahertz planar antennas for future wireless communication: A technical review," *infrared physics & Technology*, vol. 60, pp. 71–80, 2013.
- [2] M. J. Fitch and R. Oslander, "Terahertz waves for communications and sensing," *Johns Hopkins APL technical digest*, vol. 25, no. 4, pp. 348–355, 2004.
- [3] C. Kulesa, "Terahertz spectroscopy for astronomy: From comets to cosmology," *IEEE Transactions on Terahertz Science and Technology*, vol. 1, no. 1, pp. 232–240, 2011.
- [4] J. A. Zeitler and L. F. Gladden, "In-vitro tomography and non-destructive imaging at depth of pharmaceutical solid dosage forms," *European Journal of Pharmaceutics and Biopharmaceutics*, vol. 71, no. 1, pp. 2–22, 2009.
- [5] P. H. Siegel, "Terahertz technology in biology and medicine," *IEEE transactions on microwave theory and techniques*, vol. 52, no. 10, pp. 2438–2447, 2004.
- [6] P. Hillger, J. Grzyb, R. Jain, and U. R. Pfeiffer, "Terahertz imaging and sensing applications with silicon-based technologies," *IEEE Transactions on Terahertz Science and Technology*, vol. 9, no. 1, pp. 1–19, 2018.
- [7] M. Naftaly and R. E. Miles, "Terahertz time-domain spectroscopy for material characterization," *Proceedings of the IEEE*, vol. 95, no. 8, pp. 1658–1665, 2007.
- [8] P. H. Siegel, "Terahertz technology," *IEEE Transactions on microwave theory and techniques*, vol. 50, no. 3, pp. 910–928, 2002.
- [9] H.-B. Liu, H. Zhong, N. Karpowicz, Y. Chen, and X.-C. Zhang, "Terahertz spectroscopy and imaging for defense and security applications," *Proceedings of the IEEE*, vol. 95, no. 8, pp. 1514–1527, 2007.
- [10] S. S. Gao, H.-M. Qiao, and J.-L. Li, "Multibeam holographic antenna for terahertz applications," *Optik*, vol. 181, pp. 538–544, 2019.
- [11] M. E. Benlakehal, A. Hocini, D. Khedrouche, M. N. e. Temmar, T. A. Denidni, and I. Shayea, "Design and simulation of  $1 \times 2$ ,  $1 \times 4$  and  $2 \times 8$  microstrip patch antenna arrays based on photonic crystals for improved gain performance in thz," *Journal of Optics*, pp. 1–12, 2023.
- [12] M. E. Benlakehal, A. Hocini, D. Khedrouche, T. A. Denidni, *et al.*, "Design and analysis of novel microstrip patch antenna array based on photonic crystal in thz," *Optical and Quantum Electronics*, vol. 54, no. 5, pp. 1–16, 2022.
- [13] M. E. Benlakehal, A. Hocini, D. Khedrouche, M. N. E. Temmar, and T. A. Denidni, "Design and analysis of a  $2 \times 2$  microstrip patch antenna array based on periodic and non-periodic photonic crystals substrate in thz," *OPTICAL AND QUANTUM ELECTRONICS*, vol. 54, no. 3, 2022.

- 
- [14] M. E. Benlakehal, A. Hocini, D. Khedrouche, M. N. E. Temmar, and T. A. Denidni, "Design and analysis of a  $1 \times 2$  microstrip patch antenna array based on periodic and aperiodic photonic crystals in terahertz," *OPTICAL AND QUANTUM ELECTRONICS*, vol. 54, no. 10, 2022.
- [15] M. E. Benlakehal, A. Hocini, D. Khedrouche, M. N. E. Temmar, D. Ahmed, and I. Shayea, "Gain enhancement of a novel  $1 \times 2$  microstrip patch antenna array based on cylindrical and cuboid photonic crystal substrate in thz," *Analog Integrated Circuits and Signal Processing*, vol. 114, no. 1, pp. 159–170, 2023.
- [16] M. E. Benlakehal, A. Hocini, D. Khedrouche, M. N. E. Temmar, D. Ahmed, and I. Shayea, "Design and analysis of a  $1 \times 2$  microstrip patch antenna array based on photonic crystals with a graphene load in thz," *Optics*, vol. 52, no. 2, pp. 483–493, 2022.
- [17] M. E. Benlakehal, A. Hocini, D. Khedrouche, M. N. E. Temmar, and T. A. Denidni, "Design and analysis of mimo system for thz communication using terahertz patch antenna array based on photonic crystals with graphene," *OPTICAL AND QUANTUM ELECTRONICS*, vol. 54, no. 11, 2022.
- [18] D. L. Woolard, R. Brown, M. Pepper, and M. Kemp, "Terahertz frequency sensing and imaging: A time of reckoning future applications?," *Proceedings of the IEEE*, vol. 93, no. 10, pp. 1722–1743, 2005.
- [19] J. Chamberlain, "Where optics meets electronics: recent progress in decreasing the terahertz gap," *Philosophical Transactions of the Royal Society of London. Series A: Mathematical, Physical and Engineering Sciences*, vol. 362, no. 1815, pp. 199–213, 2004.
- [20] R. Piesiewicz, T. Kleine-Ostmann, N. Krumbholz, D. Mittleman, M. Koch, J. Schoebel, and T. Kurner, "Short-range ultra-broadband terahertz communications: Concepts and perspectives," *IEEE Antennas and Propagation Magazine*, vol. 49, no. 6, pp. 24–39, 2007.
- [21] M. Toyoshima, "Trends in satellite communications and the role of optical free-space communications," *Journal of Optical Networking*, vol. 4, no. 6, pp. 300–311, 2005.
- [22] T. Kleine-Ostmann and T. Nagatsuma, "A review on terahertz communications research," *Journal of Infrared, Millimeter, and Terahertz Waves*, vol. 32, pp. 143–171, 2011.
- [23] E. Brown, K. McIntosh, K. Nichols, and C. Dennis, "Photomixing up to 3.8 thz in low-temperature-grown gaas," *Applied Physics Letters*, vol. 66, no. 3, pp. 285–287, 1995.
- [24] S. Matsuura, M. Tani, and K. Sakai, "Generation of coherent terahertz radiation by photomixing in dipole photoconductive antennas," *Applied Physics Letters*, vol. 70, no. 5, pp. 559–561, 1997.
- [25] S. Schiller, B. Roth, F. Lewen, O. Ricken, and M. Wiedner, "Ultra-narrow-linewidth continuous-wave thz sources based on multiplier chains," *Applied Physics B*, vol. 95, pp. 55–61, 2009.
- [26] I. Mehdi, P. Siegel, D. Humphrey, T. Lee, R. Dengler, J. Oswald, A. Pease, R. Lin, H. Eisele, R. Zimmermann, *et al.*, "An all solid-state 640 ghz subharmonic mixer," in *1998 IEEE MTT-S International Microwave Symposium Digest (Cat. No. 98CH36192)*, vol. 2, pp. 403–406, IEEE, 1998.
- [27] G. Carr, M. Martin, W. McKinney, K. Jordan, G. Neil, and G. Williams, "Very high power thz radiation sources," *Journal of Biological Physics*, vol. 29, pp. 319–325, 2003.
- [28] G. P. Williams, "Filling the thz gap—high power sources and applications," *Reports on Progress in Physics*, vol. 69, no. 2, p. 301, 2005.
- [29] P. Mukherjee and B. Gupta, "Terahertz (thz) frequency sources and antennas—a brief review," *International Journal of Infrared and Millimeter Waves*, vol. 29, pp. 1091–1102, 2008.

- [30] T. Minotani, A. Hirata, and T. Nagatsuma, "A broadband 120-ghz schottky-diode receiver for 10-gbit/s wireless links," *IEICE transactions on electronics*, vol. 86, no. 8, pp. 1501–1505, 2003.
- [31] H.-J. Song, K. Ajito, A. Hirata, A. Wakatsuki, Y. Muramoto, T. Furuta, N. Kukutsu, T. Nagatsuma, and Y. Kado, "8 gbit/s wireless data transmission at 250 ghz," *Electronics Letters*, vol. 45, no. 22, pp. 1121–1122, 2009.
- [32] M. Mukherjee, N. Mazumder, S. K. Roy, and K. Goswami, "Gan impatt diode: a photo-sensitive high power terahertz source," *Semiconductor Science and Technology*, vol. 22, no. 12, p. 1258, 2007.
- [33] Y. Ren, J. Hovenier, R. Higgins, J. Gao, T. Klapwijk, S. Shi, A. Bell, B. Klein, B. Williams, S. Kumar, *et al.*, "Terahertz heterodyne spectrometer using a quantum cascade laser," *Applied Physics Letters*, vol. 97, no. 16, 2010.
- [34] M. A. Belkin, F. Capasso, F. Xie, A. Belyanin, M. Fischer, A. Wittmann, and J. Faist, "Room temperature terahertz quantum cascade laser source based on intracavity difference-frequency generation," *Applied Physics Letters*, vol. 92, no. 20, 2008.
- [35] T. Kleine-Ostmann, K. Pierz, G. Hein, P. Dawson, and M. Koch, "Audio signal transmission over thz communication channel using semiconductor modulator," *Electron. Lett.*, vol. 40, no. 2, pp. 124–126, 2004.
- [36] A. Hirata, T. Kosugi, H. Takahashi, R. Yamaguchi, F. Nakajima, T. Furuta, *et al.*, "Ieee trans. microwave theory tech.," *IEEE Trans. Microwave Theory Tech.*, vol. 54, no. 5, pp. 1937–1944, 2006.
- [37] W. Yin, *Efficient Terahertz Antennas Using Photomixer and Resonant Tunneling diodes sources*. PhD thesis, University of Sheffield, 2017.
- [38] B. Thomas, A. Maestrini, J. Gill, C. Lee, R. Lin, I. Mehdi, and P. de Maagt, "A broadband 835–900-ghz fundamental balanced mixer based on monolithic gaas membrane schottky diodes," *IEEE Transactions on Microwave Theory and Techniques*, vol. 58, no. 7, pp. 1917–1924, 2010.
- [39] M. A. Belkin, F. Capasso, A. Belyanin, D. L. Sivco, A. Y. Cho, D. C. Oakley, C. J. Vineis, and G. W. Turner, "Terahertz quantum-cascade-laser source based on intracavity difference-frequency generation," *Nature Photonics*, vol. 1, no. 5, pp. 288–292, 2007.
- [40] B. S. Williams, S. Kumar, Q. Hu, and J. L. Reno, "Operation of terahertz quantum-cascade lasers at 164 k in pulsed mode and at 117 k in continuous-wave mode," *Optics express*, vol. 13, no. 9, pp. 3331–3339, 2005.
- [41] A. Hirata, T. Kosugi, H. Takahashi, R. Yamaguchi, F. Nakajima, T. Furuta, H. Ito, H. Sugahara, Y. Sato, and T. Nagatsuma, "120-ghz-band millimeter-wave photonic wireless link for 10-gb/s data transmission," *IEEE transactions on microwave theory and techniques*, vol. 54, no. 5, pp. 1937–1944, 2006.
- [42] H. Elayan, O. Amin, B. Shihada, R. M. Shubair, and M.-S. Alouini, "Terahertz band: The last piece of rf spectrum puzzle for communication systems," *IEEE Open Journal of the Communications Society*, vol. 1, pp. 1–32, 2019.
- [43] K. Cooper, R. Dengler, G. Chattopadhyay, E. Schlecht, J. Gill, A. Skalare, I. Mehdi, and P. Siegel, "A high-resolution imaging radar at 580 ghz," *IEEE Microwave and wireless components letters*, vol. 18, no. 1, pp. 64–66, 2008.
- [44] J. Kraus and R. Marhefka, "Antenna temperature, remote sensing and radar cross section," *Antennas for All Applications 3rd Edition, McGraw Hill, NY: New York*, pp. 401–426, 2002.
- [45] E. Brown, "Fundamentals of terrestrial millimeter-wave and thz remote sensing," *International journal of high speed electronics and systems*, vol. 13, no. 04, pp. 995–1097, 2003.

- [46] C. A. Balanis, "Antenna theory: A review," *Proceedings of the IEEE*, vol. 80, no. 1, pp. 7–23, 1992.
- [47] H. Röser, E. Durwen, R. Wattenbach, and G. Schultz, "Investigation of a heterodyne receiver with open structure mixer at 324 ghz and 693 ghz," *International journal of infrared and millimeter waves*, vol. 5, pp. 301–314, 1984.
- [48] J. Zmuidzinis, A. Betz, and R. Boreiko, "A corner-reflector mixer mount for far infrared wavelengths," *Infrared physics*, vol. 29, no. 1, pp. 119–131, 1989.
- [49] S. S. Gearhart, C. C. Ling, G. M. Rebeiz, H. Davee, and G. Chin, "Integrated 119- $\mu$ m linear corner-cube array," *IEEE microwave and guided wave letters*, vol. 1, no. 7, pp. 155–157, 1991.
- [50] G. Bansal, A. Singh, R. Bala, *et al.*, "A triband slotted bow-tie wideband thz antenna design using graphene for wireless applications," *Optik*, vol. 185, pp. 1163–1171, 2019.
- [51] M. Runge, D. Engel, M. Schneider, K. Reimann, M. Woerner, and T. Elsaesser, "Spatial distribution of electric-field enhancement across the gap of terahertz bow-tie antennas," *Optics Express*, vol. 28, no. 17, pp. 24389–24398, 2020.
- [52] W. Miao, Y. Delorme, F. Dauply, R. Lefevre, B. Lecomte, A. Feret, G. Beaudin, J. Krieg, W. Zhang, S. Cheng, *et al.*, "Investigation of a 600-ghz membrane-based twin slot antenna for heb mixers," in *Proceedings of 19th international symposium on space terahertz technology*, pp. 28–30, 2008.
- [53] J. Van Rudd and D. M. Mittleman, "Influence of substrate-lens design in terahertz time-domain spectroscopy," *JOSA B*, vol. 19, no. 2, pp. 319–329, 2002.
- [54] A. V. Boriskin, R. Sauleau, and A. I. Nosich, "Performance of hemielliptic dielectric lens antennas with optimal edge illumination," *IEEE Transactions on Antennas and Propagation*, vol. 57, no. 7, pp. 2193–2198, 2009.
- [55] A. Neto, "Uwb, non dispersive radiation from the planarly fed leaky lens antenna—part 1: Theory and design," *IEEE Transactions on Antennas and Propagation*, vol. 58, no. 7, pp. 2238–2247, 2010.
- [56] A. Karttunen, J. Ala-Laurinaho, R. Sauleau, and A. V. Räsänen, "A study of extended hemispherical lenses for a high-gain beam-steering antenna," in *Proceedings of the Fourth European Conference on Antennas and Propagation*, pp. 1–5, IEEE, 2010.
- [57] M. Koch, "Terahertz communications: A 2020 vision," in *Terahertz frequency detection and identification of materials and objects*, pp. 325–338, Springer, 2007.
- [58] A. Sharma, V. K. Dwivedi, and G. Singh, "Thz rectangular patch microstrip antenna design using photonic crystal as substrate," in *Progress in Electromagnetic Research Symposium, Cambridge, USA*, pp. 161–165, 2008.
- [59] A. Sharma and G. Singh, "Rectangular microstrip patch antenna design at thz frequency for short distance wireless communication systems," *Journal of Infrared, Millimeter, and Terahertz Waves*, vol. 30, pp. 1–7, 2009.
- [60] K. R. Jha and G. Singh, "Improved performance analysis of square patch microstrip antenna at terahertz frequency," in *2009 International Conference on Advances in Recent Technologies in Communication and Computing*, pp. 676–679, IEEE, 2009.
- [61] K. R. Jha, G. Singh, K. R. Jha, and G. Singh, "Performance analysis of an open-loop resonator loaded terahertz microstrip antenna," *Terahertz Planar Antennas for Next Generation Communication*, pp. 125–145, 2014.
- [62] G. Singh, "Design considerations for rectangular microstrip patch antenna on electromagnetic crystal substrate at terahertz frequency," *Infrared Physics & Technology*, vol. 53, no. 1, pp. 17–22, 2010.

- [63] K. R. Jha and G. Singh, "Dual-band rectangular microstrip patch antenna at terahertz frequency for surveillance system," *Journal of computational electronics*, vol. 9, pp. 31–41, 2010.
- [64] A. K. Bhattacharyya, "Characteristics of space and surface waves in a multilayered structure (microstrip antennas)," *IEEE Transactions on Antennas and Propagation*, vol. 38, no. 8, pp. 1231–1238, 1990.
- [65] R. Gonzalo, I. Ederra, C. Mann, and P. De Maagt, "Radiation properties of terahertz dipole antenna mounted on photonic crystal," *Electronics Letters*, vol. 37, no. 10, p. 1, 2001.
- [66] K. R. Jha and G. Singh, "Analysis and design of enhanced directivity microstrip antenna at terahertz frequency by using electromagnetic bandgap material," *International Journal of Numerical Modelling: Electronic Networks, Devices and Fields*, vol. 24, no. 5, pp. 410–424, 2011.
- [67] A. Sharma, V. K. Dwivedi, and G. Singh, "Thz rectangular microstrip patch antenna on multilayered substrate for advance wireless communication systems," in *Progress in electromagnetics research symposium, Beijing, China*, pp. 627–631, 2009.
- [68] K. R. Jha and G. Singh, "Microstrip patch array antenna on photonic crystal substrate at terahertz frequency," *Infrared Physics & Technology*, vol. 55, no. 1, pp. 32–39, 2012.
- [69] G. R. DeJean and M. M. Tentzeris, "A new high-gain microstrip yagi array antenna with a high front-to-back (f/b) ratio for wlan and millimeter-wave applications," *IEEE Transactions on Antennas and Propagation*, vol. 55, no. 2, pp. 298–304, 2007.
- [70] Y. Doraisingam, *Bandwidth enhancement of microstrip antenna for wireless local area network applications*. PhD thesis, Universiti Putra Malaysia, 2007.
- [71] M. H. Khatun, R. Inum, and N. Tasnim, "Design of rectangular patch antenna array using different feeding technique," in *2017 2nd International Conference on Electrical & Electronic Engineering (ICEEE)*, pp. 1–4, IEEE, 2017.
- [72] K. K. Singh and S. Gupta, "Review and analysis of microstrip patch array antenna with different configurations," *International Journal of scientific & engineering research*, vol. 4, no. 2, p. 6, 2013.
- [73] K. K. Singh and S. Gupta, "Design and simulation of microstrip patch array antenna for c band application at imt (4400-4900 mhz) advanced spectrum with series feed and parallel feed," *International Journal of Scientific & Engineering Research*, vol. 4, no. 12, 2013.
- [74] T. A. Milligan, *Modern antenna design*. John Wiley & Sons, 2005.
- [75] R. Waterhouse, "Microstrip patch antennas," in *Handbook of Antennas in Wireless Communications*, pp. 6–1, CRC Press, 2018.
- [76] K. Chen, Z. He, and C. Han, "A modified real ga for the sparse linear array synthesis with multiple constraints," *IEEE Transactions on Antennas and Propagation*, vol. 54, no. 7, pp. 2169–2173, 2006.
- [77] R. Bala and A. Marwaha, "Analysis of graphene based triangular nano patch antenna using photonic crystal as substrate for wireless applications," in *2015 2nd International Conference on Recent Advances in Engineering & Computational Sciences (RAECS)*, pp. 1–7, IEEE, 2015.
- [78] R. Garg, *Microstrip antenna design handbook*. Artech house, 2001.
- [79] C. A. Balanis, *Antenna theory: analysis and design*. John wiley & sons, 2016.
- [80] H. J. Visser, *Array and phased array antenna basics*. John Wiley & Sons, 2006.

- [81] R. Mailloux, J. McIlvenna, and N. Kernweis, "Microstrip array technology," *IEEE transactions on antennas and propagation*, vol. 29, no. 1, pp. 25–37, 1981.
- [82] C.-C. Hu, C. Jsu, and J.-J. Wu, "An aperture-coupled linear microstrip leaky-wave antenna array with two-dimensional dual-beam scanning capability," *IEEE Transactions on Antennas and Propagation*, vol. 48, no. 6, pp. 909–913, 2000.
- [83] G.-c. Kang, H.-y. Lee, J.-k. Kim, M.-j. Park, F. J. Harackiewicz, N.-Y. Kim, and B. Lee, "Ku-band high efficiency antenna with corporate-series-fed microstrip array," in *IEEE Antennas and Propagation Society International Symposium. Digest. Held in conjunction with: US-NC/CNC/URSI North American Radio Sci. Meeting (Cat. No. 03CH37450)*, vol. 4, pp. 690–693, IEEE, 2003.
- [84] D. Pozar and D. Schaubert, "Analysis of an infinite array of rectangular microstrip patches with idealized probe feeds," *IEEE Transactions on Antennas and Propagation*, vol. 32, no. 10, pp. 1101–1107, 1984.
- [85] S. Datto, M. R. I. Sheikh, and N. M. Sohayeb, "Optimized microstrip patch antenna (mpa) array design to enhance gain for s-band application," *IOSR Journal of Electrical and Electronics Engineering*, vol. 12, pp. 74–78, 2017.
- [86] N. Capet, C. Martel, J. Sokoloff, and O. Pascal, "Optimum high impedance surface configuration for mutual coupling reduction in small antenna arrays," *Progress In Electromagnetics Research B*, vol. 32, pp. 283–297, 2011.
- [87] M. F. Abedin and M. Ali, "Effects of a smaller unit cell planar ebg structure on the mutual coupling of a printed dipole array," *IEEE Antennas and Wireless Propagation Letters*, vol. 4, pp. 274–276, 2005.
- [88] M. S. Alam, M. T. Islam, and N. Misran, "A novel compact split ring slotted electromagnetic bandgap structure for microstrip patch antenna performance enhancement," *Progress In Electromagnetics Research*, vol. 130, pp. 389–409, 2012.
- [89] D. Guha, S. Biswas, M. Biswas, J. Y. Siddiqui, and Y. M. Antar, "Concentric ring-shaped defected ground structures for microstrip applications," *IEEE antennas and wireless propagation letters*, vol. 5, pp. 402–405, 2006.
- [90] C.-Y. Chiu, C.-H. Cheng, R. D. Murch, and C. R. Rowell, "Reduction of mutual coupling between closely-packed antenna elements," *IEEE transactions on antennas and propagation*, vol. 55, no. 6, pp. 1732–1738, 2007.
- [91] D. Sievenpiper, L. Zhang, R. F. Broas, N. G. Alexopolous, and E. Yablonovitch, "High-impedance electromagnetic surfaces with a forbidden frequency band," *IEEE Transactions on Microwave Theory and techniques*, vol. 47, no. 11, pp. 2059–2074, 1999.
- [92] K. Buell, H. Mosallaei, and K. Sarabandi, "Electromagnetic metamaterial insulator to eliminate substrate surface waves," in *2005 IEEE Antennas and Propagation Society International Symposium*, vol. 2, pp. 574–577, IEEE, 2005.
- [93] F. Yang and Y. Rahmat-Samii, "Microstrip antennas integrated with electromagnetic band-gap (ebg) structures: A low mutual coupling design for array applications," *IEEE transactions on antennas and propagation*, vol. 51, no. 10, pp. 2936–2946, 2003.
- [94] H.-Y. Yang, N. G. Alexopoulos, and E. Yablonovitch, "Photonic band-gap materials for high-gain printed circuit antennas," *IEEE Transactions on Antennas and Propagation*, vol. 45, no. 1, pp. 185–187, 1997.
- [95] B. Wan, L. Zhu, X. Ma, T. Li, and J. Zhang, "Characteristic analysis and structural design of hollow-core photonic crystal fibers with band gap cladding structures," *Sensors*, vol. 21, no. 1, p. 284, 2021.



- [96] E. Yablonovitch, "Photonic crystals: semiconductors of light," *Scientific American*, vol. 285, no. 6, pp. 46–55, 2001.
- [97] E. Yablonovitch, T. Gmitter, and K.-M. Leung, "Photonic band structure: The face-centered-cubic case employing nonspherical atoms," *Physical review letters*, vol. 67, no. 17, p. 2295, 1991.
- [98] M. Mulot, *Two-Dimensional Photonic Crystals in InP-based Materials*. PhD thesis, Mikroelektronik och informationsteknik, 2004.
- [99] P. R. Villeneuve and M. Piche, "Photonic band gaps in two-dimensional square and hexagonal lattices," *Physical Review B*, vol. 46, no. 8, p. 4969, 1992.
- [100] M. Plihal and A. Maradudin, "Photonic band structure of two-dimensional systems: The triangular lattice," *Physical Review B*, vol. 44, no. 16, p. 8565, 1991.
- [101] K. R. Jha and G. Singh, "Analysis and design of terahertz microstrip antenna on photonic bandgap material," *Journal of Computational Electronics*, vol. 11, no. 4, pp. 364–373, 2012.
- [102] M. V. Hidayat and C. Apriono, "Design of 0.312 thz microstrip linear array antenna for breast cancer imaging application," in *2018 International Conference on Signals and Systems (ICSigSys)*, pp. 224–228, IEEE, 2018.
- [103] H. Kanaya, M. Koga, K. Tsugami, G. C. Eu, and K. Kato, "4x4 planar array antenna on indium phosphide substrate for 0.3-thz band application," in *Terahertz, RF, Millimeter, and Submillimeter-Wave Technology and Applications X*, vol. 10103, p. 101031N, International Society for Optics and Photonics, 2017.
- [104] A. Azarbar, M. Masouleh, and A. Behbahani, "A new terahertz microstrip rectangular patch array antenna," *International Journal of Electromagnetics and Applications*, vol. 4, no. 1, pp. 25–29, 2014.
- [105] R. K. Kushwaha, P. Karuppanan, and Y. Srivastava, "Proximity feed multiband patch antenna array with srr and pbg for thz applications," *Optik*, vol. 175, pp. 78–86, 2018.
- [106] K.-C. Huang and Z. Wang, "Terahertz terabit wireless communication," *IEEE Microwave Magazine*, vol. 12, no. 4, pp. 108–116, 2011.
- [107] I. F. Akyildiz, J. M. Jornet, and C. Han, "Terahertz band: Next frontier for wireless communications," *Physical Communication*, vol. 12, pp. 16–32, 2014.
- [108] J. Federici and L. Moeller, "Review of terahertz and subterahertz wireless communications," *Journal of Applied Physics*, vol. 107, no. 11, p. 6, 2010.
- [109] J.-i. Nishizawa, T. Sasaki, K. Suto, T. Yamada, T. Tanabe, T. Tanno, T. Sawai, and Y. Miura, "Thz imaging of nucleobases and cancerous tissue using a gap thz-wave generator," *Optics communications*, vol. 244, no. 1-6, pp. 469–474, 2005.
- [110] J.-H. Son, "Terahertz electromagnetic interactions with biological matter and their applications," *Journal of Applied Physics*, vol. 105, no. 10, p. 102033, 2009.
- [111] Z. Li, L. Guan, C. Li, and A. Radwan, "A secure intelligent spectrum control strategy for future thz mobile heterogeneous networks," *IEEE Communications Magazine*, vol. 56, no. 6, pp. 116–123, 2018.
- [112] M. Siegel and R. King, "Ieee trans. antennas propag.," 1971.
- [113] I. Malhotra, K. R. Jha, and G. Singh, "Terahertz antenna technology for imaging applications: A technical review," *International Journal of Microwave and Wireless Technologies*, vol. 10, no. 3, p. 271, 2018.

- [114] S. Galoda and G. Singh, "Fighting terrorism with terahertz," *Ieee Potentials*, vol. 26, no. 6, pp. 24–29, 2007.
- [115] Y. B. Ji, S. J. Oh, S.-G. Kang, J. Heo, S.-H. Kim, Y. Choi, S. Song, H. Y. Son, S. H. Kim, J. H. Lee, *et al.*, "Terahertz reflectometry imaging for low and high grade gliomas," *Scientific reports*, vol. 6, no. 1, pp. 1–9, 2016.
- [116] T. Schneider, A. Wiatrek, S. Preußler, M. Grigat, and R.-P. Braun, "Link budget analysis for terahertz fixed wireless links," *IEEE Transactions on Terahertz Science and Technology*, vol. 2, no. 2, pp. 250–256, 2012.
- [117] R. K. Kushwaha, P. Karuppanan, and L. Malviya, "Design and analysis of novel microstrip patch antenna on photonic crystal in thz," *Physica B: Condensed Matter*, vol. 545, pp. 107–112, 2018.
- [118] K. Han, T. K. Nguyen, I. Park, and H. Han, "Terahertz yagi-uda antenna for high input resistance," *Journal of Infrared, Millimeter, and Terahertz Waves*, vol. 31, no. 4, pp. 441–454, 2010.
- [119] K. H. Alharbi, A. Khalid, A. Ofiare, J. Wang, and E. Wasige, "Diced and grounded broadband bow-tie antenna with tuning stub for resonant tunnelling diode terahertz oscillators," *IET Microwaves, Antennas & Propagation*, vol. 11, no. 3, pp. 310–316, 2016.
- [120] B. Khamaisi, S. Jameson, and E. Socher, "A 210–227 ghz transmitter with integrated on-chip antenna in 90 nm cmos technology," *IEEE Transactions on Terahertz Science and Technology*, vol. 3, no. 2, pp. 141–150, 2013.
- [121] K. Wu, Y. J. Cheng, T. Djerafi, and W. Hong, "Substrate-integrated millimeter-wave and terahertz antenna technology," *Proceedings of the IEEE*, vol. 100, no. 7, pp. 2219–2232, 2012.
- [122] K.-M. Mak, K.-K. So, H.-W. Lai, and K.-M. Luk, "A magnetoelectric dipole leaky-wave antenna for millimeter-wave application," *IEEE Transactions on Antennas and Propagation*, vol. 65, no. 12, pp. 6395–6402, 2017.
- [123] F. Formanek, M.-A. Brun, T. Umetsu, S. Omori, and A. Yasuda, "Aspheric silicon lenses for terahertz photoconductive antennas," *Applied Physics Letters*, vol. 94, no. 2, 2009.
- [124] E. C. Britto, S. K. Danasegaran, and W. Johnson, "Design of slotted patch antenna based on photonic crystal for wireless communication," *International Journal of Communication Systems*, vol. 34, no. 1, p. e4662, 2021.
- [125] M. N. E. Temmar, A. Hocini, D. Khedrouche, and M. Zamani, "Analysis and design of a terahertz microstrip antenna based on a synthesized photonic bandgap substrate using bpsq," *Journal of Computational Electronics*, vol. 18, no. 1, pp. 231–240, 2019.
- [126] J. N. Burghartz, "Silicon rf technology—the two generic approaches," in *Proceeding of the 27th European Solid-State Device Research Conference*, pp. 143–153, 1997.
- [127] A. Karmakar and K. Singh, "Silicon implementation of planar topologies," in *Si-RF Technology*, pp. 1–9, Springer, 2019.
- [128] S. Reinecke Taub and S. A. Alterovitz, "Silicon technologies adjust to rf applications," *Microwaves & Rf*, vol. 33, no. E-9322, 1994.
- [129] P. G. Huray, O. Oluwafemi, J. Loyer, E. Bogatin, and X. Ye, "Impact of copper surface texture on loss: A model that works," *DesignCon 2010*, vol. 1, pp. 462–483, 2010.
- [130] A. Karmakar, B. Biswas, and A. Chauhan, "Investigation of various commonly associated imperfections in radiofrequency micro-electro-mechanical system devices and its empirical modeling," *IETE Journal of Research*, pp. 1–10, 2021.

- [131] V. Adhikar, A. Karmakar, B. Biswas, and C. Saha, "Recent trends in terahertz antenna development implementing planar geometries," in *Advances in Terahertz Technology and Its Applications*, pp. 1–17, Springer, 2021.
- [132] S. Shukla and S. S. Ojha, "Review of various techniques available to modify parameters of microstrip patch antenna,"
- [133] N. Jin, A. Yu, and X. Zhang, "An enhanced  $2 \times 2$  antenna array based on a dumbbell ebg structure," *Microwave and Optical Technology Letters*, vol. 39, no. 5, pp. 395–399, 2003.
- [134] A. Hocini, M. Temmar, D. Khedrouche, and M. Zamani, "Novel approach for the design and analysis of a terahertz microstrip patch antenna based on photonic crystals," *Photonics and Nanostructures-Fundamentals and Applications*, vol. 36, p. 100723, 2019.
- [135] M. N. eddine Temmar, A. Hocini, D. Khedrouche, and T. A. Denidni, "Enhanced flexible terahertz microstrip antenna based on modified silicon-air photonic crystal," *Optik*, vol. 217, p. 164897, 2020.
- [136] M. N. E. Temmar, A. Hocini, D. Khedrouche, and T. A. Denidni, "Analysis and design of mimo indoor communication system using terahertz patch antenna based on photonic crystal with graphene," *Photonics and Nanostructures-Fundamentals and Applications*, vol. 43, p. 100867, 2021.
- [137] H. Boutayeb and T. A. Denidni, "Gain enhancement of a microstrip patch antenna using a cylindrical electromagnetic crystal substrate," *IEEE transactions on antennas and propagation*, vol. 55, no. 11, pp. 3140–3145, 2007.
- [138] D. Jackson, J. Williams, A. K. Bhattacharyya, R. L. Smith, S. J. Buchheit, and S. Long, "Microstrip patch designs that do not excite surface waves," *IEEE Transactions on antennas and propagation*, vol. 41, no. 8, pp. 1026–1037, 1993.
- [139] A. Singh and S. Singh, "A trapezoidal microstrip patch antenna on photonic crystal substrate for high speed thz applications," *Photonics and Nanostructures-Fundamentals and applications*, vol. 14, pp. 52–62, 2015.
- [140] A. Nejati, R. A. Sadeghzadeh, and F. Geran, "Effect of photonic crystal and frequency selective surface implementation on gain enhancement in the microstrip patch antenna at terahertz frequency," *Physica B: Condensed Matter*, vol. 449, pp. 113–120, 2014.
- [141] S. Anand, D. S. Kumar, R. J. Wu, and M. Chavali, "Graphene nanoribbon based terahertz antenna on polyimide substrate," *Optik*, vol. 125, no. 19, pp. 5546–5549, 2014.
- [142] P. Hall and C. Hall, "Coplanar corporate feed effects in microstrip patch array design," in *IEE Proceedings H (Microwaves, Antennas and Propagation)*, vol. 135, pp. 180–186, IET, 1988.
- [143] K.-L. Wu, M. Spenuk, J. Litva, and D.-G. Fang, "Theoretical and experimental study of feed network effects on the radiation pattern of series-fed microstrip antenna arrays," in *IEE Proceedings H (Microwaves, Antennas and Propagation)*, vol. 138, pp. 238–242, IET, 1991.
- [144] R. K. Kushwaha and P. Karuppanan, "Enhanced radiation characteristics of graphene-based patch antenna array employing photonic crystals and dielectric grating for thz applications," *Optik*, vol. 200, p. 163422, 2020.
- [145] R. Waterhouse, *Microstrip Patch Antennas: A Designer's Guide: A Designer's Guide*. Springer Science & Business Media, 2003.
- [146] B. Biswas, A. Karmakar, and V. Adhikar, "Liquid crystal polymer: Potential bio-compatible substrate for antenna application.," *Microwave Review*, vol. 27, no. 1, 2021.
- [147] C. A. Balanis, "Microstrip antennas," *Antenna theory: analysis and design*, vol. 3, pp. 811–882, 2005.

- [148] M. Rabbani and H. Ghafouri-Shiraz, "Size improvement of rectangular microstrip patch antenna at mm-wave and terahertz frequencies," *Microwave and Optical Technology Letters*, vol. 57, no. 11, pp. 2585–2589, 2015.
- [149] M. A. Rahim, I. Ibrahim, R. Kamaruddin, Z. Zakaria, and N. Hassim, "Characterization of microstrip patch array antenna at 28 ghz," *Journal of Telecommunication, Electronic and Computer Engineering (JTEC)*, vol. 9, no. 2-8, pp. 137–141, 2017.
- [150] A. G. Bole, A. Wall, and A. Norris, *Radar and ARPA manual: radar, AIS and target tracking for marine radar users*. Butterworth-Heinemann, 2013.
- [151] P. Russer and N. Fichtner, "Nanoelectronics in radio-frequency technology," *IEEE Microwave Magazine*, vol. 11, no. 3, pp. 119–135, 2010.
- [152] M. Biabanifard and M. S. Abrishamian, "Circuit modeling of tunable terahertz graphene absorber," *Optik*, vol. 158, pp. 842–849, 2018.
- [153] W. L. Chan, J. Deibel, and D. M. Mittleman, "Imaging with terahertz radiation," *Reports on progress in physics*, vol. 70, no. 8, p. 1325, 2007.
- [154] N. Surkamp, B. Döpke, Y. Hu, C. Brenner, M. Hofmann, A. Klehr, A. Knigge, and G. Tränkle, "Terahertz time-domain spectroscopy by asynchronous sampling with modelocked semiconductor lasers," in *2018 First International Workshop on Mobile Terahertz Systems (IWMTS)*, pp. 1–4, IEEE, 2018.
- [155] S. U. Hwu, K. B. deSilva, and C. T. Jih, "Terahertz (thz) wireless systems for space applications," in *2013 IEEE Sensors Applications Symposium Proceedings*, pp. 171–175, IEEE, 2013.
- [156] S. Poorgholam-Khanjari and F. B. Zarrabi, "Reconfigurable vivaldi thz antenna based on graphene load as hyperbolic metamaterial for skin cancer spectroscopy," *Optics Communications*, vol. 480, p. 126482, 2021.
- [157] D. L. Woolard, J. O. Jensen, and R. J. Hwu, *Terahertz science and technology for military and security applications*, vol. 46. world scientific, 2007.
- [158] A. A. Althuwayb, "On-chip antenna design using the concepts of metamaterial and siw principles applicable to terahertz integrated circuits operating over 0.6–0.622 thz," *International Journal of Antennas and Propagation*, vol. 2020, 2020.
- [159] D. Tse and P. Viswanath, *Fundamentals of wireless communication*. Cambridge university press, 2005.
- [160] Y. D. Sirmaci, C. K. Akin, and C. Sabah, "Fishnet based metamaterial loaded thz patch antenna," *Optical and Quantum Electronics*, vol. 48, no. 2, pp. 1–10, 2016.
- [161] C. Cheng, Y. Lu, D. Zhang, F. Ruan, and G. Li, "Gain enhancement of terahertz patch antennas by coating epsilon-near-zero metamaterials," *Superlattices and Microstructures*, vol. 139, p. 106390, 2020.
- [162] D. Pozar, "Considerations for millimeter wave printed antennas," *IEEE Transactions on antennas and propagation*, vol. 31, no. 5, pp. 740–747, 1983.
- [163] H. Chu, Y.-X. Guo, T.-G. Lim, Y. M. Khoo, and X. Shi, "135-ghz micromachined on-chip antenna and antenna array," *IEEE Transactions on Antennas and Propagation*, vol. 60, no. 10, pp. 4582–4588, 2012.
- [164] E. Semouchkina, R. Duan, N. P. Gandji, S. Jamilan, G. Semouchkin, and R. Pandey, "Superluminal media formed by photonic crystals for transformation optics-based invisibility cloaks," *Journal of Optics*, vol. 18, no. 4, p. 044007, 2016.

- [165] A. I. Il'in, V. T. Volkov, O. V. Trofimov, and M. Y. Barabanenkov, "Technological problems in forming si waveguide lamellar diffraction gratings and 2d photonic crystals by plasma and wet etching of si," in *2015 IEEE 15th International Conference on Nanotechnology (IEEE-NANO)*, pp. 983–986, IEEE, 2015.
- [166] I. Ahmad, S. Ullah, S. Ullah, U. Habib, S. Ahmad, A. Ghaffar, M. Alibakhshikenari, S. Khan, and E. Limiti, "Design and analysis of a photonic crystal based planar antenna for thz applications," *Electronics*, vol. 10, no. 16, p. 1941, 2021.
- [167] V. M. Lubecke, K. Mizuno, and G. M. Rebeiz, "Micromachining for terahertz applications," *IEEE transactions on microwave theory and techniques*, vol. 46, no. 11, pp. 1821–1831, 1998.
- [168] Z. Lu and D. W. Prather, "Calculation of effective permittivity, permeability, and surface impedance of negative-refraction photonic crystals," *Optics Express*, vol. 15, no. 13, pp. 8340–8345, 2007.
- [169] M. Rabbani and H. Ghafouri-Shiraz, "Improvement of microstrip antenna's bandwidth and fabrication tolerance at terahertz frequency bands," 2015.
- [170] M. S. Rabbani and H. Ghafouri-Shiraz, "Liquid crystalline polymer substrate-based thz microstrip antenna arrays for medical applications," *IEEE Antennas and Wireless Propagation Letters*, vol. 16, pp. 1533–1536, 2017.
- [171] L. Lewin, "Spurious radiation from microstrip," in *Proceedings of the Institution of Electrical Engineers*, vol. 125, pp. 633–642, IET, 1978.
- [172] S. H. Kim, K.-D. Lee, J.-Y. Kim, M.-K. Kwon, and S.-J. Park, "Fabrication of photonic crystal structures on light emitting diodes by nanoimprint lithography," *Nanotechnology*, vol. 18, no. 5, p. 055306, 2007.
- [173] S. M. Palhade and S. Yawale, "Design and photo-lithographic fabrication of microstrip patch antenna," *Int. J. Sci. Res*, vol. 4, no. 2, p. 2021, 2015.
- [174] J. Cao, Z. Xue, and M. Cao, "Beam tilt-angle estimation for monopole end-fire array mounted on a finite ground plane," *International Journal of Antennas and Propagation*, vol. 2015, 2015.
- [175] S. Ullah, C. Ruan, T. U. Haq, and X. Zhang, "High performance thz patch antenna using photonic band gap and defected ground structure," *Journal of Electromagnetic Waves and Applications*, vol. 33, no. 15, pp. 1943–1954, 2019.
- [176] N. Kushwaha, R. Kumar, R. R. Krishna, and T. Oli, "Design and analysis of new compact uwb frequency selective surface and its equivalent circuit," *Progress In Electromagnetics Research C*, vol. 46, pp. 31–39, 2014.
- [177] S. Sharma, C. Tripathi, and R. Rishi, "Impedance matching techniques for microstrip patch antenna," *Indian Journal of Science and Technology*, vol. 10, no. 28, pp. 1–16, 2017.
- [178] S. Shamim, M. S. Uddin, M. Hasan, M. Samad, *et al.*, "Design and implementation of miniaturized wideband microstrip patch antenna for high-speed terahertz applications," *Journal of Computational Electronics*, vol. 20, no. 1, pp. 604–610, 2021.
- [179] K. Vasu Babu, S. Das, G. Varshney, G. N. J. Sree, and B. T. P. Madhav, "A micro-scaled graphene-based tree-shaped wideband printed mimo antenna for terahertz applications," *Journal of Computational Electronics*, vol. 21, no. 1, pp. 289–303, 2022.
- [180] R. Piesiewicz, C. Jansen, D. Mittleman, T. Kleine-Ostmann, M. Koch, and T. Kurner, "Scattering analysis for the modeling of thz communication systems," *IEEE Transactions on Antennas and Propagation*, vol. 55, no. 11, pp. 3002–3009, 2007.
- [181] H.-J. Song and T. Nagatsuma, "Present and future of terahertz communications," *IEEE transactions on terahertz science and technology*, vol. 1, no. 1, pp. 256–263, 2011.

- [182] P. Boronin, V. Petrov, D. Moltchanov, Y. Koucheryavy, and J. M. Jornet, "Capacity and throughput analysis of nanoscale machine communication through transparency windows in the terahertz band," *Nano Communication Networks*, vol. 5, no. 3, pp. 72–82, 2014.
- [183] C. Jansen, S. Priebe, C. Moller, M. Jacob, H. Dierke, M. Koch, and T. Kurner, "Diffuse scattering from rough surfaces in thz communication channels," *IEEE Transactions on Terahertz Science and Technology*, vol. 1, no. 2, pp. 462–472, 2011.
- [184] S. Mujumdar, K. Chau, and A. Elezzabi, "Experimental and numerical investigation of terahertz transmission through strongly scattering sub-wavelength size spheres," *Applied physics letters*, vol. 85, no. 25, pp. 6284–6286, 2004.
- [185] G. M. Whitman, Q. Wang, P. Spector, and F. K. Schwering, "Gaussian beam scattering from a deterministic rough metal surface," *IEEE Transactions on Antennas and Propagation*, vol. 64, no. 5, pp. 1868–1876, 2016.
- [186] A. G. Alharbi and V. Sorathiya, "Ultra-wideband graphene-based micro-sized circular patch-shaped yagi-like mimo antenna for terahertz wireless communication," *Electronics*, vol. 11, no. 9, p. 1305, 2022.
- [187] A. K. Geim and K. S. Novoselov, "The rise of graphene," in *Nanoscience and technology: a collection of reviews from nature journals*, pp. 11–19, World Scientific, 2010.
- [188] S. Ghosh, S. Harish, K. A. Rocky, M. Ohtaki, and B. B. Saha, "Graphene enhanced thermoelectric properties of cement based composites for building energy harvesting," *Energy and Buildings*, vol. 202, p. 109419, 2019.
- [189] L. A. Falkovsky, "Optical properties of graphene," in *Journal of Physics: conference series*, vol. 129, p. 012004, IOP Publishing, 2008.
- [190] T. Gan and S. Hu, "Electrochemical sensors based on graphene materials," *Microchimica Acta*, vol. 175, no. 1, pp. 1–19, 2011.
- [191] M. Pumera, "Graphene in biosensing," *Materials today*, vol. 14, no. 7-8, pp. 308–315, 2011.
- [192] Y. Cheng, H. Zhao, and C. Li, "Broadband tunable terahertz metasurface absorber based on complementary-wheel-shaped graphene," *Optical Materials*, vol. 109, p. 110369, 2020.
- [193] J. Perruisseau-Carrier, "Graphene for antenna applications: Opportunities and challenges from microwaves to thz," in *2012 Loughborough Antennas & Propagation Conference (LAPC)*, pp. 1–4, IEEE, 2012.
- [194] R. Bala and A. Marwaha, "Characterization of graphene for performance enhancement of patch antenna in thz region," *Optik*, vol. 127, no. 4, pp. 2089–2093, 2016.
- [195] M. Dragoman, A. Muller, D. Dragoman, F. Coccetti, Plana, and R, "Terahertz antenna based on graphene," *Journal of Applied Physics*, vol. 107, no. 10, p. 104313, 2010.
- [196] P. Maraghechi and A. Y. Elezzabi, "Experimental confirmation of design techniques for effective bow-tie antenna lengths at thz frequencies," *Journal of Infrared, Millimeter, and Terahertz Waves*, vol. 32, no. 7, pp. 897–901, 2011.
- [197] M. Alibakhshikenari, B. S. Virdee, M. Khalily, C. H. See, R. Abd-Alhameed, F. Falcone, T. A. Denidni, and E. Limiti, "High-gain on-chip antenna design on silicon layer with aperture excitation for terahertz applications," *IEEE Antennas and Wireless Propagation Letters*, vol. 19, no. 9, pp. 1576–1580, 2020.
- [198] Z. Wu, M. Liang, W.-R. Ng, M. Gehm, and H. Xin, "Terahertz horn antenna based on hollow-core electromagnetic crystal (emxt) structure," *IEEE Transactions on Antennas and Propagation*, vol. 60, no. 12, pp. 5557–5563, 2012.

- [199] L. Guo, H. Meng, L. Zhang, and J. Ge, "Design of mems on-chip helical antenna for thz application," in *2016 IEEE MTT-S International Microwave Workshop Series on Advanced Materials and Processes for RF and THz Applications (IMWS-AMP)*, pp. 1–4, IEEE, 2016.
- [200] H. Guerboukha, R. Shrestha, J. Neronha, O. Ryan, M. Hornbuckle, Z. Fang, and D. Mittleman, "Efficient leaky-wave antennas at terahertz frequencies generating highly directional beams," *Applied Physics Letters*, vol. 117, no. 26, p. 261103, 2020.
- [201] G. B. Wu, Y.-S. Zeng, K. F. Chan, S.-W. Qu, and C. H. Chan, "High-gain circularly polarized lens antenna for terahertz applications," *IEEE Antennas and Wireless Propagation Letters*, vol. 18, no. 5, pp. 921–925, 2019.
- [202] S. Shamim, S. Das, M. Hossain, B. T. P. Madhav, *et al.*, "Investigations on graphene-based ultra-wideband (uwb) microstrip patch antennas for terahertz (thz) applications," *Plasmonics*, vol. 16, no. 5, pp. 1623–1631, 2021.
- [203] J.-J. Tiang, M. T. Islam, N. Misran, and M. Singh, "Circular microstrip slot antenna for dual-frequency rfid application," *Progress In Electromagnetics Research*, vol. 120, pp. 499–512, 2011.
- [204] M. Turduev, I. H. Giden, C. Babayigit, Z. Hayran, E. Bor, Ç. Boztuğ, H. Kurt, and K. Stalinas, "Mid-infrared t-shaped photonic crystal waveguide for optical refractive index sensing," *Sensors and Actuators B: Chemical*, vol. 245, pp. 765–773, 2017.
- [205] H. C. C. Fernandes, A. R. Rocha, and A. Teixeira, "Analysis of antennas with pbg substrate," in *Proceedings of the 2003 SBMO/IEEE MTT-S International Microwave and Optoelectronics Conference-IMOC 2003.(Cat. No. 03TH8678)*, vol. 1, pp. 207–209, IEEE, 2003.
- [206] M.-S. Lin, C.-H. Huang, and C.-N. Chiu, "Use of high-impedance screens for enhancing antenna performance with electromagnetic compatibility," *Progress In Electromagnetics Research*, vol. 116, pp. 137–157, 2011.
- [207] M. Qi, E. Lidorikis, P. T. Rakich, S. G. Johnson, J. Joannopoulos, E. P. Ippen, and H. I. Smith, "A three-dimensional optical photonic crystal with designed point defects," *Nature*, vol. 429, no. 6991, pp. 538–542, 2004.
- [208] Y. A. Vlasov, X.-Z. Bo, J. C. Sturm, and D. J. Norris, "On-chip natural assembly of silicon photonic bandgap crystals," *Nature*, vol. 414, no. 6861, pp. 289–293, 2001.
- [209] K. Agi, K. Malloy, E. Schamiloglu, M. Mojahedi, and E. Niver, "Integration of a microstrip patch antenna with a two-dimensional photonic crystal substrate," *Electromagnetics*, vol. 19, no. 3, pp. 277–290, 1999.
- [210] E. Chow, S. Lin, S. Johnson, P. Villeneuve, J. Joannopoulos, J. R. Wendt, G. A. Vawter, W. Zubrzycki, H. Hou, and A. Alleman, "Three-dimensional control of light in a two-dimensional photonic crystal slab," *Nature*, vol. 407, no. 6807, pp. 983–986, 2000.
- [211] H. Benisty, C. Weisbuch, D. Lailly, M. Rattier, C. Smith, T. Krauss, R. M. De La Rue, R. Houdré, U. Oesterle, C. Jouanin, *et al.*, "Optical and confinement properties of two-dimensional photonic crystals," *Journal of Lightwave Technology*, vol. 17, no. 11, pp. 2063–2077, 1999.
- [212] J. Ren, G. Wang, W. Qiu, Z. Lin, H. Chen, P. Qiu, J.-X. Wang, Q. Kan, and J.-Q. Pan, "Optimization of the fano resonance lineshape based on graphene plasmonic hexamer in mid-infrared frequencies," *Nanomaterials*, vol. 7, no. 9, p. 238, 2017.
- [213] G.-W. Cheng, K. Chu, J. S. Chen, and J. T. Tsai, "Fabrication of graphene from graphite by a thermal assisted vacuum arc discharge system," *Superlattices and Microstructures*, vol. 104, pp. 258–265, 2017.

- [214] R. Aloui, Z. Houaneb, and H. Zairi, "Substrate integrated waveguide circular antenna for terahertz application," *Progress In Electromagnetics Research C*, vol. 96, pp. 229–242, 2019. [https:// DOI:10.2528/PIERC19080607](https://doi.org/10.2528/PIERC19080607).
- [215] G. W. Hanson, "Erratum:"dyadic green's functions and guided surface waves for a surface conductivity model of graphene"[j. appl. phys. 103, 064302 (2008)]," *Journal of Applied Physics*, vol. 113, no. 2, p. 029902, 2013.
- [216] Y. Yao, M. A. Kats, P. Genevet, N. Yu, Y. Song, J. Kong, and F. Capasso, "Broad electrical tuning of graphene-loaded plasmonic antennas," *Nano letters*, vol. 13, no. 3, pp. 1257–1264, 2013.
- [217] M. Esfandiyari, S. Jarchi, and M. Ghaffari-Miab, "Channel capacity enhancement by adjustable graphene-based mimo antenna in thz band," *Optical and Quantum Electronics*, vol. 51, no. 5, pp. 1–11, 2019.
- [218] W. Kemp, *Organic spectroscopy*. Bloomsbury Publishing, 2017.
- [219] G. W. Hanson, "Dyadic green's functions and guided surface waves for a surface conductivity model of graphene," *Journal of Applied Physics*, vol. 103, no. 6, p. 064302, 2008.
- [220] M. A. K. Khan, T. A. Shaem, and M. A. Alim, "Analysis of graphene based miniaturized terahertz patch antennas for single band and dual band operation," *Optik*, vol. 194, p. 163012, 2019.
- [221] M. A. K. Khan, T. A. Shaem, and M. A. Alim, "Graphene patch antennas with different substrate shapes and materials," *Optik*, vol. 202, p. 163700, 2020.
- [222] S. A. Naghdehforushha and G. Moradi, "High directivity plasmonic graphene-based patch array antennas with tunable thz band communications," *Optik*, vol. 168, pp. 440–445, 2018.
- [223] S. M. Razavizadeh, "Simulation of graphene in cst microwave v2015 and comsol multiphysics 5.2 a," *IRIB Univ., Tehran, Iran, Tech. Rep.*, 2017.
- [224] I. Llatser, C. Kremers, A. Cabellos-Aparicio, J. M. Jornet, E. Alarcón, and D. N. Chigrin, "Graphene-based nano-patch antenna for terahertz radiation," *Photonics and Nanostructures-Fundamentals and Applications*, vol. 10, no. 4, pp. 353–358, 2012.
- [225] F. Wen, S. David, X. Chécoury, M. El Kurdi, and P. Boucaud, "Two-dimensional photonic crystals with large complete photonic band gaps in both te and tm polarizations," *Optics express*, vol. 16, no. 16, pp. 12278–12289, 2008.
- [226] R. Wang, X.-H. Wang, B.-Y. Gu, and G.-Z. Yang, "Effects of shapes and orientations of scatterers and lattice symmetries on the photonic band gap in two-dimensional photonic crystals," *Journal of Applied Physics*, vol. 90, no. 9, pp. 4307–4313, 2001.
- [227] M. Younssi, A. Jaoujal, M. D. Yaccoub, A. El Moussaoui, and N. Akin, "Study of a microstrip antenna with and without superstrate for terahertz frequency," *International Journal of Innovation and Applied Studies*, vol. 2, no. 4, pp. 369–371, 2013.
- [228] M. Singh, S. Singh, and M. T. Islam, "Highly efficient ultra-wide band mimo patch antenna array for short range thz applications," in *Emerging Trends in Terahertz Engineering and System Technologies*, pp. 193–207, Springer, 2021.
- [229] C. Han, A. O. Bicen, and I. F. Akyildiz, "Multi-ray channel modeling and wideband characterization for wireless communications in the terahertz band," *IEEE Transactions on Wireless Communications*, vol. 14, no. 5, pp. 2402–2412, 2014.
- [230] J. M. Jornet and I. F. Akyildiz, "Channel modeling and capacity analysis for electromagnetic wireless nanonetworks in the terahertz band," *IEEE Transactions on Wireless Communications*, vol. 10, no. 10, pp. 3211–3221, 2011.



- 
- [231] Z. Xu, X. Dong, and J. Bornemann, "Design of a reconfigurable mimo system for thz communications based on graphene antennas," *IEEE Transactions on Terahertz science and technology*, vol. 4, no. 5, pp. 609–617, 2014.
- [232] A. Goldsmith, *Wireless communications*. Cambridge university press, 2005.